

# TECHNICAL GUIDANCE AND ANALYTIC SERVICES IN SUPPORT OF SEASAT-A

(NASA-CR-141399) TECHNICAL GUIDANCE AND  
ANALYTIC SERVICES IN SUPPORT OF SEASAT-A  
Final Report, Feb. - Nov. 1974 (Technology  
Service Corp., Silver Spring, Md.) 148 p HC  
\$5.75

N75-20803

Unclas

CSCL 22A G3/43 - 18700 -

L.W. Brooks and R.P. Dooley

## FINAL REPORT

Report No. TSC-W3-20

Prepared Under Contract No. NAS6-2447 by

Technology Service Corporation

Washington Division

Silver Spring, Maryland 20910



for

NATIONAL AERONAUTICS AND SPACE ADMINISTRATION

WALLOPS FLIGHT CENTER

WALLOPS ISLAND, VIRGINIA 23337

April 1975

|   |  |  |  |  |            |
|---|--|--|--|--|------------|
| 1. Report No.<br>NASA CR-141399   |  | 2. Government Accession No.                          |  | 3. Recipient's Catalog No.   |            |
| 4. Title and Subtitle<br>Technical Guidance and Analytic Services in Support of SEASAT-A  |  |  |  | 5. Report Date<br>April 1975   |            |
|   |  |  |  | 6. Performing Organization Code  |            |
| 7. Author(s)<br>L. W. Brooks and R. P. Dooley   |  |  |  | 8. Performing Organization Report No.<br>TSC-W3-20   |            |
| 9. Performing Organization Name and Address<br>Technology Service Corporation<br>8555 Sixteenth Street<br>Silver Spring, MD 20910   |  |  |  | 10. Work Unit No.  |            |
|   |  |  |  | 11. Contract or Grant No.<br>Contract No. NAS6-2447  |            |
| 12. Sponsoring Agency Name and Address<br>National Aeronautics and Space Administration<br>Wallops Flight Center<br>Wallops Island, VA 23337  |  |  |  | 13. Type of Report and Period Covered<br>Contractor Report<br>February 1974 to November 1974 |            |
|   |  |  |  | 14. Sponsoring Agency Code   |            |
| 15. Supplementary Notes<br><br>This is a final report.  |  |  |  |  |            |
| 16. Abstract<br><p>The design of a high resolution radar for altimetry and ocean wave height estimation is studied. From basic principles, it is shown that a short pulse wide beam radar is the most appropriate and recommended technique for measuring both altitude and ocean wave height. To achieve a topographic resolution of <math>\pm 10</math> cm RMS at 5.0 meter RMS wave heights, as required for SEASAT-A, it is recommended that the altimeter design include an onboard adaptive processor. The resulting design, which assumes a Maximum Likelihood Estimation (MLE) processor is shown to satisfy all performance requirements. A design summary is given for the recommended radar altimeter, which includes a full deramp STRETCH pulse compression technique followed by an analog filter bank to separate range returns as well as the assumed MLE processor.</p> <p>The feedback loop implementation of the MLE on a digital computer is examined in detail. Computer "size", estimation accuracies, and bias due to range sidelobes are given for the MLE with typical SEASAT-A parameters. The standard deviation of the altitude estimate is developed and evaluated for several adaptive and nonadaptive split-gate trackers. Split-gate tracker biases due to range sidelobes and transmitter noise are examined. An approximate closed form solution for the altimeter power return is derived and evaluated.</p> <p>The feasibility of utilizing the basic radar altimeter design for the measurement of ocean wave spectra as well, is examined. A preliminary design analysis shows the resulting system parameters for the ocean wave spectrometer to correspond very closely to those of the radar altimeter design. The required modifications are that the transmitter output is switched to a 2 meter antenna which is steered <math>20^\circ</math> away from nadir and scanned conically with a period of 5 seconds. On receive, the full deramp processor is replaced by a surface wave pulse compressor and detector followed by a bank of 11 one-third (<math>1/3</math>) octave filters to perform the spectral analysis. The filter outputs are then detected and integrated for a period of 26 <math>\mu</math>sec per pulse. This preliminary design meets all specified performance requirements.</p> |  |  |  |  |            |
| 17. Key Words (Suggested by Author(s))<br>Radar<br>Radar Altimetry<br>High Resolution<br>Pulse Compression<br>STRETCH<br>Split-Gate Tracker   |  |  | 18. Distribution Statement<br><br>Unclassified - Unlimited<br><br>STAR Category 43 |  |            |
| 19. Security Classif. (of this report)<br>Unclassified  |  | 20. Security Classif. (of this page)<br>Unclassified |  | 21. No. of Pages<br>148  | 22. Price* |

\*For sale by the National Technical Information Service, Springfield, Virginia 22151

**ORIGINAL PAGE IS  
OF POOR QUALITY**

## ABSTRACT

The design of a high resolution radar for altimetry and ocean wave height estimation is studied. From basic principles, it is shown that a short pulse wide beam radar is the most appropriate and recommended technique for measuring both altitude and ocean wave height. To achieve a topographic resolution of  $\pm 10$  cmRMS at 5.0 meter RMS wave heights, as required for SEASAT-A, it is recommended that the altimeter design include an onboard adaptive processor. The resulting design, which assumes a Maximum Likelihood Estimation (MLE) processor is shown to satisfy all performance requirements. A design summary is given for the recommended radar altimeter, which includes a full deramp STRETCH pulse compression technique followed by an analog filter bank to separate range returns as well as the assumed MLE processor.

A feedback loop implementation of the MLE on a digital computer is examined in detail. Computer "size", estimation accuracies, and bias due to range sidelobes are given for the MLE with typical SEASAT-A parameters. The standard deviation of the altitude estimate is developed and evaluated for several adaptive and nonadaptive split-gate trackers. Split-gate tracker biases due to range sidelobes and transmitter noise are examined. An approximate closed form solution for the altimeter power return is derived and evaluated.

The feasibility of utilizing the basic radar altimeter design for the measurement of ocean wave spectra as well, is examined. A preliminary design analysis shows the resulting system parameters for the ocean wave spectrometer to correspond very closely to those of the radar altimeter design. The required modifications are that the transmitter output is switched to a 2 meter antenna which is steered  $20^\circ$  away from nadir and scanned conically with a period of 5 seconds. On receive, the full deramp processor is replaced by a surface wave pulse compressor and detector followed by a bank of 11 one-third ( $1/3$ ) octave filters to perform the spectral analysis. The filter outputs are then detected and integrated for a period of 26  $\mu$ sec per pulse. This preliminary design meets all specified performance requirements.

CONTENTS

Page

PART I - ALTIMETRY AND OCEAN WAVE HEIGHT

|  |   |        |
|--|---|--------|
| 1.0  | INTRODUCTION AND SUMMARY.....                   | I-1-1  |
| 2.0  | HIGH RESOLUTION RADAR IMPLEMENTATION.....       | I-2-1  |
| 2.1  | Basic Principles and Recommended Approach.....  | I-2-2  |
| 2.2  | System Design Summary.....                      | I-2-6  |
| 3.0  | MAXIMUM LIKELIHOOD ESTIMATOR.....               | I-3-1  |
| 3.1  | Feedback Loop Implementation.....               | I-3-2  |
| 3.2  | Computer Sizing.....                            | I-3-19 |
| 3.3  | Estimation Accuracies.....                      | I-3-27 |
| 3.4  | Range Sidelobe Bias.....                        | I-3-31 |
| 4.0  | SPLIT-GATE TRACKERS.....                        | I-4-1  |
| 4.1  | Tracker Accuracy.....                           | I-4-1  |
| 4.2  | Range Sidelobe Bias.....                        | I-4-9  |
| 4.3  | Transmitter Noise Bias.....                     | I-4-16 |
| 5.0  | ALTIMETER POWER RETURN.....                     | I-5-1  |
| 5.1  | Theoretical Development.....                    | I-5-1  |
| 5.2  | Approximate Evaluation.....                     | I-5-6  |
| 6.0  | REFERENCES - PART I.....                        | I-6-1  |
| APPENDIX A - THEORETICAL DERIVATIONS FOR THE MLE ANALYSIS..... A-1 |   |        |
| A.0  | Introduction.....                               | A-1    |
| A.1  | Problem Definition.....                         | A-1    |
| A.2  | Asymptotic Bias and Variance.....               | A-2    |
| A.3  | Special Case: MLE.....                          | A-4    |
| A.4  | A Feedback Loop Implementation.....             | A-5    |
| A.5  | Evaluation of the Satellite Altimetry Case..... | A-9    |
| A.6  | Bias in the MLE Due to Range Sidelobes.....     | A-17   |

**PRECEDING PAGE BLANK NOT FILMED**

CONTENTS (CONTINUED)

|   | <u>Page</u> |
|---|-------------|
| PART II - OCEAN WAVE SPECTRA                        |             |
| 1.0 INTRODUCTION AND SUMMARY.....                   | II-1-1      |
| 2.0 HIGH RESOLUTION RADAR IMPLEMENTATION.....       | II-2-1      |
| 2.1 Basic Principles and Recommended Approach.....  | II-2-2      |
| 2.2 System Design Summary.....                      | II-2-5      |
| 3.0 THEORETICAL ANALYSIS.....                       | II-3-1      |
| 3.1 Detection of Modulation on a Noise Process..... | II-3-2      |
| 3.2 Measurement of Ocean Wavelength.....            | II-3-6      |
| 4.0 REFERENCES - PART II.....                       | II-4-1      |

Part I  
ALTIMETRY AND OCEAN WAVE HEIGHT

1.0 INTRODUCTION AND SUMMARY

The design of a high resolution radar for altimetry and ocean wave height estimation is examined in this part of the report. To achieve a topographic resolution of 10 cm RMS over practically all sea surface roughness, as required for SEASAT-A, it is recommended that the design include an on-board adaptive processor. The resulting design, which assumes a Maximum Likelihood Estimation (MLE) processor, satisfies all the specified SEASAT-A performance requirements for altitude and wave height measurements.

Section 2.0 examines the basic principles involved in the measurement of altitude and wave height. Consideration of both the short pulse radar and two frequency interferometer technique with either a wide or narrow antenna beam, leads to the conclusion that a short pulse wide beam radar is the most appropriate and recommended technique for measuring both altitude and wave height. A design summary is given for the recommended radar which includes a full deramp STRETCH pulse compression technique followed by an analog filter bank to separate range returns as well as the assumed MLE processor.

Section 3.0 describes the implementation and performance of a joint MLE which would simultaneously estimate altitude, wave height, and signal-to-noise ratio. A step-by-step description of a feedback loop implementation of the MLE on a digital computer is presented to show the simplicity of the concepts involved. It is shown that a relatively modest mini-computer would be of adequate "size" for implementing the processor. Estimation accuracies as well as biases associated with range sidelobes are given for typical SEASAT-A parameters. Performance requirements are shown to be achieved with a signal-to-noise ratio greater than 5 dB even at 20 meter significant wave height. The biases due to range sidelobes are shown to be negligible when the average RMS sidelobes are less than -50 dB. This sidelobe level can be achieved in practice.

Section 4.0 examines the performance of a split-gate tracker. An easily interpreted expression for the variance of a split-gate tracker is derived and used to show the effect of changing gate widths and placement of the early gate. A comparison of tracker accuracies for several adaptive and nonadaptive split-gate trackers is given for typical SEASAT-A parameters. Altitude bias due to range sidelobes is examined. It is shown that while receiver weighting to reduce peak sidelobes will not be necessary, the average far out sidelobe level must be less than -50 dB RMS in order to keep the altitude bias less than 6 cm. It is also shown that an altitude bias is caused by the additive transmit noise burst resulting from gating the TWT on prior to (and keeping in on after) transmitting the linear FM signal. To maintain the bias due to this effect at an acceptable level, the ratio of total transmit signal energy to total transmit noise energy must be at least 17 dB.

Section 5.0 derives an approximate closed form solution for the shape of the altimeter mean power return. The radar equation for a distributed target is derived and applied to the particular case of a satellite altimeter. The resulting closed form solution is given in terms of the usual radar parameters, an "effective" range distribution, which is a combination of RMS wave height and RMS range resolution, and an "effective" beamwidth which is a combination of ocean surface slope distribution and two-way antenna beamwidth. Illustrations showing the shape of the mean power return as a function of RMS wave height and "effective" beamwidth are given for typical SEASAT-A parameters. It is shown that a small "effective" beamwidth causes a distortion in the shape of leading edge of the mean return and produces a wave height dependent altitude bias. To eliminate this bias, an antenna beamwidth of  $5^\circ$  to  $10^\circ$  would be required for SEASAT-A. Such a small antenna would, however, require a corresponding increase in peak transmitter power and/or compression ratio to achieve the recommended signal-to-noise ratio. It is recommended that a study be made of all of the trade-offs involved (including the effects of antenna pointing error) in order to determine an optimum antenna beamwidth.

Appendix A presents the theoretical derivations for a broad class of estimators which are obtained by minimizing a penalty functional that depends on both the observed data and on the parameters to be estimated. Maximum Likelihood Estimators (MLE) are special cases of this class of estimators. Formulas for computing the asymptotic bias and variance of the estimators are derived. A feedback loop implementation scheme is described and formulas for computing the mean response and the variance of the loop estimates are derived. The general solutions are then evaluated for the satellite altimetry case. The resulting formulas provide the basis for the results described in Section 3.0 of the report.

It is desirable, for geodetic purposes as well as the measurement of many oceanographic phenomena of interest, to measure the position of the mean sea surface to an accuracy of  $\pm 10$  cm RMS. The design of a satellite radar altimeter with this accuracy would be quite simple were it not for the unavoidable degradation in performance caused by sea surface roughness. Recent studies<sup>(1)</sup> have shown that the standard deviation of the altitude measurement is directly proportional to sea surface roughness. Thus an altimeter design having a 10 cm RMS accuracy at 2 meter wave heights (peak-to-trough) would only provide a 100 cm RMS accuracy at 20 meter wave height. The design of a satellite altimeter having a topographic resolution of 10 cm RMS over practically all sea surface roughness (1 to 20 meters peak-to-trough) cannot be achieved on board the spacecraft with standard "split gate" tracking algorithms.

To circumvent this problem, it is recommended that the altimeter design include an on board adaptive processor. At the present time several candidate adaptive processors are under consideration. These include a Maximum Likelihood Estimate (MLE) processor<sup>(1)</sup>, a Minimum Mean Square Error (MMSE) processor<sup>(1)</sup>, and several Adaptive Split-Gate (ASG) trackers<sup>(1,2)</sup> which either continuously or discretely approximate the weighting functions of the MLE or MMSE processors. The theoretical basis for both the MLE and MMSE processor was developed by Technology Service Corporation for NASA/Wallops under Contract No. NAS6-2241. From a performance point of view, the MLE is best since it would provide optimum (minimum variance) estimates of satellite altitude, ocean wave height, and electromagnetic ocean surface reflectivity. As such, only the salient parameter estimates need to be transmitted to the ground instead of the large amount of raw data otherwise required for ground processing. The MMSE processor and continuous ASG tracker represent progressive simplifications, respectively, in processor design and complexity with a corresponding reduction in performance. Finally, the discrete ASG tracker approximation to the weighting functions of the MMSE processor proposed by MacArthur<sup>(2)</sup> represents the simplest processor design and complexity with a corresponding performance that marginally meets the requirements for SEASAT-A.

In addition to the obvious trade offs between performance and complexity, the recommendation of a particular on board adaptive processor for SEASAT-A requires further study and evaluation of the many subtleties associated with each processor. However, in order to specify a complete system design, the remainder of this section of the report assumes the selection of an on board MLE processor.

Section 2.1 examines the basic principles involved in the measurement of altitude and wave height. Consideration is given to both the short pulse radar and two frequency interferometer techniques operating with either a wide or narrow antenna beam. The ensuing discussion leads to the conclusion that a short pulse wide beam radar is the most appropriate and recommended technique for measuring both altitude and wave height.

Section 2.2 summarizes the design of the recommended radar which includes an on board MLE processor. The recommended pulse compression technique, because of bandwidth considerations, is a full deramp STRETCH followed by an analog filter bank to separate range returns. The resulting design achieves all specified performance requirements for altitude and wave height measurements.

## 2.1 Basic Principles and Recommended Approach

The basic purpose of a satellite altimeter is to measure the height from the satellite to the mean sea surface. For a nadir looking altimeter this requires the measurement of the mean of the density of specular point scatterers with respect to height. A measurement of wave height may also be obtained with the altimeter if the spread (standard deviation) of the density of specular point scatterers with height is available. Rigorous theoretical developments of techniques for achieving altitude and wave height measurements are readily available in the literature<sup>(3,4,5)</sup>. For the most part these works by the very nature of their rigorous and precise developments tend to obscure the simplicity of the concepts involved. The following is an attempt to explain the principles involved at the expense of rigorous justification.

First consider a short pulse radar altimeter which, depending upon the geometry, can be operated in either a narrow antenna beam or wide antenna beam mode. The impulse response (mean power response of a matched filter receiver) of a smooth flat ocean would correspond to the radar cross section versus range,  $\sigma(R)$ , and would appear as shown in Figure 2.1-b. In the wide beam (pulse limited) mode  $\sigma(R)$  is a step response which occurs at the location of the surface and lasts until the intersection of pulse and surface passes out of the antenna beamwidth. In the narrow beam (beam limited) mode, the  $\sigma(R)$  is simply the transmit pulse with an epoch corresponding to the location of the surface. Next consider a discrete distribution of specular points with height as shown in Figure 2.1-c. Now the composite return signals are simply the superposition of impulse responses weighted by the distribution function.

Thus, in the wide beam mode the leading edge of the impulse response corresponds to the integral of the specular point density (specular point cumulative distribution function). Here an altitude measurement can be obtained by tracking the half power point of the leading edge of the return signal (the median) and an estimate of wave height is obtained by measuring the rise time (shape) of the leading edge. In the narrow beam mode the impulse response corresponds to the specular point density itself. Thus, altitude measurement is obtained by tracking the centroid of the return signal and an estimate of wave height is obtained from the width of the return signal. Passing now to a realistic model for the specular point density of the sea surface, Barrick<sup>(3)</sup> has shown to a first order approximation that the density is normal. Thus the impulse responses for the wide and narrow beam modes would be as shown in Figure 2.1-d.

Now a comparison of the two modes of operation at typical satellite altitudes shows the narrow beam mode to be impractical because of the large antenna required. That is, in order to have an impulse response which adequately corresponds to the wave height density, the differential path length at the edge of the beam  $\Delta R$ , is required to be less than the smallest wave height of interest and the range resolution must be about half the smallest wave height of interest. For a 1 meter wave height and satellite altitude of 725 km this

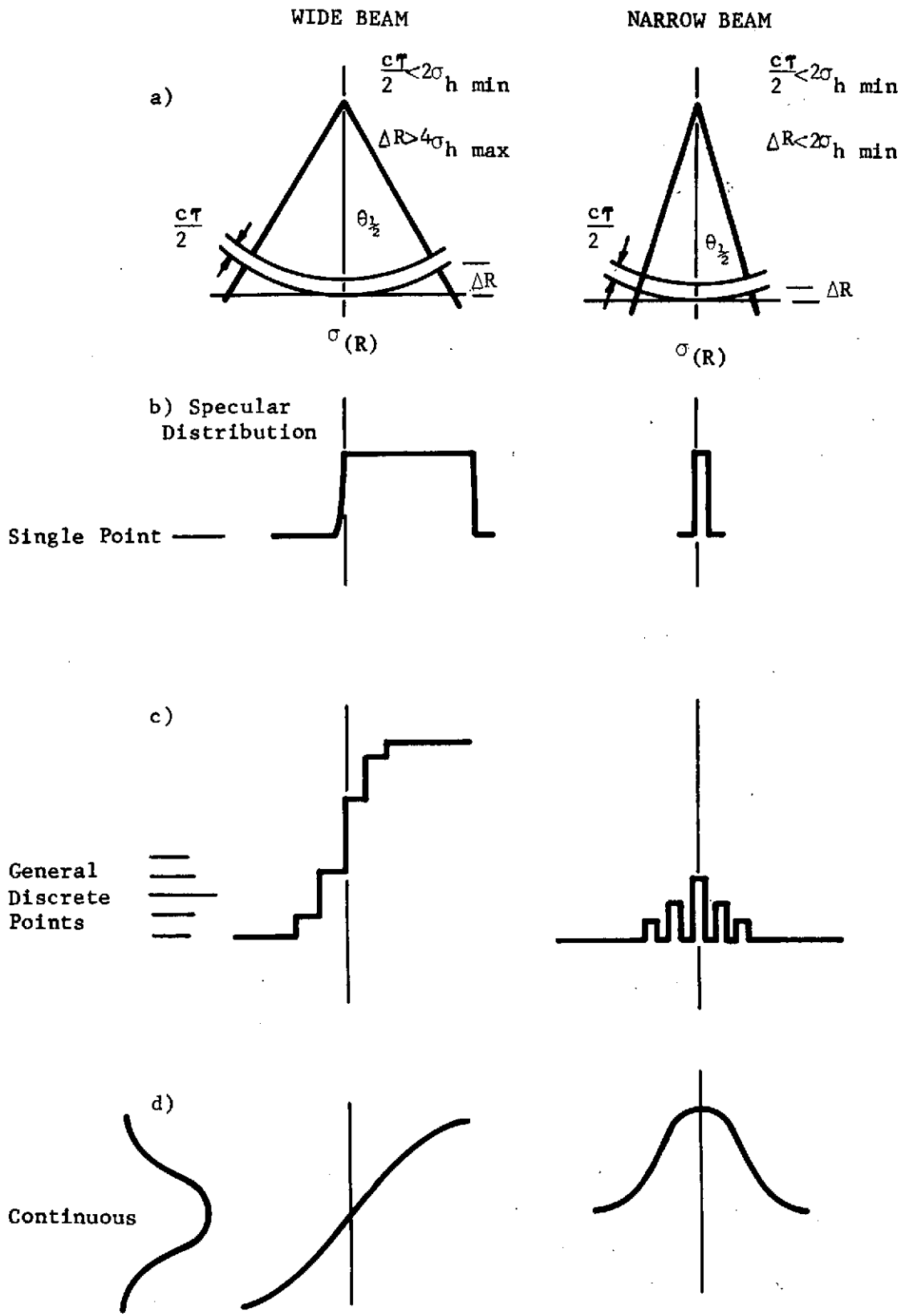


Figure 2.1. Impulse Response of a Short-Pulse Radar For Narrow- and Wide-Beam Antenna.

translates to an antenna diameter of at least 20 meters and a pulse width of about 3 nsec. On the other hand, the wide beam mode simply requires that the differential path length  $\Delta R$  be much greater than the largest wave heights of interest and the range resolution be about half the smallest peak-to-trough wave height of interest. For the present SEASAT application this corresponds to an antenna smaller than 1.1 meter and a pulse width of about 3 nsec, which is readily achievable in the recommended design.

Note that in the comparison of the two modes of operation the emphasis is placed on the ability to faithfully reproduce the wave height density or distribution function so that an estimate of wave height may be obtained. It is also seen that both modes required a wide bandwidth signal ( $\sim 330$  MHz) in order to resolve the smallest (1 meter) wave height of interest. As will be shown, this bandwidth requirement is basic to the measurement of wave height regardless of the technique employed.

Consider now the two frequency correlation techniques suggested by Weissman<sup>(5)</sup> for the measurement of wave height. With this method two very long (essentially CW) signals separated in frequency by the amount  $\Delta f = f_1 - f_2$  are simultaneously transmitted. Two homodyne receivers are then used to separate the return signals at frequencies  $f_1$  and  $f_2$  and measure the cross correlation  $R(\Delta f)$  at the frequency separation  $\Delta f$ . Thus changing the transmitter frequency separation  $\Delta f$  provides a measure of  $R(\Delta f)$ . It can be shown<sup>(6)</sup> that the cross correlation,  $R(\Delta f)$ , is simply the Fourier transform of the radar cross section versus range  $\sigma(R)$ . Now if the radar is operating in a narrow beam mode (for which the antenna requirement for  $\Delta R < 2\sigma_{\text{hmin}}$  has already been shown to be impractical at satellite altitudes) the Fourier transform of  $\sigma(R)$ ,  $\text{FT}[\sigma(R)]$ , is the characteristic function of the specular point density. Note also that the wave height resolution of this implementation is the reciprocal of the transmitter frequency separation,  $1/\Delta f$ , and hence would require the same 330 MHz for the measurement of 1 meter (peak-to-trough) wave heights as the short pulse radar. The point to be made here is that the measurement of the wave height density or characteristic function both require the same overall system bandwidth and antenna requirements.

Finally, consider operating the two frequency interferometer in a wide beam mode for measuring wave height. Here, the measured output  $R(\Delta f)$  would again correspond to the  $FT[\sigma(R)]$ , but in this situation the transform is not only that of the cumulative wave height distribution (corresponding to the leading edge of  $\sigma(R)$ ) but also includes the so called plateau region of  $\sigma(R)$ . Unfortunately, most of the energy in  $\sigma(R)$  is contained within the plateau region and hence also in  $FT[\sigma(R)]$ . Thus, changes in wave height would have little effect on the main response of  $FT[\sigma(R)]$  and would probably have to be determined by the measurement of the sidelobe structure of  $FT[\sigma(R)]$ . While such a measurement technique has not been examined in depth (and in fact might even be feasible) it certainly cannot compare favorably with the short pulse wide beam radar which provides altimetry as well as wave height information. Table 2.1 summarizes the more important characteristics of a short pulse radar and two frequency interferometer technique for measuring wave height.

From the above discussion it is seen that a short pulse wide beam radar is the most appropriate (and recommended) technique for measuring both altitude and wave height. The following sections summarize the design of such a radar, which includes an on board MLE processor.

## 2.2 System Design Summary

The design of a high resolution satellite radar for measuring altitude and wave height is described on the following pages. The resulting design achieves all specified performance requirements. These performance requirements are summarized in Table 2.2 and the system design is summarized in Table 2.3.

A simplified block diagram of the proposed radar is shown in Figure 2.2. The CHIRP transmitter generates a 2.8  $\mu$ sec 360 MHz bandwidth linear FM signal. When the chirp transmitter receives both a PRF trigger and a transmit pulse gate, the output signal is fed to a TWT string identical to that used in GEOS-C. Full deramp pulse compression is achieved by generating a second identical linear FM signal by means of a properly timed range trigger from the MLE processor. This second linear FM signal is not

Table 2.1

Short Summary of Wave Height Measurements

| Quantity         | Type of Radar             |                          |
|------------------|---------------------------|--------------------------|
|                  | Short Pulse               | Two-Freq. Interferometer |
| Resolution       | $1/B$                     | $1/\Delta f$             |
| Max data rate    | $B$                       | $1/\tau$                 |
| Energy on target | $\tau$                    | $\tau$ (50% loss)        |
| Measured output  | $\sigma(R)$               | FT [ $\sigma(R)$ ]       |
| a) Narrow beam   | Density                   | Characteristic           |
| b) Wide beam     | Cumulative dist. function | F.T. [C.D.F. + Plateau]  |

Table 2.2

System Performance Requirements

|      |   |   |
|------|---|---|
| I.   | Geodetic accuracy   | 50 cm                                       |
| II.  | Topographic resolution  | 10 cm RMS (7 cm allocated to system error)  |
| III. | Wave height range:<br>Accuracy:                                 | 1-20 m crest-to-trough<br>max (0.5 m., 25%) |
| IV.  | Correlation between pulses                                      | $<1/e$                                      |
| V.   | Oceanographic phenomena of interest (maximum spacial frequency) | 0.25 Hz                                     |

Table 2.3

## Design Summary

|   |                                  |
|---|----------------------------------|
| I. <u>Orbit Parameters</u>  |                                  |
| a) Height   | 725 km                           |
| b) Inclination  | 82° retrograde                   |
| c) Eccentricity   | 0.0064 maximum                   |
| II. <u>Radar Parameters</u>                                       |                                  |
| a) Antenna beamwidth  | 2.6°                             |
| b) Pointing accuracy  | $2\sigma_{\theta} = 0.1^{\circ}$ |
| c) Antenna gain   | 36.4 dB                          |
| d) Peak power   | 2 kW                             |
| e) System Losses other than processing losses in pulse compressor | 5 dB                             |
| f) Noise figure   | 5.5 dB                           |
| g) Frequency  | 13.9 GHz                         |
| h) Uncompressed pulse width                                       | 2.8 $\mu$ s                      |
| i) Uncompressed pulse bandwidth                                   | 360 MHz                          |
| j) Compressed pulse width   | 3.0 ns                           |
| k) Compression ratio  | 1000/1                           |
| l) PRF <sub>max</sub> (uncorrelated returns)                      | 1.6 kHz                          |
| m) PRF  | 1500 Hz                          |
| n) S/N (single pulse)   | 10 dB                            |
| o) Ocean cross section  | +6 dB                            |
| p) Receiver weighting*  | -26 dB Modified Taylor           |
| q) Pulse compression * processing loss                            | 0.55 dB                          |
| r) Main lobe broadening due to tapering*                          | 23%                              |
| III. <u>Pulse Compression</u>                                     |                                  |
| Type  | Full deramp stretch              |
| Range processing  | Analog filter bank               |
| Filter bank   | Discrete passive                 |
| Number of filters   | 60                               |
| Frequency range   | 9.2 to 20.8 MHz                  |
| Filter bandwidth  | 385 kHz                          |
| Output data form  | Two TTL parallel words           |
|   | A. Range bin number, 6 bits      |
|   | B. Range bin amplitude, 13 bits  |
| * Included in design but considered optional:                     |                                  |

Table 2.3 (cont.)

|      |   |  |
|------|---|--|
| III. | <u>Pulse Compression</u>  |  |
|      | Time required for full sampling                                       | 450 microseconds, max.                   |
|      | A/D sampling frequency  | 1 MHz                                    |
| IV.  | <u>Linear FM Generation</u>   |  |
|      | Type*   | Surface wave                             |
|      | Bandwidth   | 60 MHz                                   |
|      | Multiplier chain  | X6                                       |
|      | Pulse length  | 2.8 $\mu$ s                              |
|      | Linearity of FM   | 0.2%                                     |
|      | Peak frequency deviation<br>(one circle of variation<br>across pulse) | 25 kHz                                   |
| V.   | <u>Altitude and Wave Height Processing</u>                            |  |
|      | Type  | MLE processor                            |
|      | Implementation  | Digital interface with on-board computer |
|      | Interface data rate   | 200-360 Hz                               |
|      | Output data rate  | 3-5 words @ 1-10 per second              |
|      | Tracking bandwidth  | 1.0 Hz                                   |

I-2-10

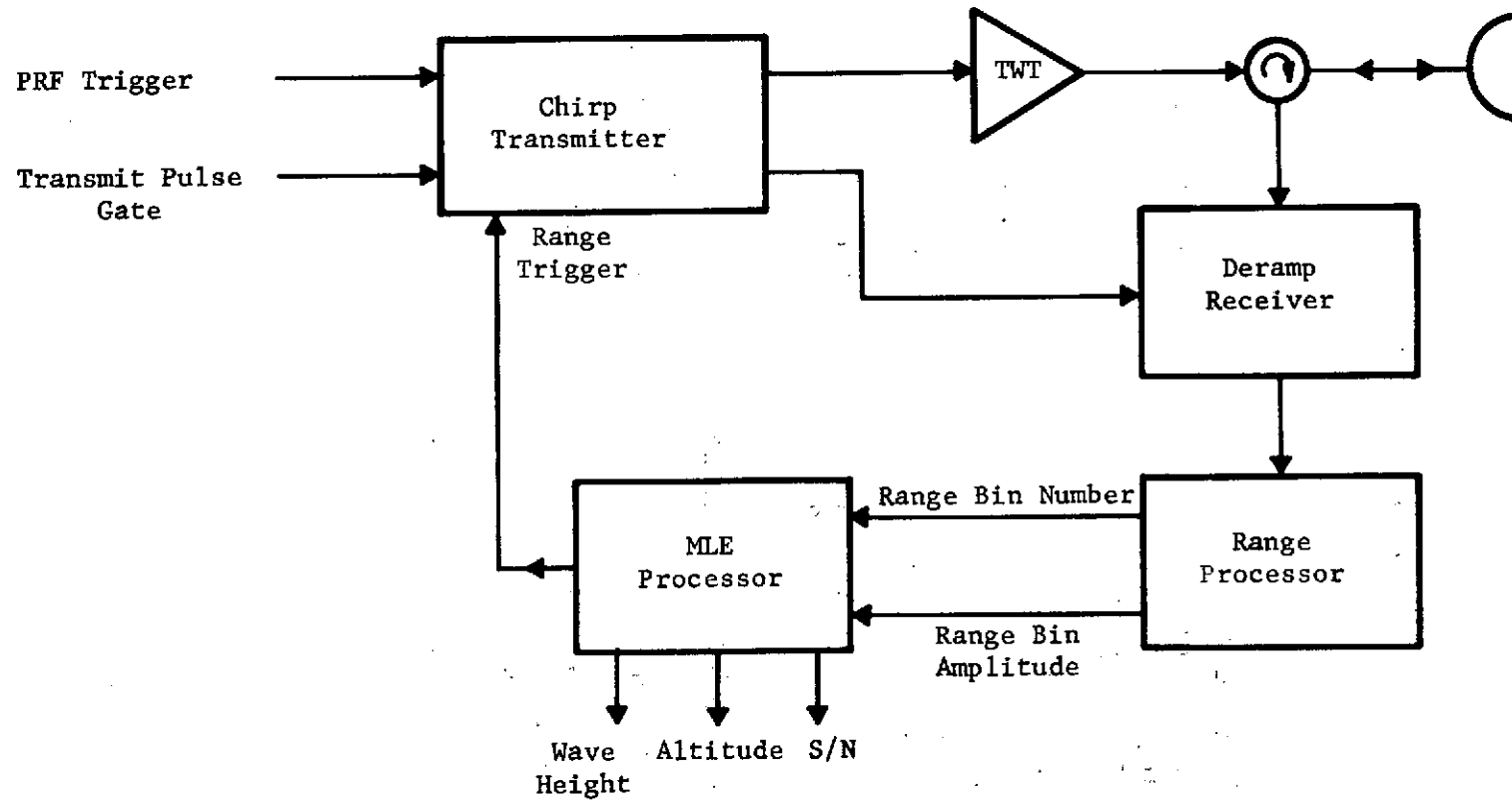


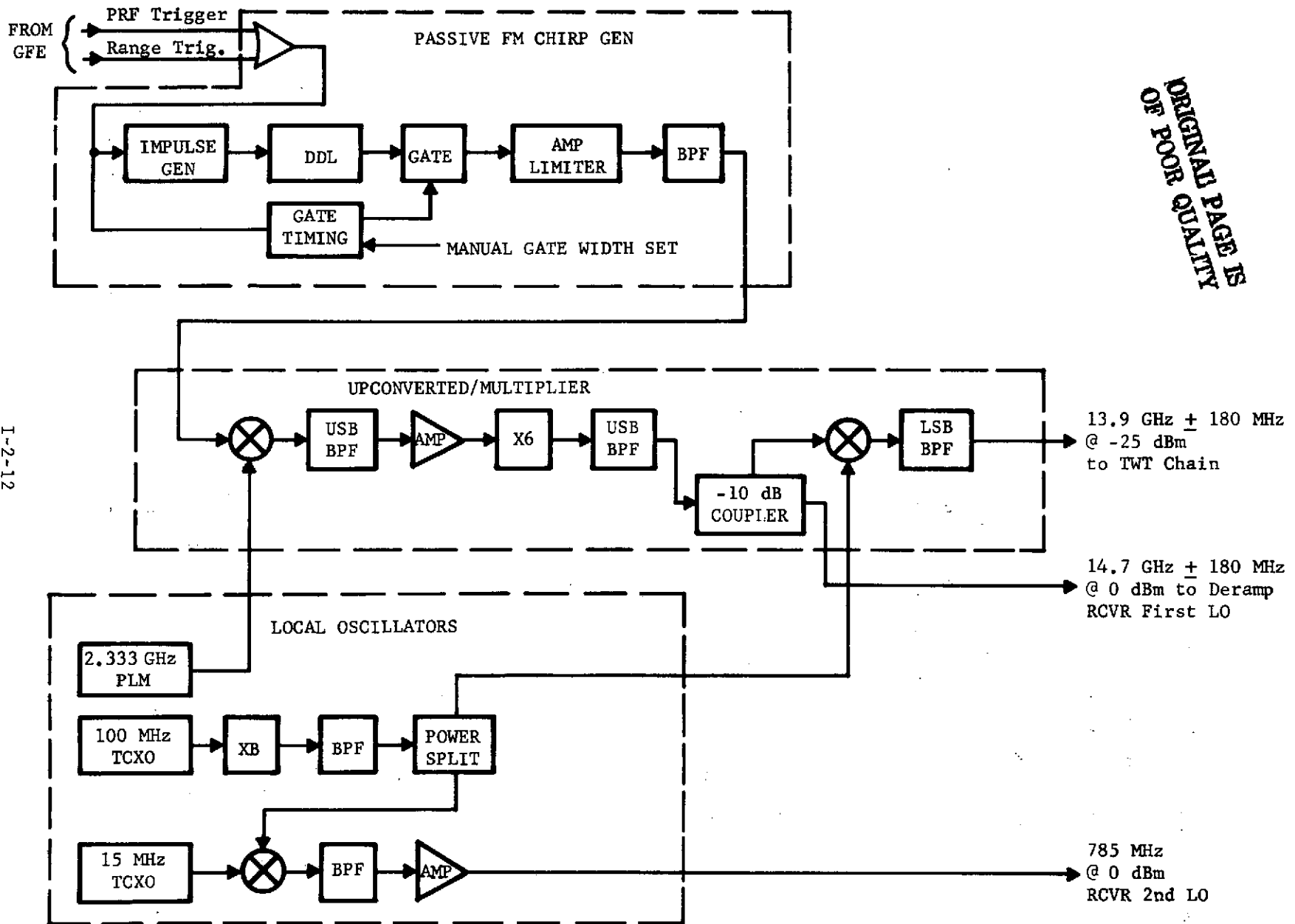
Figure 2.2 High Resolution Radar Altimeter Block Diagram

transmitted but instead fed to the deramp receiver where it is mixed with the ocean return signal. This process converts the return signal as a function of time into an identical signal as a function of frequency.

This return signal as a function of frequency is then fed at an IF frequency into the range processor unit. There an analog filter bank consisting of 60 discrete filters is used to provide 60 samples of the leading edge of the return signal (i.e., cumulative wave height distribution function). The 60 range samples are then detected and fed into an analog multiplexer and A/D converter. The output of the range processor unit then consists of two TTL parallel words, range bin number (6 bits) and range bin amplitude (13 bits).

A more detailed breakdown of the recommended design for the chirp transmitter, deramp receiver, and range processor is shown in Figures 2.3, 2.4 and 2.5 respectively. This particular design is the result of a previous NASA/Wallops study<sup>(1)</sup>. An in depth description of the rationale and tradeoffs involved in arriving at this design is available in the above referenced final report. The most important aspect of the above design is the selection of a full deramp pulse compression technique followed by an analog filter bank to separate individual range returns. With this technique the A/D converter bandwidth is less than 1 MHz as compared to other forms of pulse compression which would require a rather impractical 330 MHz A/D converter.

The MLE processor accepts the digital output of the range processor and simultaneously performs an optimum (minimum variance) estimate of epoch, wave height, and signal-to-noise ratio. In addition, the MLE processor also provides a range trigger to the chirp transmitter unit for deramping the return signal and hence closing the altitude tracking loop. As shown in Figure 2.6, the digital input from the range processing unit is fed into a buffer storage and inverted to produce negative digital video samples,  $-V$ , which when summed with the estimated mean power return  $\hat{V}$  produces a difference signal,  $\hat{V} - V$ . This difference signal is then normalized by dividing by the variance of the estimated return  $\hat{V}^2$ , multiplied by the appropriate parameter weighting function  $(\frac{\partial \hat{V}}{\partial \hat{\tau}_0}, \frac{\partial \hat{V}}{\partial \hat{\sigma}_0}, \text{ or } \frac{\partial \hat{V}}{\partial \hat{\sigma}_h})$ , and range summed in each loop to produce the error signals



ORIGINAL PAGE IS  
OF POOR QUALITY

I-2-12

Figure 2.3 Chirped Transmitter Section

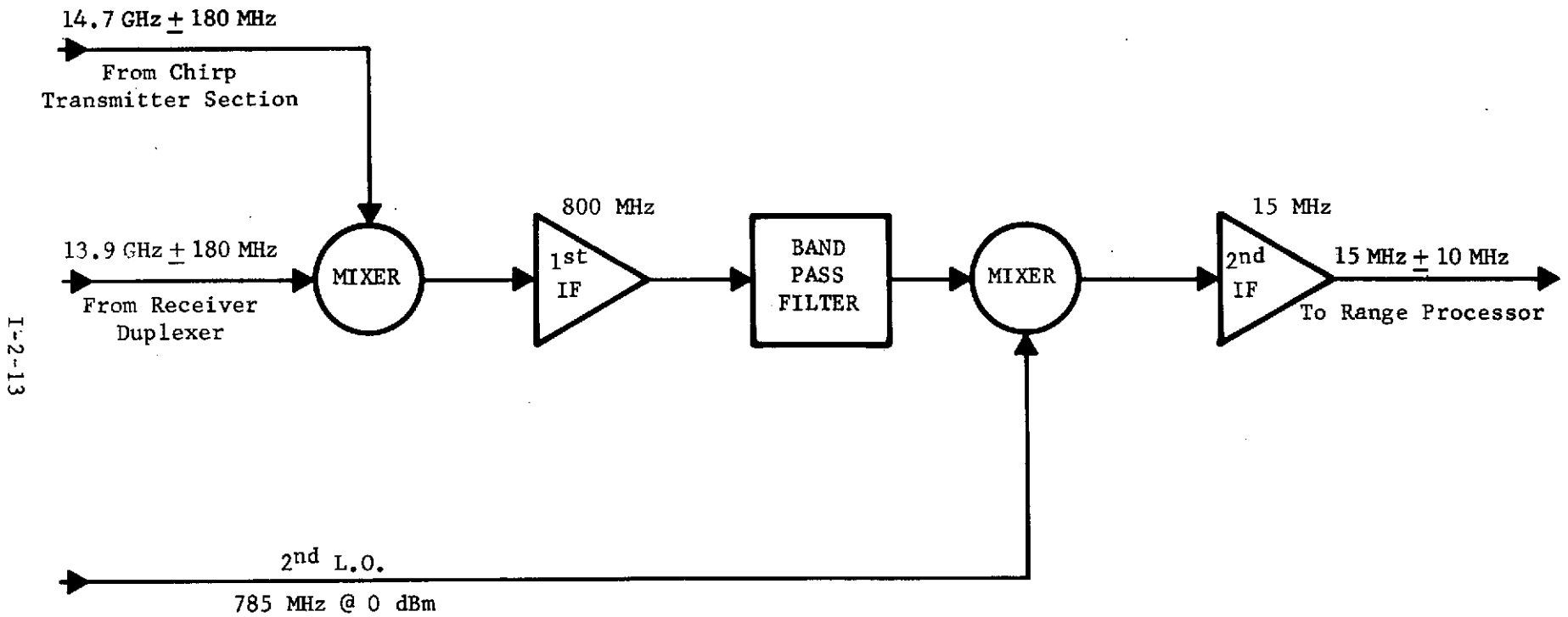
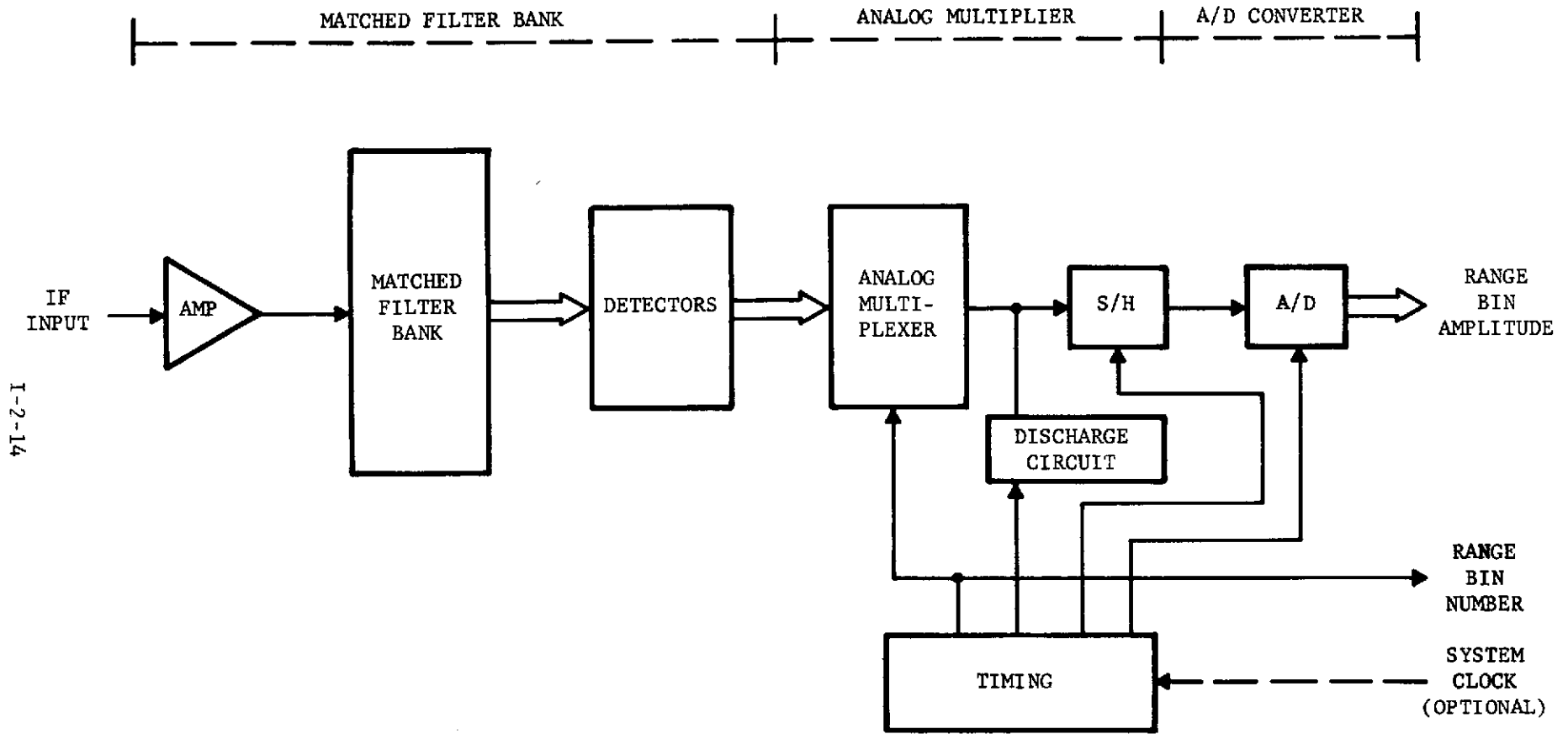
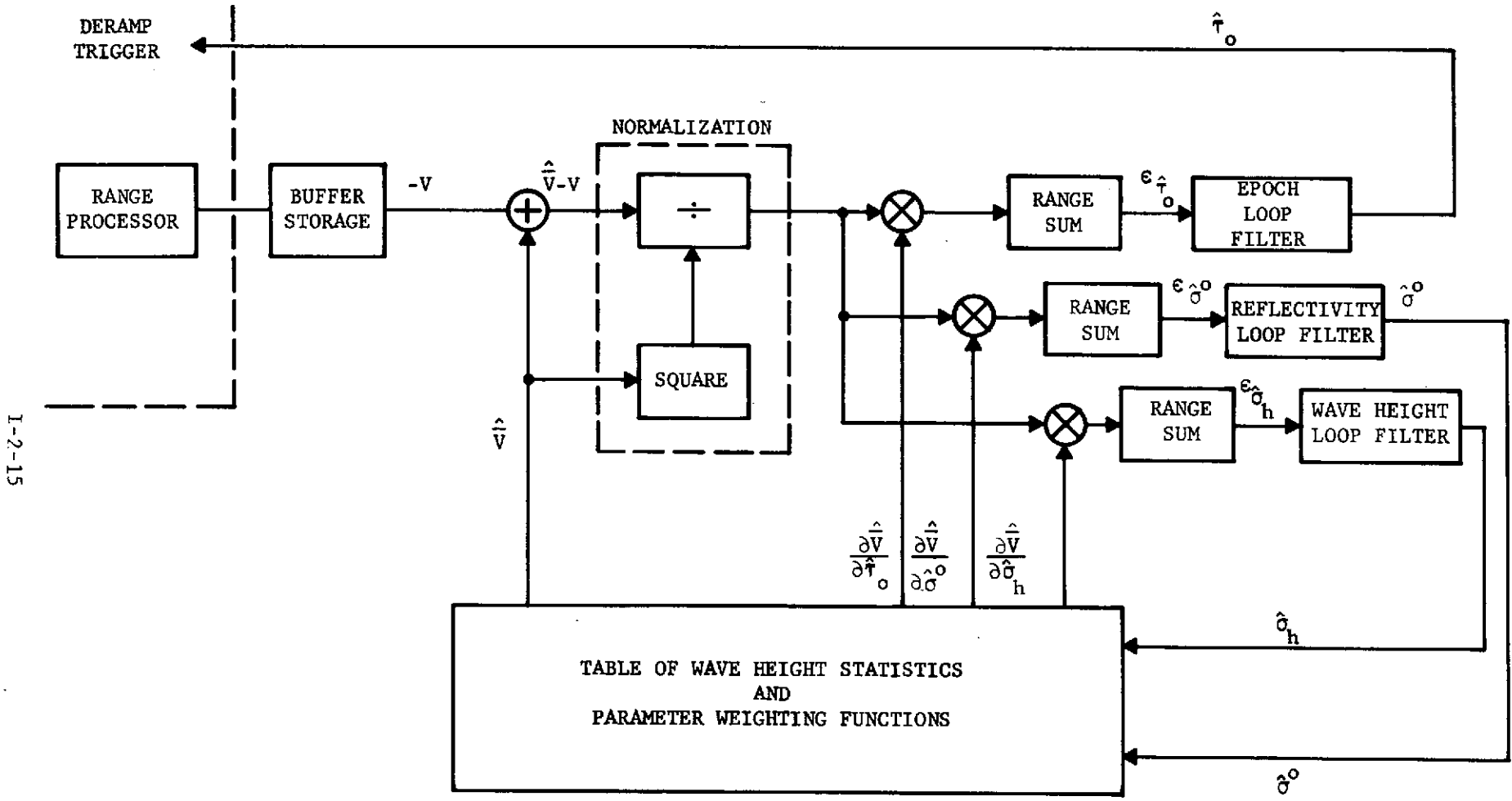


Figure 2.4 Deramp Receiver Section Block Diagram



I-2-14

Figure 2.5 Range Processor Section



I-2-15

Figure 2.6 Onboard MLE Processor

$\hat{\epsilon}_{\tau_0}$ ,  $\hat{\epsilon}_{\sigma_0}$ , and  $\hat{\epsilon}_{\sigma_h}$ . After passing through the loop filters, the estimates are fed back as follows: the epoch estimate is used to control the range trigger of the chirp transmitter for deramping the ocean return signal. The wave height estimate is used to control the table look up of the mean return signal as well as the parameter weighting functions. The signal-to-noise ratio estimate is used as a scale factor in the generation of the estimated mean return and as a scale factor in the generation of the epoch and wave height weighting functions.

The implementation of a MLE processor could take one of two forms; a complete special purpose digital logic unit or a digital interface with a minicomputer. If a minicomputer is included in the proposed SEASAT-A configuration, a digital interface would be the recommended approach. The interface data rate would be 62 words at a nominal 200 - 360 Hz rate. The MLE output data rate would be 3 - 5 words at a 1 - 10 per second rate.

Complete details of the mathematical development of the MLP processor are given in Reference (1), and further delineated in Section 3.0 and Appendix A of this report. Again, it should be pointed out that some sort of adaptive processor — whether it be an MLE, MMSE, or ASG — is necessary (and recommended) to achieve the performance requirements on board the spacecraft. A comparison of tracking accuracies, Figure 2.7, shows that a 5.0 meter RMS wave height, a factor of four reduction in RMS tracking error is achieved by the MLE when compared with a conventional half power split-gate tracker. The accuracies and biases associated with these split-gate trackers (conventional and adaptive) are examined in detail in Section 4.0 of this report.

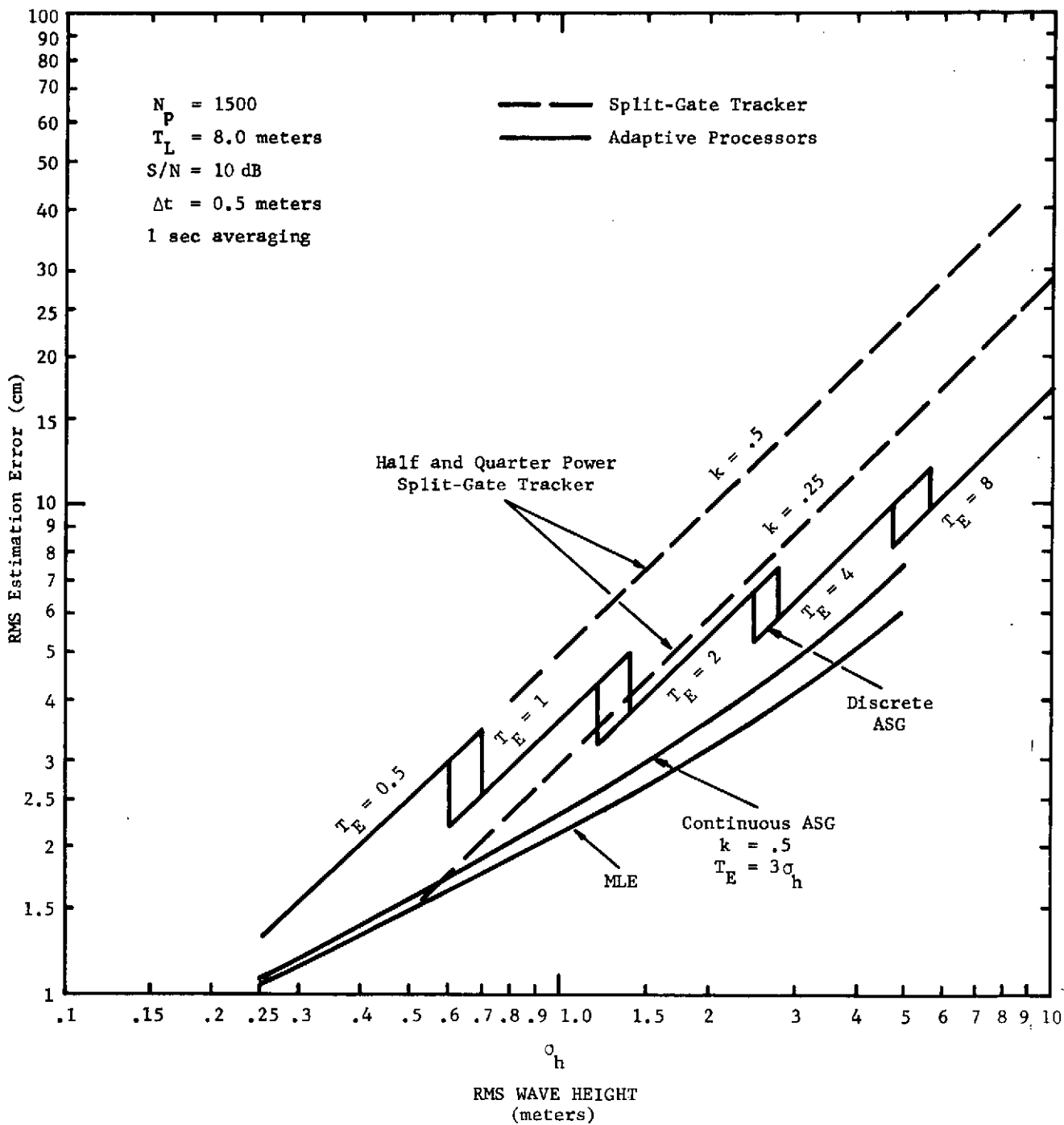


Figure 2.7 Comparison of Tracking Accuracies of Split-Gate Trackers and Adaptive Processors

### 3.0 MAXIMUM LIKELIHOOD ESTIMATOR

A joint Maximum Likelihood Estimator (MLE) which would simultaneously estimate the epoch, wave height, and signal-to-noise ratio for a satellite altimeter was originally described in Reference (1). This section of the report describes a method of implementing a MLE processor on a digital computer. Estimation accuracies as well as biases associated with range sidelobes are given for typical SEASAT-A altimeter parameters. The intention of this section of the report is to describe results and explain the simplicity of the concepts involved in the implementation. The theoretical basis for all of the material described here is provided in Appendix A.

Section 3.1 describes a feedback loop implementation of the MLE processor. It is shown that for such an implementation, the logarithms of the likelihood ratio must converge with time to a local minimum of the likelihood function. A step-by-step description of the implementation is presented. Simulated examples which illustrate the shape of the functions used to generate the error signals of the processor are described in detail. Some of these functions are shown to be generalizations of the gating functions used in split-gate trackers, thus providing further insight into the nature of the feedback loop implementation.

Section 3.2 describes the approximate "size" of the MLE processor when implemented as a software program in a general purpose digital computer. It is shown that the total data storage required is about 2000 words, and the total program storage is also about 2000 words. These results indicate that a relatively modest mini-computer would be adequate for implementing the processor.

Section 3.3 presents the theoretical estimation accuracies of the MLE for typical SEASAT-A system parameters. An evaluation example is given for each of the three parameter estimates. A table of estimation accuracies shows that the performance requirements for SEASAT-A could be achieved with a signal-to-noise ratio greater than 5 dB even at 20 meter significant wave height.

Section 3.4 provides expressions for the biases in the three parameter estimates caused by range sidelobes of the pulse compression network. It is shown that all biases can be maintained at a negligible level (less than 1 percent), provided that the average RMS sidelobes are less than or equal to -50 dB. Since these sidelobe levels can be achieved in practice, the resulting biases for the MLE should not cause any problems.

### 3.1 Feedback Loop Implementation

The implementation of a joint Maximum Likelihood Estimator (MLE) for epoch, normalized surface reflectivity, and RMS wave height ( $\tau_o$ ,  $\sigma^o$ ,  $\sigma_h$ ) is examined in this section of the report. Here, the intention is to explain the simplicity of the concepts involved, at the expense of rigorous theoretical justification. The theoretical developments are given in Appendix A of this report.

First consider the recommended altimeter design, which consists of a full deramp pulse compression technique followed by an analog filter bank to separate individual range returns. Then, the altimeter receiver can be modeled as (nearly) matched filtering, square law detection and sampling as shown in Figure 3.1. The description of the MLE and its properties are simplified with this model, since the problem is now constrained to that of finding the optimum processor for the sampled video outputs. In the sense that only the video processing is optimized, the resulting processor is suboptimal; however, this is not thought to be a serious limitation. Aside from the fact that the optimum video processing to be described will show considerable improvement over existing tracking schemes, it also readily lends itself to a practical implementation with a small scale digital computer.

The procedure to be followed will be to find a suitable approximation to the likelihood function (i.e., the joint probability density) of the video outputs given the three parameters of interest  $\tau_o$ ,  $\sigma^o$  and  $\sigma_h$ . Then, for any set of observed video samples, the joint MLE are those values ( $\hat{\tau}_o$ ,  $\hat{\sigma}^o$ ,  $\hat{\sigma}_h$ ) which maximize the logarithm of the likelihood function. The maximum, of course, occurs at a point in the parameter space for which the three partial derivatives with respect to the parameters are zero. This

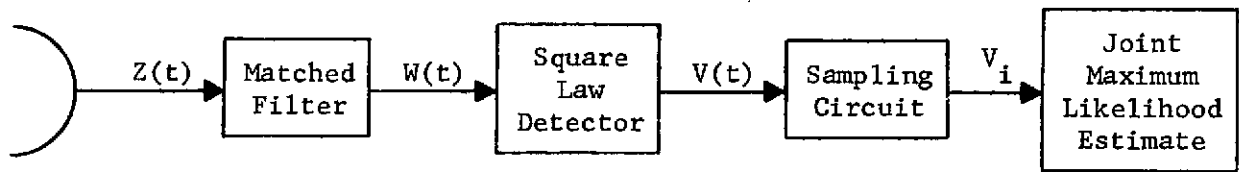


Figure 3.1  
Functional Model of the Altimeter Receiver

fact suggests a technique for implementing the MLE which uses the partials as input error signals to three feedback loops which, in turn, solve the maximizing conditions by forcing the error signals to zero.

The form of the likelihood function for the sampled video outputs of Figure 3.1 is simple, if it is assumed that the samples are separated by at least one range resolution cell. In this case, the correlation between samples is negligible, and since the underlying process is Gaussian, it is reasonable to assume them to be independent. Thus, the likelihood function has the form:

$$\Lambda (V_{11}, V_{12}, \dots, V_{nk}/\tau_o, \sigma^o, \alpha_h) = \prod_{i,k} \bar{V}_i^{-1} \exp(-V_{ik}/\bar{V}_i) \quad (3.1)$$

where:

$V_{ik}$  is the sampled video output from the  $i^{\text{th}}$  range cell on the  $k^{\text{th}}$  pulse.

and

$\bar{V}_i$  is the expected value of the video from the  $i^{\text{th}}$  range cell.

That is, the square law detected outputs form an independent exponential process. The dependence of the likelihood function on the three parameters  $\tau_o$ ,  $\sigma^o$ ,  $\alpha_h$  is contained entirely in the variation with range of the mean value  $\bar{V}_i$ . Thus, taking the logarithm of (3.1), and differentiating, the MLE estimates must satisfy the three equations.

$$0 = \frac{\partial \log \Lambda}{\partial \alpha} = - \sum_k \sum_i (\bar{V}_i - V_{ik}) \bar{V}_i^{-2} \frac{\partial \bar{V}_i}{\partial \alpha} \quad (3.2)$$

where " $\alpha$ " stands for any of the three parameters  $\tau_o$ ,  $\sigma^o$  and  $\alpha_h$ .

The problem of determining the joint MLE of the parameters requires solving Equations (3.2). One technique for achieving this is to use the negative of the partial derivatives in Equations (3.2) as inputs to integrating-feedback filters to derive the MLE estimates as shown in Figure 3.2.

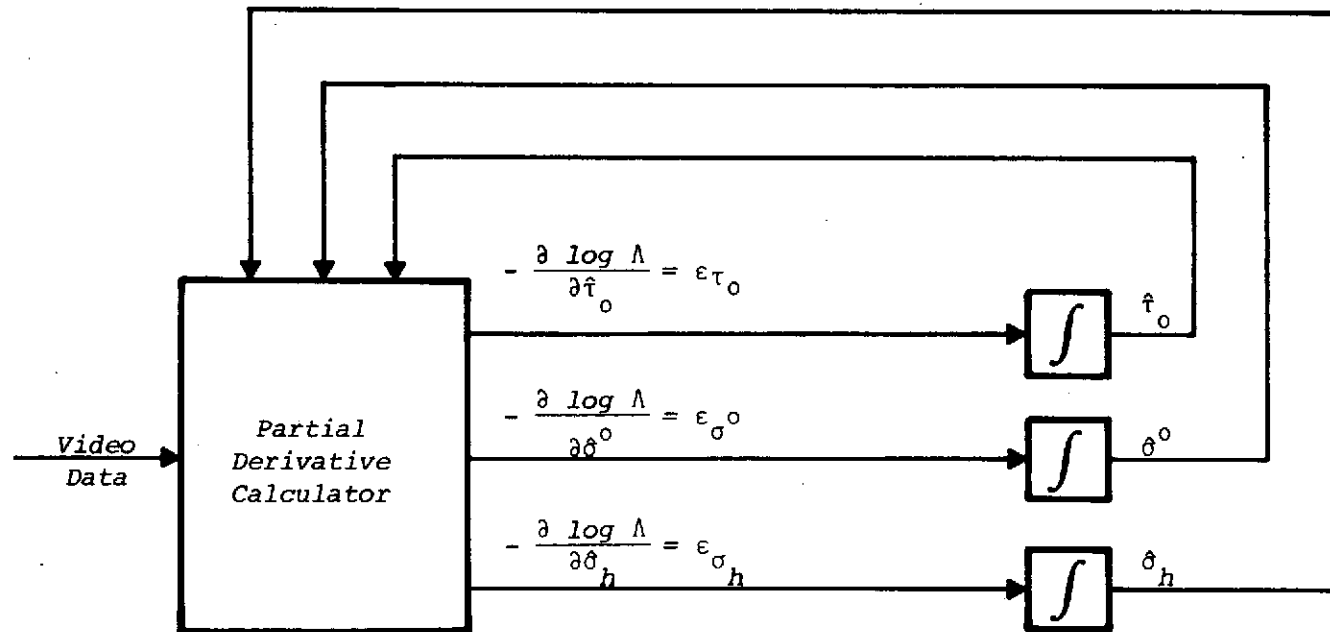


Figure 3.2 General MLE Implementation

That is, since the estimates are derived from integrating filters, one has:

$$\begin{aligned} \frac{d \hat{\tau}_o}{dt} &= - \frac{K \partial \log \Lambda}{\partial \hat{\tau}_o} \\ \frac{d \hat{\sigma}^o}{dt} &= - \frac{K \partial \log \Lambda}{\partial \hat{\sigma}^o} \end{aligned} \quad (3.3)$$

$$\frac{d \hat{\sigma}_h}{dt} = - \frac{K \partial \log \Lambda}{\partial \hat{\sigma}_h}$$

where K is a gain factor associated with the integrators.

Now, the time rate of change of the logarithm of the likelihood function is:

$$\frac{d \log \Lambda}{dt} = \left( \frac{\partial \log \Lambda}{\partial \hat{\tau}_o} \right) \frac{d \hat{\tau}_o}{dt} + \left( \frac{\partial \log \Lambda}{\partial \hat{\sigma}^o} \right) \frac{d \hat{\sigma}^o}{dt} + \left( \frac{\partial \log \Lambda}{\partial \hat{\sigma}_h} \right) \frac{d \hat{\sigma}_h}{dt} \quad (3.4)$$

or, from Equations (3.3),

$$\begin{aligned} \frac{d \log \Lambda}{dt} &= - K \left\{ \left( \frac{\partial \log \Lambda}{\partial \hat{\tau}_o} \right)^2 + \left( \frac{\partial \log \Lambda}{\partial \hat{\sigma}^o} \right)^2 + \left( \frac{\partial \log \Lambda}{\partial \hat{\sigma}_h} \right)^2 \right\} \\ &\leq 0 \end{aligned} \quad (3.5)$$

Thus, as a function of time, the logarithm of the likelihood ratio must decrease and converge to a local minimum of the likelihood function. If the initial parameter estimates are close to the correct ones, then the loops in Figure 3.2 will converge to the joint MLE of  $\tau_o$ ,  $\sigma^o$ , and  $\sigma_h$ .

The practicality of implementing the MLE depends on the complexity of the partial derivative calculator in Figure 3.2. The steps required to compute the three partial derivatives are diagrammed in Figure 3.3. As can be seen from that figure, if the mean video versus range plus the three partial derivatives are available, then the computations required to derive the error signals are relatively minor.

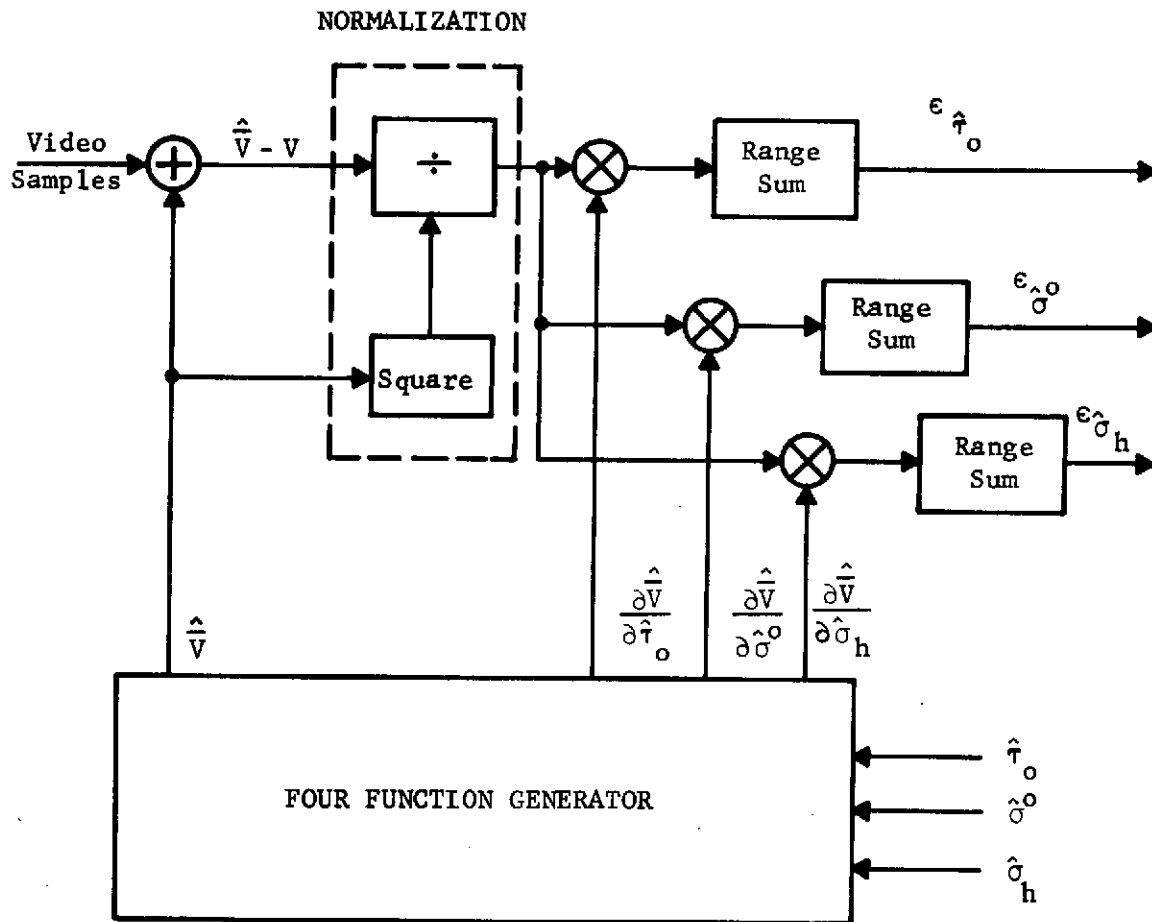


Figure 3.3 Generation of the Error Signals for the MLE

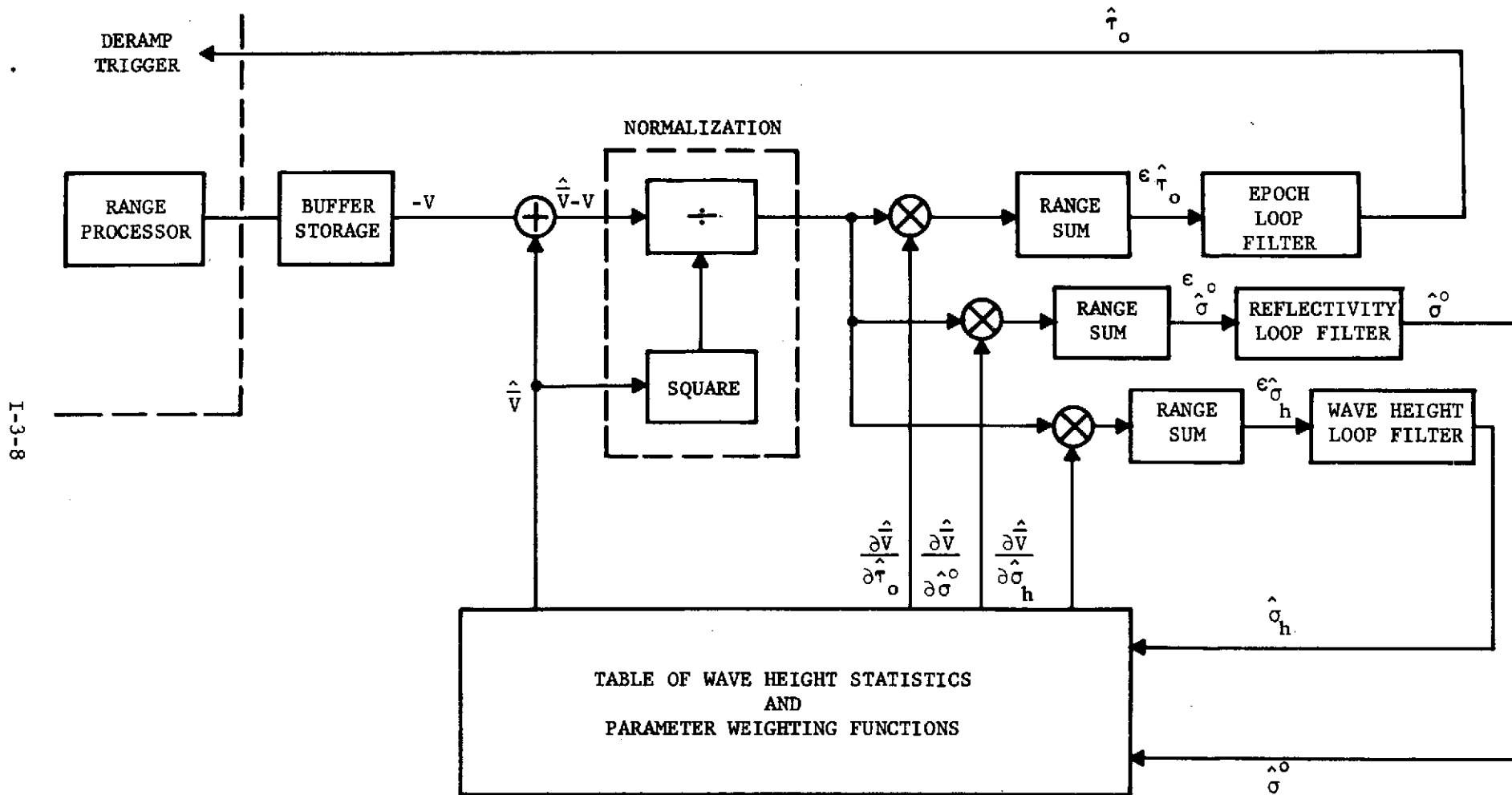


Figure 3.4 Onboard MLE Processor

Figures 3.2 and 3.3 give a fairly pleasing intuitive picture of the operation of the MLE processor. In Figure 3.3, it is seen that the error signals for the tracking loops in Figure 3.2 are derived as follows. First, an error signal versus range,  $\hat{V} - V$ , is generated which represents the difference between the measured return as a function of range and the estimated mean return. Secondly, this error signal is weighted inversely proportional to its variance. That is:

$$E (V - \bar{V})^2 = \bar{V}^2 \quad (3.6)$$

Thus, after normalization, the signal may be loosely described as having uniform information content. Finally, the normalized error-versus-range signal is "gated" by the partial derivative of  $\bar{V}$ , with respect to the parameter of interest, and summed over range. The effect of multiplying (gating) by the partial derivative is to emphasize those range bins which are most affected by variations in the parameter of interest.

Thus, a very simple step-by-step description of a feedback loop implementation, Figure 3.4, for solving the minimizing conditions

$$0 = \sum_k \sum_i \frac{(\hat{V} - V_{ik})}{\hat{V}^2} \frac{\partial \hat{V}}{\partial \alpha}$$

and achieving the joint MLE is as follows:

- Step 1. Compare an estimate of the mean return signal with the sampled data to obtain a difference signal  $\hat{V} - V_{ik}$ .
- Step 2. Normalize the fluctuation of this difference signal by dividing it by the estimated variance of the return  $\hat{V}^2$ .
- Step 3. Weight this normalized difference signal to maximize its sensitivity to the parameter being estimated (multiply by  $\frac{\partial \hat{V}}{\partial \alpha}$ ).
- Step 4. Integrate the resulting signal over range to obtain the error signals  $\epsilon_\alpha$ .
- Step 5. Integrate the error signal  $\epsilon_\alpha$  with time to obtain the parameter estimates  $\hat{\alpha}$ .
- Step 6. Use the parameter estimates  $\hat{\alpha}$  to obtain a new estimate of the mean return signal  $\hat{V}$  so as to drive the error signal to zero.

### 3.1.1 Simulated Examples

The nature of the error signals generated by the feedback loop implementation of the MLE processor becomes more apparent from an examination of several simulated examples. These examples illustrate the shape of the functions utilized in generating the error signals. Three examples are given, one for an error in epoch only, one for an error in wave height only, and one for an error in ocean reflectivity only. The parameters used in simulating these examples are as follows:

Data:  $\sigma^{\circ} = 10$  dB,  $\sigma_h = 2$  m,  $\tau_o = 0$  (true values)

Sample Interval = 1.0 m

Number of Samples Averaged = 5

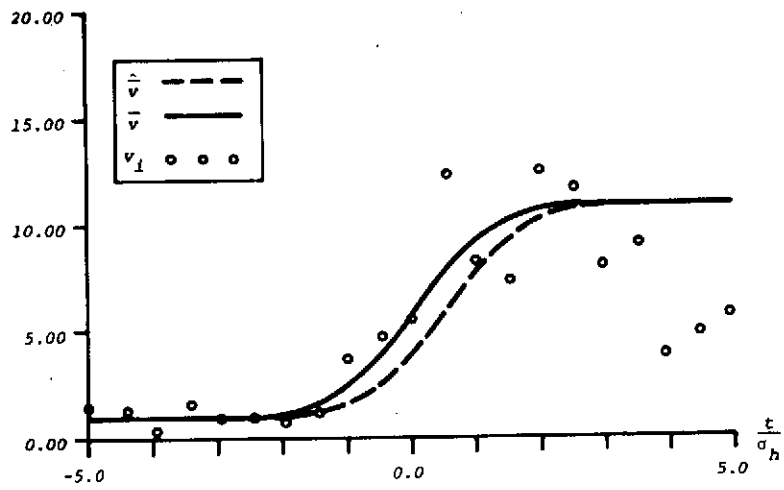
Case I:  $\hat{\tau}_o$  error = 1.0 m  
No error in  $\sigma^{\circ}$  or  $\sigma_h$

Case II:  $\hat{\sigma}_h$  error = 1.0 m  
No error in  $\sigma^{\circ}$  or  $\tau_o$

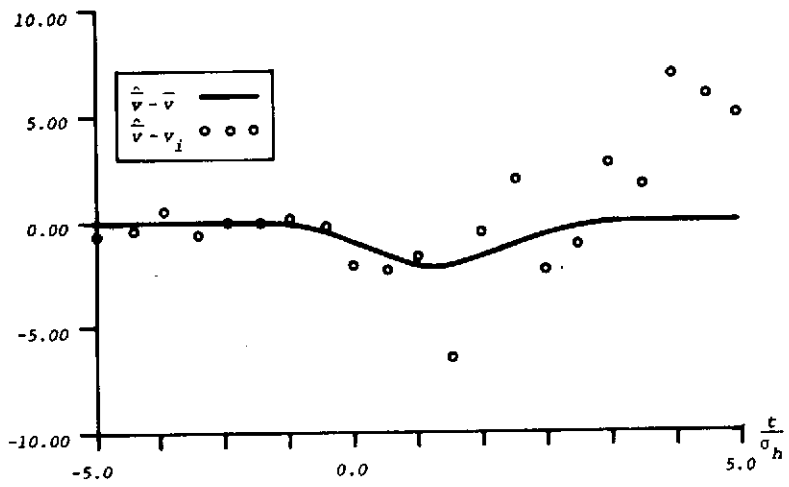
Case III:  $\hat{\sigma}^{\circ}$  error = 3.0 dB  
No error in  $\sigma_h$  or  $\tau_o$

The shape of the functions utilized in generating the error signals for Case I, epoch error only, are shown in Figure 3.5-a through 3.5-f. Figure 3.5-a shows the estimated mean  $\hat{V}$ , the data samples  $V_i$ , and the true mean of the data samples  $\bar{V}$ . Here, and throughout all the examples to be described, each data sample  $V_i$  is the average of five independent samples. That is, it is assumed that some pre-processing in the form of pulse-to-pulse averaging is performed prior to inputting the data to the MLE processor. In the actual MLE implementation, the amount of pre-processing (averaging) should be such that the averaged sample values are input to the processor at a maximum rate of 10 per second.

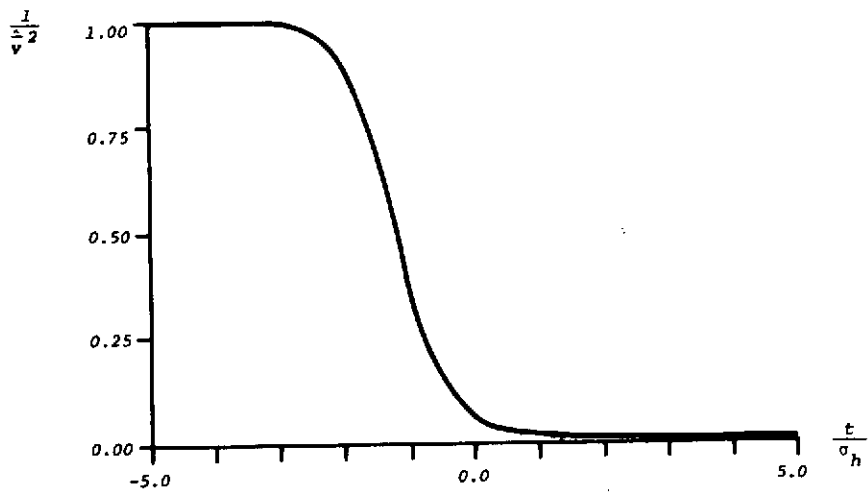
In addition to showing the 1.0 meter displacement between the true and estimated epoch, Figure 3.5-a also clearly illustrates the fact that the variance of the data samples is proportional to the mean value as shown by the fact that the fluctuation of the data samples increases as the mean value increases. This effect is even more pronounced in Figure 3.5-b,



a) Data and Estimated Mean



b) Difference Signal Between Estimated Mean and Data



c) Normalization Based on Estimated Variance

Figure 3.5 Epoch Error Example (Case I)

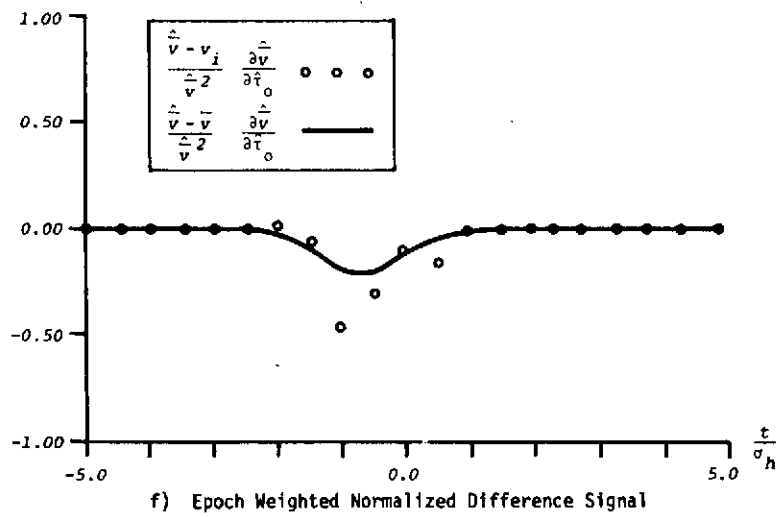
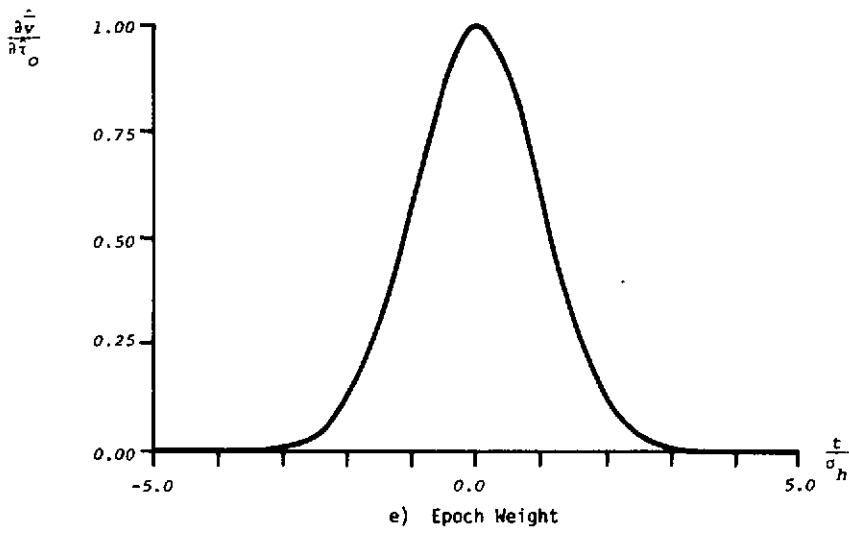
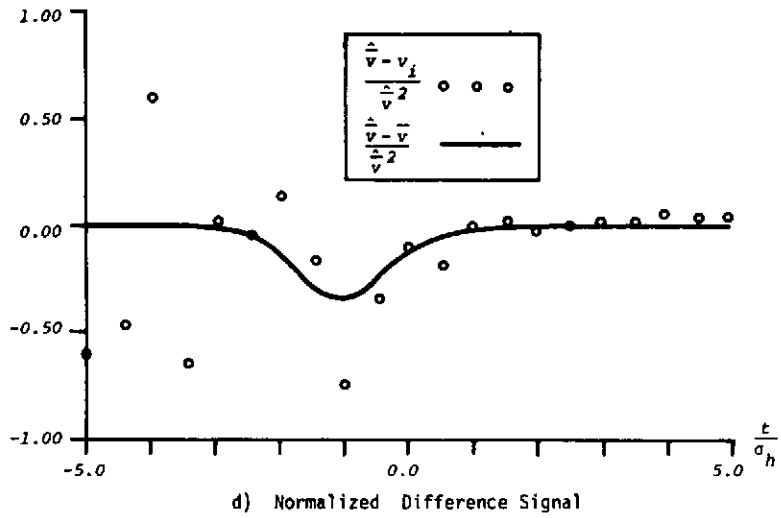


Figure 3.5 (Continued)

which shows the difference signal between the estimated mean and the data samples,  $\hat{V} - V_i$ , as well as the difference between the estimated mean and true mean,  $\hat{V} - \bar{V}$ . When this difference signal is normalized by multiplying by the reciprocal of the estimated variance  $1/\hat{V}^2$  shown in Figure 3.5-c, the normalized difference signal shown in Figure 3.5-d is obtained. The mean value of this normalized signal is also shown in the figure. Note that the fluctuation of the data samples of the normalized difference signal has been reduced to about  $\pm 0.5$ , as compared with the difference signal shown in Figure 3.5-b, which has fluctuations on the order of  $\pm 5.0$ . This type of normalization of the data for reducing and equalizing the fluctuation is characteristic of all maximum likelihood estimators.

When the normalized difference signal is multiplied by the epoch weight shown in Figure 3.5-e, the signal shown in Figure 3.5-f is obtained. Here, several observations can be made. The shape of the epoch weight shows that the maximum weight is placed at the mean of the estimated return signal. Furthermore, since this weight is the partial derivative of the estimated return, it is in fact the estimated wave height probability density function. Thus, the width of this weighting function is equal to the estimated RMS wave height  $\sigma_h$ , which of course, changes width with sea state. This epoch weight of the MLE processor is analogous to the early gate of a split-gate tracker. It is, of course, a more general type early gate in the sense that the weighting is continuous, and the width changes with wave height.

If the epoch weighted normalized difference signal shown in Figure 3.5-f were integrated (summed) over range, a single value of epoch error signal  $\epsilon_{\tau_0}$  would be obtained. Integrating successive samples of  $\epsilon_{\tau_0}$  in the epoch loop filter would thus provide a new epoch estimate  $\hat{\tau}_0$ . While it would have been desirable, time and funding limitations prevented including the shape of the error signals as a function of error for this as well as the other simulated examples. It may be shown, however, that all the error signals are strongly coupled. That is, an error in epoch estimation only (as in this example) produces not only an epoch error signal, but also error signals in the reflectivity and wave height feedback loops. The same sort of thing happens when there is an error in estimating either wave height

or reflectivity. Whether or not this coupling of the error signals presents a problem for the feedback loop implementation of the MLE remains to be determined. Since the coupled error signals are such that the total error in all three loops is driven to zero as rapidly as possible, there is reason to believe that the coupling will not be a problem. On the other hand, if error coupling proves to be a problem, the situation can be corrected by means of a decoupling network. Such a network would entail estimating (and inverting) the error correlation matrix  $R(\theta)$ , which would add to the complexity of the processor. To resolve these questions concerning the effects of error coupling requires a detailed study of the eigenvalues and eigenvectors of the error correlation matrix which was beyond the scope of the present program.

A description of the shape of the functions utilized in generating the error signals for Case II, wave height error only, shown in Figure 3.6-a through 3.6-f, and Case III, reflectivity error only, shown in Figure 3.7-a through 3.7-f, is essentially the same as the previous example except for the weighting functions. An examination of the wave height weight, Figure 3.6-e, shows a maximum negative weight applied one sigma (RMS wave height  $\sigma_h$ ) prior to the estimated epoch and a maximum positive weight applied one sigma after the estimated epoch. Functionally, this weight is formed by the product of a linear ramp and the estimated wave height density function. A gating arrangement analogous to this wave height weight would entail centering two gates symmetrically about the half power point of the return signal. The difference between these two gates would thus provide an estimate of the mean slope of the leading edge of the returns signal and hence a measure of wave height. (This is, in fact, the method suggested by MacArthur, Reference (2), for estimating wave height.) The wave height weight of the MLE processor is of course, more general in the sense that the weighting is continuous, and the separation and width of the positive and negative portions change continuously with wave height.

An examination of the reflectivity weight, Figure 3.7-e, shows the maximum weight being applied well after the estimated epoch. Since this weight is the partial derivative of the estimated return with respect to  $\sigma^0$ , it is simply a scaled version of the estimated return, and hence, corresponds to the estimated cumulative wave height distribution function. Quite obviously, this reflectivity weight is the more general analogy to the late gate of a split-gate tracker.

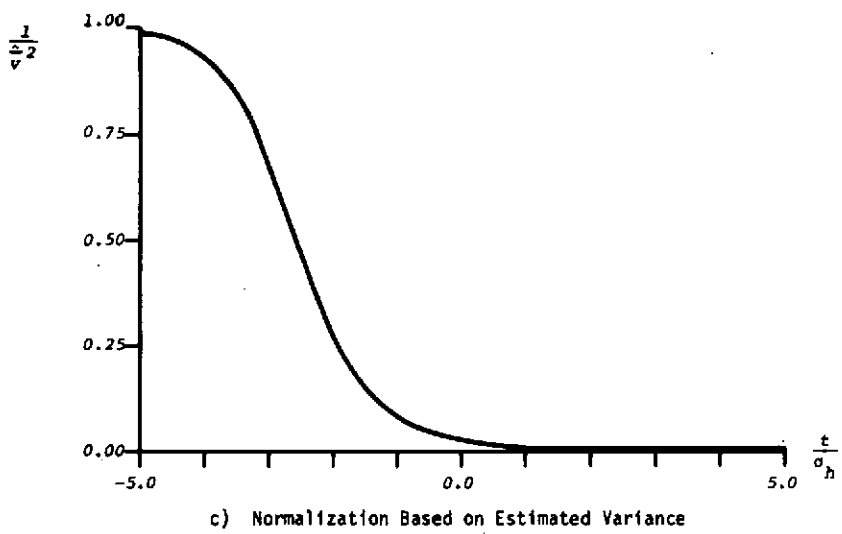
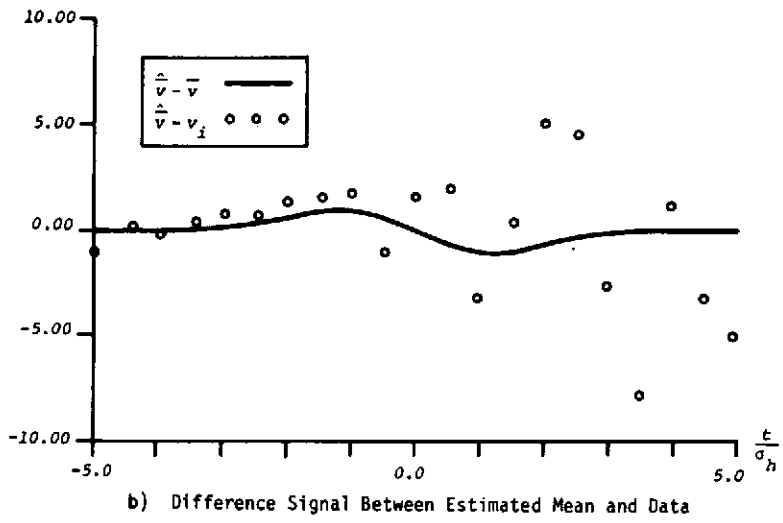
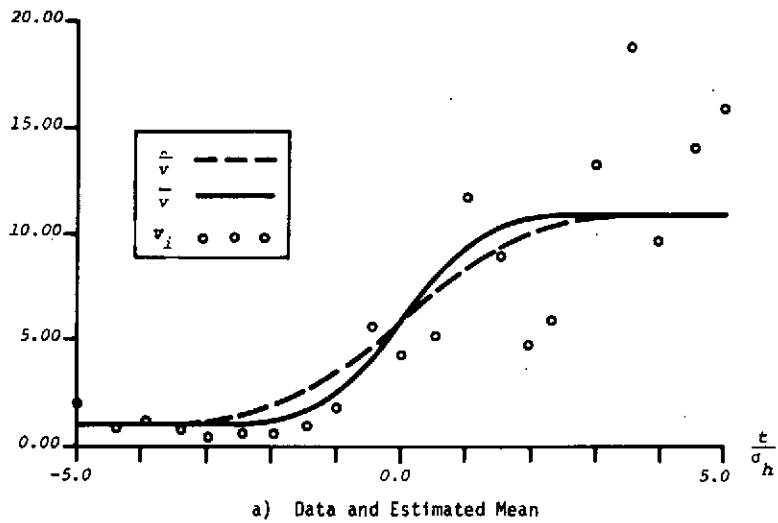


Figure 3.6 Wave Height Error Example (Case II)

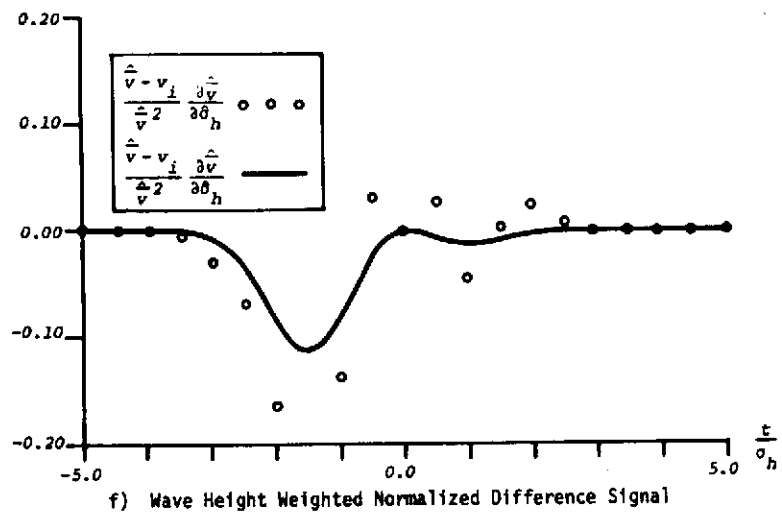
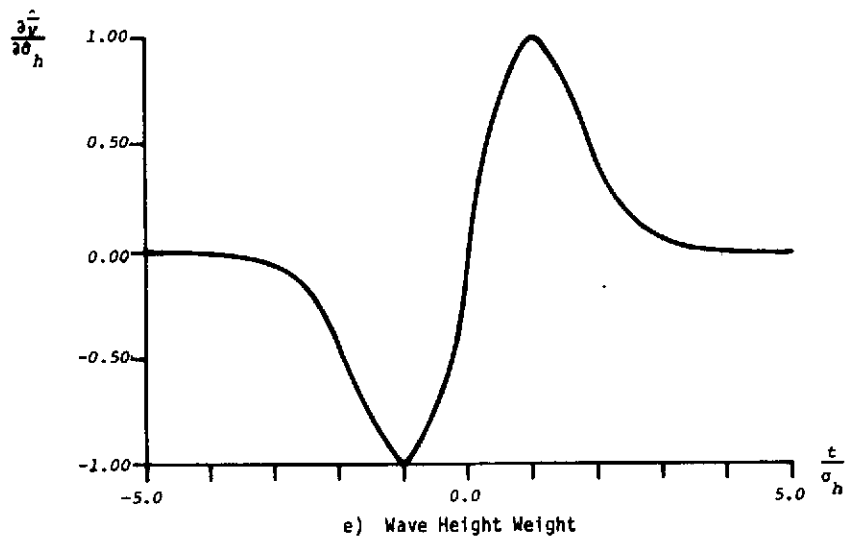
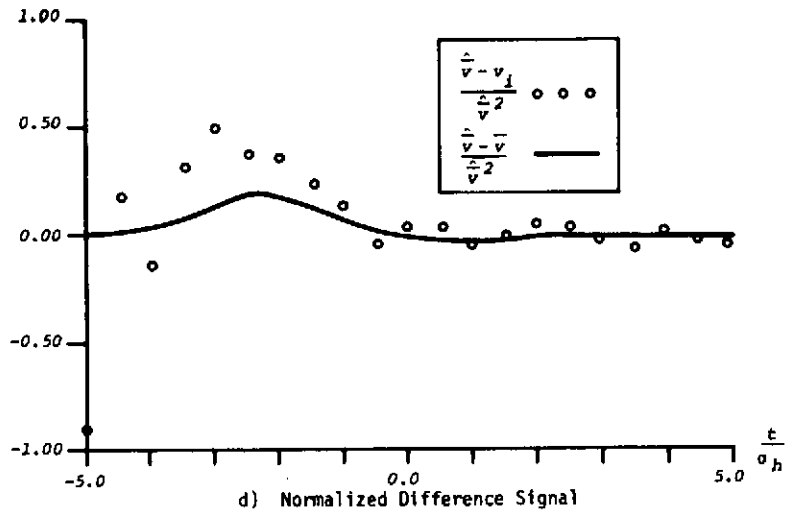


Figure 3.6 (Continued)

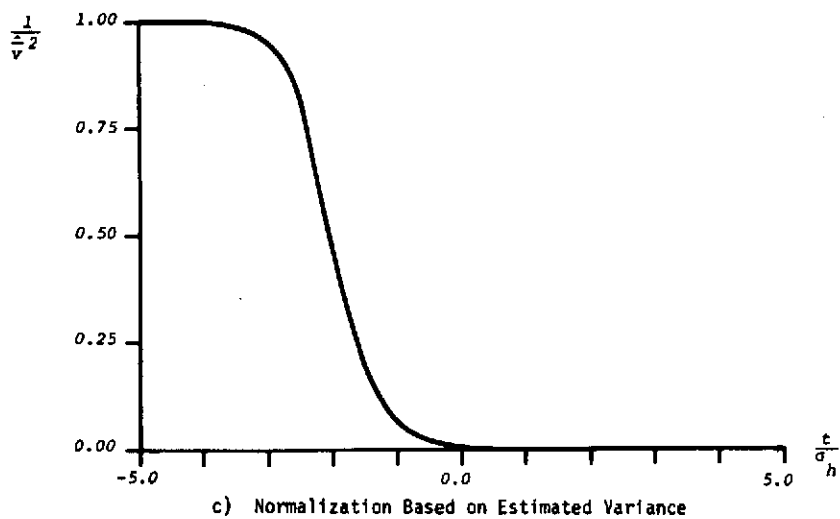
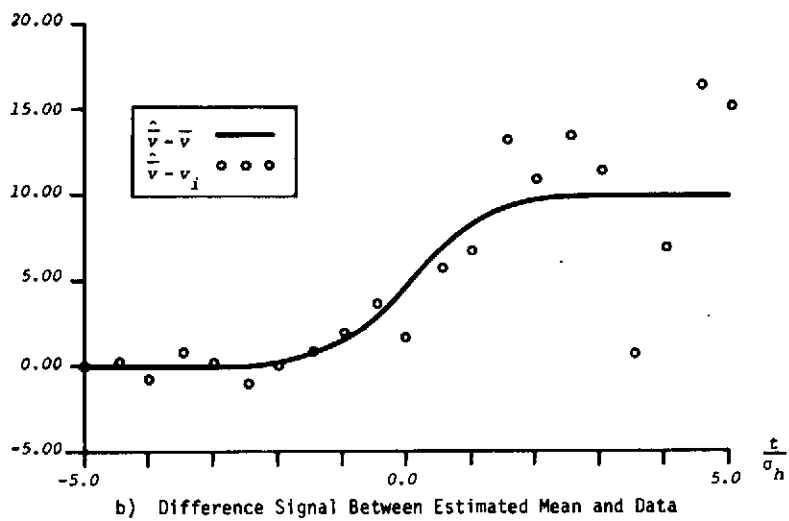
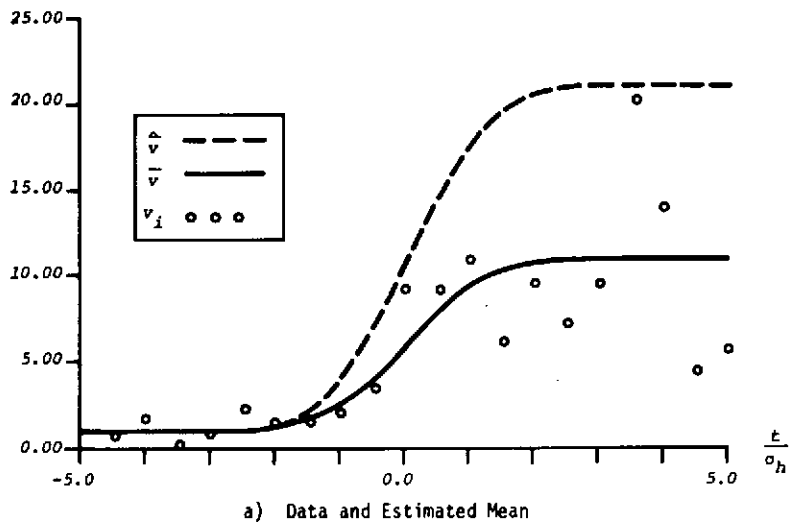


Figure 3.7 Reflectivity Error Example (Case III)

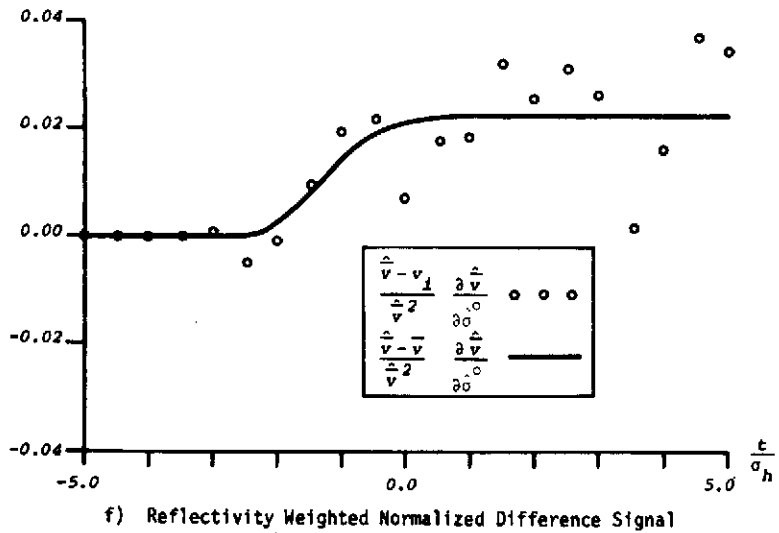
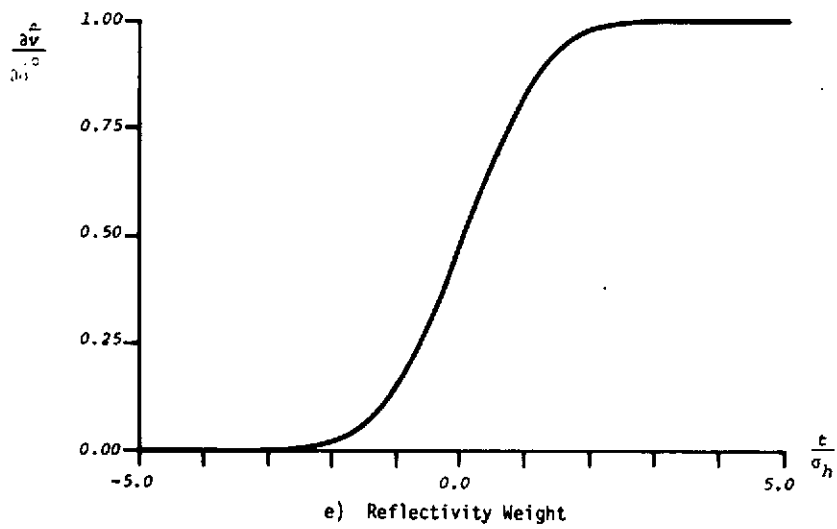
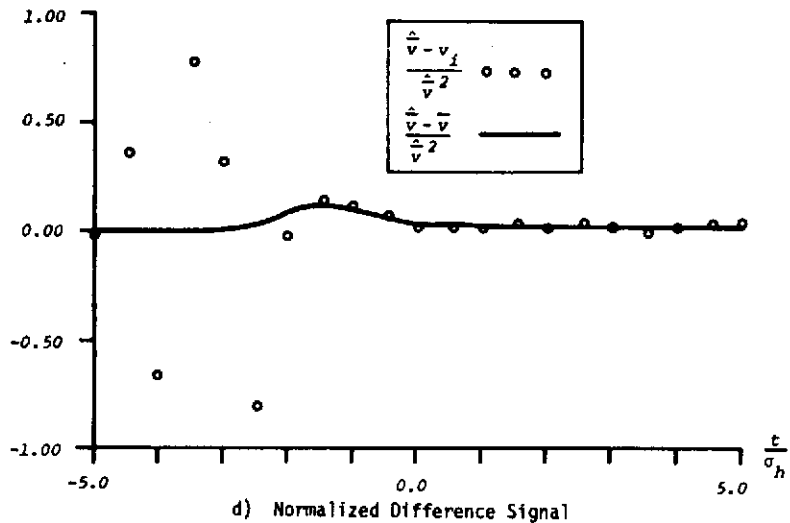


Figure 3.7 (Continued)

In summary then, it is seen that the feedback loop implementation of the MLE processor is simply a generalization of the split-gate tracker and gating technique for estimating wave height. (Actually, the gating technique for estimating wave height was developed as a simplification of the MLE wave height weighting function.) Aside from the more general weighting functions, the feedback loop implementation of the MLE also differs from the gating techniques, in that a replica (or template) is compared with the return signal, and the fluctuation of the data is then reduced by normalizing with the estimated variance. It might also be noted that if the normalization by the estimated variance is eliminated, the feedback loop implementation would be that of a MMSE processor!

### 3.2 Computer Sizing

In this section, an approximate "size" of an MLE is obtained. For this estimate, it is assumed that the processor will be implemented as a software program in a general purpose computer. The size is then determined as the total program and data storage required, plus the total compute time required during each data cycle. The results indicate that a relatively modest mini-computer is required. It is shown that the total data storage is approximately 2000 words and the total program storage is about 2000 words; thus, only about 4k memory words are required. Further, assuming a compute speed roughly equivalent to the NOVA, the total computing time per data cycle is about 28 ms. If the data is averaged for 0.1 sec (100 ms) before the MLE acquires it, then the computer will be relatively lightly loaded.

#### 3.2.1 Approach

This study was intended only as a "quick look" estimate; thus, the approach was correspondingly simple. First, a detailed block diagram of the processor was developed. This is shown as Figure 3.8. In that figure, the data is supplied to the MLE at 10 Hz. Thus for each .1 sec data cycle 62 power values are transferred into the buffer. The levels represent the integrated power for .1 sec (150 pulses) for each of the 60 range gates on the leading edge plus a noise gate and a plateau gate. The diagram to the right of the dotted line represents a detailed breakdown of the computations performed in the MLE.



The computation speed estimate was obtained from Figure 3.8 as follows:

- On a per "data cycle" basis, count the number of arithmetic operations and I/O requests indicated in the diagram.
- Using "typical" computer speeds, and the above counts, estimate the compute time per data cycle.
- Apply 25 percent increase for program housekeeping, (loop initialization, data shuffling, etc.)
- Apply 15 percent increase for the real time executive.

The above approach is obviously somewhat crude, however, to obtain better estimates, one would have to write a sample code and then count the number of operations in the code. Further, that approach would probably not yield particularly accurate estimates until it was actually run in a real-time environment. Either of these approaches are beyond the scope of this study.

The percentage increase in the running time for housekeeping and the real-time executive have not been documented. They are "engineering judgments" based on discussions with several people who have had experience in programming mini-computers in a real-time environment.

The computation of the core storage requirement was obtained from Figure 3.8 as follows:

- Data Storage  
From the block diagram, count the data storage.
- Program Storage  
For the tracking phase, identify major function blocks and estimate the number of instructions per block.  
  
Assume that the code for the acquisition phase approximately equals that for the tracking phase.  
  
Add 250 instructions for initialization.  
  
Add 200 instructions for the executive.

Again, the constants for the initialization and the executive represent "engineering judgment" rather than documented fact.

### 3.2.2 Details of the Estimates

As stated previously, it is assumed that 60 leading edge samples plus one noise gate plus one plateau gate are transferred to the MLE each data cycle. The data cycle rate is 10 Hz; thus, for a 1500 Hz PRF, the altimeter averages 150 pulses before transferring the data to the MLE.

The total number of arithmetic operations per data cycle is given in Table 3.1. To convert the totals to required computing time, it is assumed that, on the average, about five total instructions requiring approximately 10  $\mu$ sec are needed for each addition or subtraction. For multiplication and division, about eight instructions and 20  $\mu$ sec are required. These numbers assume that the registers are loaded from memory, and the results may be normalized before storage. The compute time corresponds approximately to fixed point operations on the NOVA II computer built by Data General Corporation.

Table 3.2 summarizes the total compute time per data cycle. The compute time, housekeeping, and executive have been explained previously. The I/O handling represents a pessimistic estimate. It is assumed that the computer supplies trigger information to the altimeter at the PRF, and thus must provide 150 numbers per data cycle. Further, it is assumed that for each number, the system must process an interrupt and store working registers before processing the data. This is assumed to take 30  $\mu$ sec per interrupt.

From Table 3.2, it is seen that the total compute time is estimated to be  $\approx$  28 ms. Thus, the computer would be 28 percent loaded. This seems to be an adequate margin for a computer dedicated entirely to the MLE function. Conversely, this probably represents a significant load on a time share system in which the computer would be performing additional system functions.

The data storage and program storage are detailed in Tables 3.3 and 3.4. The numbers there should be self-explanatory. The major data storage is in the tables of the wave height cumulative distribution function (CDF) and the probability density function (PDF). These tables are used to generate an estimate of the mean return,  $\bar{V}$ .

TABLE 3-1  
Speed Requirements

| FUNCTION                               | ADDS | MULTIPLIES | DIVIDES |
|--|------|------------|---------|
| Noise Integration<br>and Normalization | 1    | 1          |         |
| Plateau Normalization                  |      | 1          |         |
| Error Signal Generation                |      |            |         |
| $\bar{V}$                              | 62   | 62         |         |
| $\epsilon_o$                           | 62   | 62         | 62      |
| $\epsilon_{\tau_o}$                    | 62   | 62         |         |
| $\epsilon_{\sigma_o}$                  | 62   | 62         |         |
| $\epsilon_{\sigma_h}$                  | 62   | 124        |         |
| Loop Filters                           |      |            |         |
| $\dot{\tau}_o$                         | 2    | 3          |         |
| $\tau_o$                               | 150  |            |         |
| $\sigma_o$                             | 3    | 3          |         |
| $\sigma_h$                             | 3    | 3          |         |
| Calib. Normalization                   |      | 4          | 1       |
| Ramp Generator                         | 120  | 2          | 2       |
| Offset                                 | 150  |            |         |
| Totals                                 | 739  | 389        | 65      |

TABLE 3.2

## Compute Time Per Data Cycle

| "Typical" Computer:            |                |              |
|--------------------------------|----------------|--------------|
| Add Time                       | 5 Instructions | 10 $\mu$ sec |
| Multi/Div Time                 | 8 Instructions | 20 $\mu$ sec |
| Compute Time<br>Per Data Cycle |                | 16.5 msec    |
| Housekeeping (25%)             |                | 4.1 msec     |
| Exec. (15%)                    |                | 2.5 msec     |
| I/O Data Handling              |                | 4.5 msec     |
| Total                          |                | 27.6 msec    |

TABLE 3.3  
Data Storage Locations

|                      |       |  |
|----------------------|-------|--|
| Input Buffer         | 124   |  |
| $\tau_o$ Buffer      | 150   |  |
| Output Data          | 6     |  |
| Intermediate Storage | 20    |  |
| Loop Filters         | 9     | (Constants)                                  |
|                      | 6     | (Previous Values)                            |
| Ramp Generator       | 6     |  |
| Calibration          | 20    |  |
| CDF Table            | 600   | } at 5 cm Resolution<br>for 20 m Wave Height |
| PDF Table            | 600   |  |
|                      | < 2 k |  |

TABLE 3.4  
Program Storage

| Tracking Mode:     |                               |
|--------------------|-------------------------------|
| <u>Major Block</u> | <u>Number of Instructions</u> |
| Input Buffer       | 50                            |
| Noise Integrator   | 75                            |
| Error Signals      | 200                           |
| Loop Filters       | 225                           |
| Ramp Generator     | 50                            |
| Calibration        | 25                            |
| Total              | 625                           |
| Acquisition Mode:  | 625                           |
| Initialization     | 250                           |
| Executive          | 200                           |
| ~2 k               |                               |

The program storage estimates again were in the nature of "engineering judgments" rather than actual instruction counts. It was beyond the scope of this task to do the coding which would be required for more accurate counts. It should also be pointed out that these counts assume that all code has been generated from scratch. In particular, no manufacturer supplied standard I/O, or executive routines have been used. Such routines would usually be more general purpose than is needed, and would increase the storage requirements considerably (e.g., as much as a factor of 2 or more).

In sum, the size requirements from the first cut estimates appear to be modest, but not trivial. Approximately 4 k of memory is required, and a computing speed comparable to existing mini-computers (NOVA II) appears to be adequate with a reasonable safety margin (28 percent loaded). This is true, provided the computer is dedicated to the MLE, or performs only a few additional tasks.

### 3.3 Estimation Accuracies

The theoretical accuracies of the joint maximum likelihood estimates of epoch, wave height, and reflectivity are evaluated in this section of the report. These accuracies are given in terms of the standard deviation of the estimates due to random fluctuations only. System errors (such as clock and timing errors) as well as errors associated with the feedback loop implementation as described in Appendix A, are not included in the evaluation. The theoretical basis for the expressions used in evaluating these accuracies was originally derived in Reference (1), and is rederived and expressed in a much simpler and more useful format in Appendix A. An example showing the method of evaluation is given for each of the three estimates. A table of estimation accuracies as a function of signal-to-noise ratio and wave height is provided for each parameter estimate under typical SEASAT-A conditions.

The following typical SEASAT-A parameter values are used in each of the sample calculations:

|                       |                        |   |       |
|-----------------------|------------------------|---|-------|
| Number of Pulses      | N                      | = | 1500  |
| Range Resolution      | $\frac{c\Delta t}{2}$  | = | .5 m  |
| Data Interval         | $\frac{c T_{\max}}{2}$ | = | 23 m  |
| RMS Wave height       | $\sigma_h$             | = | 5 m   |
| Signal-to-Noise Ratio | a                      | = | 10 dB |

Here the data interval is assumed to contain half of the 60 samples on the leading edge of the return plus an additional 16 samples contained in a late gate. This results in a total of 46 independent range samples per pulse.

### 3.3.1 Epoch Example

From Appendix A the variance of the epoch estimate is

$$\sigma_{\tau_o \tau_o}^2 = [N^{-1} R(\theta)^{-1}]_{\tau_o \tau_o} \quad (3.7)$$

where

$$R(\theta)^{-1} = \alpha \beta \Delta t D^{-1} C^{-1} D^{-1} \quad (A-67)$$

$D^{-1} = \text{diag}(a, \beta^{-1}, \beta)$  is a diagonal matrix, the (i,j) element of  $C^{-1}$  is

$$C^{ij} = F_{ij} - \frac{d}{1+d F_{11}} F_{1i} F_{1j} \quad (A-66)$$

and

$$d = (\alpha \beta T_{\max} - 1) \left(\frac{a}{1+a}\right)^2 \quad (A-68)$$

Table A-I of Appendix A tabulates  $F_{ij}$  versus signal-to-noise ratio from -10 dB to 30 dB in 5 dB steps. The parameter  $\beta$  is related to RMS wave height via

$$\beta = \frac{c}{2 \sigma_h} \quad (3.8)$$

and the constant  $\alpha = .3227$  arises from fitting a linear ramp to the leading edge of the return signal in a minimum mean square sense. Also, the subscripts of Equation (A-66) are related to the parameter being estimated via:

$$\begin{aligned} 1 &\leftrightarrow a \\ 2 &\leftrightarrow \tau_o \\ 3 &\leftrightarrow \beta \end{aligned} \tag{3.9}$$

Now substituting in Equation A-68,

$$\begin{aligned} d &= \left( \frac{\alpha}{\alpha_h} \frac{c T_{\max}}{2} - 1 \right) \left( \frac{a}{a+1} \right)^2 = \left( \frac{.3227}{5} (23) - 1 \right) \left( \frac{10}{11} \right)^2 \\ &= .4003 \end{aligned}$$

From Table A-I (using 10 dB signal-to-noise ratio),

$$F_{11} = 2.42, \quad F_{12} = 3.75, \quad F_{22} = 9.82, \quad \text{and from Equation A-66}$$

$$\begin{aligned} C^{\tau_o \tau_o} &= C^{22} = F_{22} - \frac{d}{1 + d F_{11}} F_{12}^2 \\ &= 9.82 - \frac{.4003}{1 + (.4003)(2.42)} (3.75)^2 \\ &= 6.961 \end{aligned}$$

Substituting Equations A-67 into Equation 3.7 yields:

$$\sigma_{\tau_o \tau_o}^2 = (\alpha \beta \Delta t) N^{-1} \beta^{-2} C^{\tau_o \tau_o}$$

or

$$\begin{aligned} \sigma_R &= \frac{c}{2} \sigma_{\tau_o} = \sqrt{\alpha \left( \frac{c \Delta t}{2} \right) \sigma_h N^{-1} C^{\tau_o \tau_o}} \\ &= \sqrt{.3227 (.5) (5) \left( \frac{1}{1500} \right) 6.961} \\ &= .061 \text{ meters or } \boxed{6.1 \text{ cm}} \end{aligned} \tag{3.10}$$

### 3.3.2 Wave Height Example

The variance in estimating the parameter  $\beta$

$$\sigma_{\beta\beta}^2 = [N^{-1} R(\theta)^{-1}]_{\beta\beta} = (\alpha\beta \Delta t) N^{-1} \beta^2 C^{\beta\beta} \quad (3.11)$$

after substituting Equation A-67.

From Table A-I,  $F_{11} = 2.42$ ;  $F_{13} = -2.42$ ;  $F_{33} = 5.14$ ; and as in the previous example  $d = .4003$ . Thus:

$$\begin{aligned} C^{\beta\beta} &= C^{33} = F_{33} - \frac{d}{1+d} \frac{F_{13}^2}{F_{11}} \\ &= 5.14 - \frac{.4003}{1 + (.4003)(2.42)} (2.42)^2 \\ &= 3.95 \end{aligned} \quad (3.12)$$

Converting from the parameter  $\beta$  to  $\alpha_h$  and using Equation 3.11

$$\begin{aligned} \sigma_{\alpha_h} &= \frac{2}{c} \alpha_h^2 \sigma_{\beta} = \sqrt{\alpha \left(\frac{c\Delta t}{2}\right) \alpha_h N^{-1} C^{\beta\beta}} \\ &= \sqrt{\frac{.3227 (.5) (5)}{1500} (3.95)} \\ &= .046 \text{ meters or } \boxed{4.6 \text{ cm}} \end{aligned} \quad (3.13)$$

### 3.3.3 Reflectivity Example

The accuracy with which ocean reflectivity can be estimated is given in terms of the variance of the signal-to-noise ratio

$$\sigma_{aa}^2 = [N^{-1} R(\theta)^{-1}]_{aa} = (\alpha\beta \Delta t) N^{-1} a^2 C^{aa} \quad (3.14)$$

where again the substitution of Equation A-67 has been utilized for the inverse of the error correlation matrix.

From Table A-I,  $F_{11} = 2.42$ ; and  $d = .4003$ . Then:

$$\begin{aligned}
 C^{aa} = C^{11} &= F_{11} - \frac{d}{1+d F_{11}} F_{11}^2 \\
 &= 2.42 - \frac{.4003}{1 + (.4003)(2.42)} (2.42)^2 \\
 &= 1.229 \qquad (3.15)
 \end{aligned}$$

and

$$\begin{aligned}
 \sigma_{aa} &= a \sqrt{\alpha \left(\frac{c\Delta t}{2}\right) \sigma_h^{-1} N^{-1} C^{aa}} \\
 &= 10 \sqrt{\frac{.3227 (.5) (.2)}{1500} 1.229} \\
 &= \boxed{.051}
 \end{aligned}$$

Estimation accuracies versus signal-to-noise ratio and significant wave height are shown in Table 3.5 for typical SEASAT-A system parameters. An examination of the table entries shows that even at 20 meter significant wave height, the performance requirements for SEASAT-A could be achieved with a joint MLE operating at signal-to-noise ratios greater than 5 dB. This assumes that for the altitude estimate, the system errors (clock, timing, etc.) can be maintained to within 7.0 cm, and that any errors associated with the feedback loop implementation of the MLE processor do not significantly change the theoretical performance values given in Table 3.5.

#### 3.4 Range Sidelobe Bias

The biases associated with range sidelobes (due to pulse compression) that have not been included in the model for the estimated mean power return are summarized in this section of the report. The rather complex theoretical developments and evaluation of these biases are provided in Appendix A. There, it is shown that biases in estimating altitude, wave height, and signal-to-noise ratio caused by range sidelobes can be expressed in the following simple form:

TABLE 3.5  
Estimation Accuracies of a Joint MLE

SYSTEM PARAMETERS

PRF = 1500 Hz  
 Loop Bandwidth = 1 Hz  
 Resolution = .5 m  
 # Range Samples = 60  
 # Samples in Late Gate = 16

| <u>STANDARD DEVIATION IN ALTITUDE (cm)</u> |     |     |      |  |
|--|-----|-----|------|--|
| Significant Wave Height (m)                |     |     |      |  |
| S/N (dB)                                   | 5   | 10  | 20   |  |
| 0  | 5.7 | 8.4 | 13.1 |  |
| 5  | 3.2 | 4.8 | 7.8  |  |
| 10   | 2.5 | 3.7 | 6.1  |  |
| 20   | 2.1 | 3.1 | 5.3  |  |

| <u>STANDARD DEVIATION IN WAVE HEIGHT (cm)</u> |     |     |      |  |
|---|-----|-----|------|--|
| Significant Wave Height (m)                   |     |     |      |  |
| S/N (dB)                                      | 5   | 10  | 20   |  |
| 0   | 5.9 | 8.5 | 12.6 |  |
| 5   | 3.0 | 4.4 | 6.7  |  |
| 10  | 2.0 | 2.9 | 4.6  |  |
| 20  | 1.4 | 2.1 | 3.5  |  |

| <u>STANDARD DEVIATION IN SIGNAL-TO-NOISE RATIO</u><br><u>(ABSOLUTE UNITS [Not dB])</u> |      |      |      |  |
|--|------|------|------|--|
| Significant Wave Height (m)  |      |      |      |  |
| S/N (dB)   | 5    | 10   | 20   |  |
| 0  | .008 | .008 | .009 |  |
| 5  | .017 | .017 | .019 |  |
| 10   | .044 | .046 | .051 |  |
| 20   | .402 | .422 | .472 |  |

$$\begin{aligned}
\Delta R &= 880 \sigma_h \gamma_1 \\
\Delta \sigma_h &= 600 \sigma_h \gamma_1 \\
\Delta a &= 600 a \gamma_1
\end{aligned}
\tag{3.16}$$

where  $\gamma_1$  is the average RMS sidelobe level. In deriving these expressions it has been assumed that the 3 dB (one way) antenna beamwidth of the altimeter is  $5^\circ$  and the satellite altitude is 725 km. A rather surprising feature of these results is that the biases are independent of signal-to-noise ratio! Furthermore, the biases are all proportional to average RMS sidelobe level,  $\gamma_1$ . Thus, to maintain these biases at a few centimeters (or less than 1 percent) requires that  $\gamma_1$  be less than or equal to -50 dB. Since -50 dB average RMS sidelobes levels can be achieved with the newer pulse compression devices, such as the reflective array compressor (RAC), the biases due to range sidelobes should be negligible for the MLE processor.

#### 4.0 SPLIT-GATE TRACKERS

The performance of a split-gate tracker is examined in this section of the report. The variance of a split-gate tracker was derived previously in reference (1). In Section 4.1 the variance of a split-gate tracker is rederived to provide a much simpler expression for interpreting tracker accuracy. The effect of changing the gate widths and the placement of the early gate is examined. A comparison of tracker accuracies for several adaptive and nonadaptive split-gate trackers is given for typical SEASAT-A parameters.

Section 4.2 examines the altitude bias caused by range sidelobes in the pulse compression system. It is shown that receiver weighting to reduce peak sidelobes will not be necessary for SEASAT-A, since peak sidelobes as large as -10 dB only produce an altitude bias of about 1 cm. However, the far out sidelobe level must be less than -50 dB RMS in order to keep the altitude bias less than 6 cm.

Section 4.3 describes the altitude bias caused by the additive transmitter noise burst resulting from gating the TWT on prior to (and keeping it on after) transmitting the LFM signal. It is shown that this transmit noise burst produces uniform receiver range sidelobes extending over the entire sidelobe region. To maintain these sidelobes at -50 dB requires that the ratio of total transmit signal energy to total transmit noise energy be at least 17 dB.

#### 4.1 Tracker Accuracy

In this section the performance of a split-gate tracker is derived, and the effect of changing the gate widths and the placement of the early gate is examined. To keep the derivations relatively simple, a sampled system will be assumed. A split-gate tracker estimates the epoch of a signal by balancing the output of an early gate with that of a late gate. Specifically, let:

$t_i$ ,  $i = 0, \pm 1, \pm 2, \dots$  be the times at which the signal is sampled,

$V(t_i)$  be the square law detected output of the receiver at time  $t_i$ ,

$\sum_i \delta(t_i - t) h_i$  be the impulse response of the early gate,

$C \sum_i \delta(t_i - t) g_i$  be the impulse response of the late gate

and  $C$  be a constant which makes the tracker unbiased.

Note that the Kronecker delta functions arise from the assumption of a sampled system.

For any time delay,  $\tau_0$ , between the tracker estimated epoch and the true epoch, the error voltage of the split-gate tracker is given by:

$$\mathcal{E}(\tau_0) = \sum_i V(t_i - \tau_0) (h_i - Cg_i) \quad (4.1)$$

The tracker feedback loops function so that the error voltage is held at zero. Thus the tracker estimated epoch is given by the solution of:

$$\mathcal{E}(\tau_0) = 0 \quad (4.2)$$

If the loop time constants are long, and the tracking error is unbiased, then  $\tau_0$  will be nearly zero. Expanding  $\mathcal{E}(\tau_0)$  in a Taylor series about  $\tau_0 = 0$  and substituting into (4.2) yields:

$$\tau_0 \approx \frac{-\mathcal{E}(0)}{\left. \frac{\partial \mathcal{E}(\tau)}{\partial \tau} \right|_{\tau=0}} \quad (4.3)$$

Let  $E \left. \frac{\partial \mathcal{E}(\tau)}{\partial \tau} \right|_{\tau=0}$  be the mean tracking error slope. Using (4.3) one has:

$$\text{Var } \tau_0 = \frac{\text{Var } \mathcal{E}(0)}{\left( E \left. \frac{\partial \mathcal{E}(\tau)}{\partial \tau} \right|_{\tau=0} \right)^2} \quad (4.4)$$

The tracker will be unbiased if

$$E \mathcal{E}(0) = 0$$

Thus the normalizing constant in equation 4.1 is given by:

$$C = \frac{\sum \bar{V}(t_i) h_i}{\sum \bar{V}(t_i) g_i} \quad (4.5)$$

where  $\bar{V}(t_i) = E V(t_i)$  is the mean receiver power output at time  $t_i$ .

The mean error slope is given by

$$\left. \frac{\partial E \mathcal{E}(\tau)}{\partial \tau} \right|_{\tau=0} = \sum \dot{\bar{V}}(t_i) (h_i - C g_i) \quad (4.6)$$

And the variance of the tracking error signal is given by:

$$\text{Var } \mathcal{E}(0) = \sum \left( \text{Var } V(t_i) \right) (h_i - C g_i)^2 \quad (4.7)$$

where the samples are assumed to be uncorrelated. (i.e.,  $E(V_i - \bar{V}_i)(V_j - \bar{V}_j) = 0$ ,  $i \neq j$ ). For Gaussian processes (exponentially distributed power),

$$\text{Var } V(t_i) = \left( E V(t_i) \right)^2 = \bar{V}^2(t_i) \quad (4.8)$$

Thus the tracking error variance is given by combining (4.6), (4.7), (4.8) and (4.4) to yield:

$$\text{Var } \tau_0 = \frac{\sum \bar{V}^2(t_i) (h_i - C g_i)^2}{\left( \sum \dot{\bar{V}}(t_i) (h_i - C g_i) \right)^2} \quad (4.9)$$

From equation 4.9 it is seen that the tracking error variance depends on the shape of the early and late gates and on the characteristics of the mean power return,  $\bar{V}(t)$ . To simplify the evaluation of equation 4.9, the approximation sketched in Figure 4.1 is assumed.

4-4-1

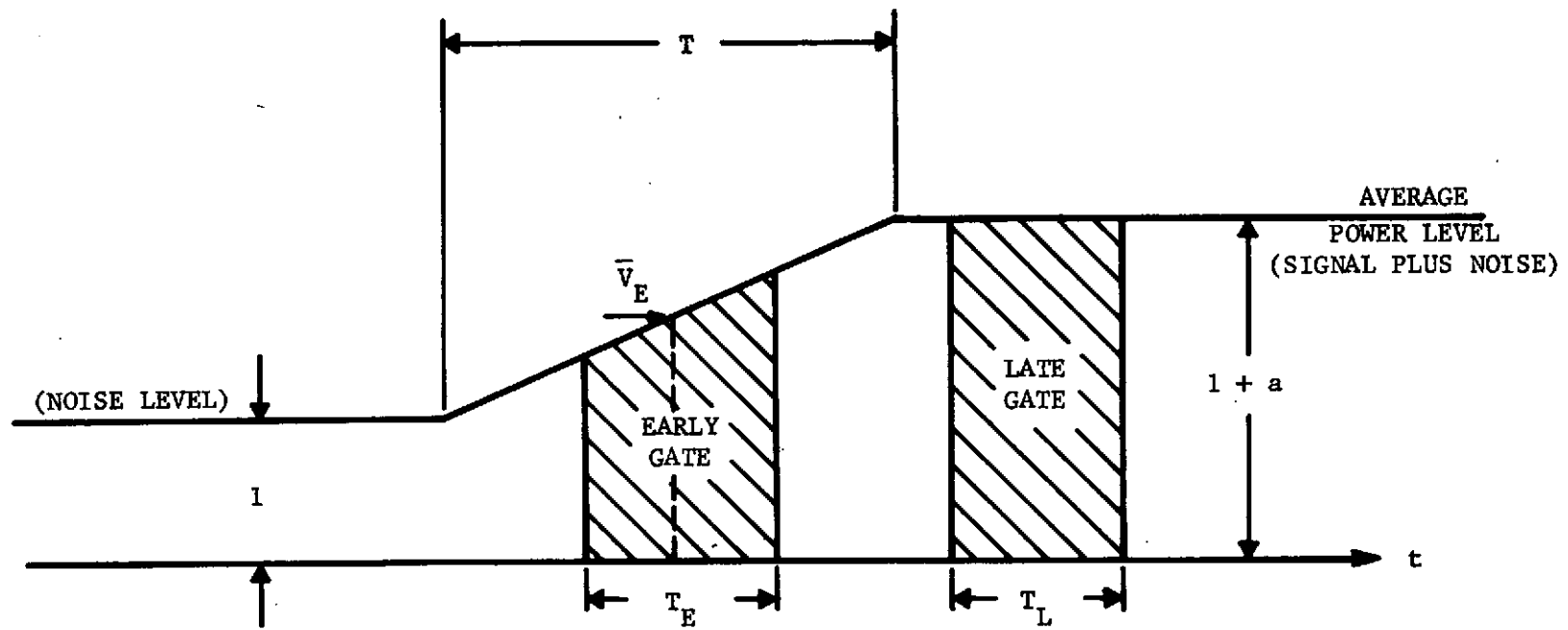


Figure 4.1 Sketch of the Average Returned Power Level and the Gate Positioning

That is, the following simplifications are made

- i) Square - non-overlapping gates are assumed.
- ii) The late gate is positioned on the plateau.
- iii) The early gate is positioned on the leading edge.
- iv) The signal return power is modeled as a linear ramp rising to a flat plateau.
- v) The receiver noise level is unity.

If the following definitions are made:

$\Delta t$  = time between independent samples

$a$  = signal-to-noise ratio

$T$  = rise time of the leading edge

$T_E$  = time duration of the early gate

$T_L$  = time duration of the **late gate**

$\bar{V}_E$  = average power return at the center of the early gate

$N_p$  = number of pulses averaged

$\beta = \frac{c}{2\sigma_h} =$  wave height parameter

$\sigma_h$  = RMS wave height

$\alpha = .3227$

the mean power return on the ramp may be expressed as

$$\bar{V}(t) = \bar{V}_E + a\alpha\beta t \quad (4.10)$$

where  $t$  is referenced to the center of the early gate and the constant  $\alpha$  has been chosen such that the ramp approximates the normal integral in a mean square sense. Thus, the mean slope of the ramp

$$\dot{\bar{V}}(t) = a\alpha\beta \quad (4.11)$$

and the term in the denominator of equation 4.9

$$\sum \dot{\bar{V}}(t_1) (h_1 - C g_1) = \sum \dot{\bar{V}}(t_1) h_1 \quad (4.12)$$

since  $\dot{\bar{V}}(t_i)$  is zero on the plateau. But using equation 4.11 and approximating the sum by an integral:

$$\begin{aligned} \sum \dot{\bar{V}}(t_i) h_i &= \frac{1}{\Delta t} \int_{-\frac{T_E}{2}}^{\frac{T_E}{2}} a\alpha\beta dt \\ &= a\alpha\beta \frac{T_E}{\Delta t} \end{aligned} \quad (4.13)$$

Similarly, the numerator of equation 4.9 is given by,

$$\sum \bar{V}^2(t_i) (h_i - C g_i)^2 = \sum \bar{V}^2(t_i) h_i^2 + \sum \bar{V}^2(t_i) C^2 g_i^2 \quad (4.14)$$

since the gates are non-overlapping. Then substituting equation 4.10 and approximating by an integral yields:

$$\begin{aligned} \sum \bar{V}^2(t_i) h_i^2 &\approx \frac{1}{\Delta t} \int_{-\frac{T_E}{2}}^{\frac{T_E}{2}} (\bar{V}_E + a\alpha\beta t)^2 dt \\ &= \frac{1}{\Delta t} \left( \bar{V}_E^2 T_E + (a\alpha\beta)^2 \frac{T_E^3}{12} \right) \end{aligned} \quad (4.15)$$

and since the return is constant on the plateau

$$\sum \bar{V}^2(t_i) C^2 g_i^2 = \frac{1}{\Delta t} (1+a)^2 C^2 T_L \quad (4.16)$$

Finally, the normalizing constant given by equation 4.5

$$\begin{aligned} C &= \frac{\sum \bar{V}(t_i) h_i}{\sum \bar{V}(t_i) g_i} = \frac{\int_{-\frac{T_E}{2}}^{\frac{T_E}{2}} (\bar{V}_E + a\alpha\beta t) dt}{(1+a) T_L} \\ &= \frac{\bar{V}_E T_E}{(1+a) T_L} \end{aligned} \quad (4.17)$$

Substituting the expressions given by equations 4.13 through 4.17 in equation 4.9 provides an expression for the tracking error variance on a per pulse basis

$$\sigma_{\tau_o}^2 = \frac{\bar{V}_E^2}{(\alpha\beta)^2} \Delta t \left( \frac{1}{T_E} + \frac{1}{T_L} \right) + \frac{T_E \Delta t}{12} \quad (4.18)$$

If the split-gate tracks the kth power point,

$$\bar{V}_E = 1+ka \quad (4.19)$$

and if  $N_p$  pulses are averaged in the tracking loop

$$\sigma_{\tau_o}^2 = \frac{1}{N_p} \left[ \frac{(k+\frac{1}{a})^2}{(\alpha\beta)^2} \left( \frac{\Delta t}{T_E} + \frac{\Delta t}{T_L} \right) + \frac{T_E \Delta t}{12} \right] \quad (4.20)$$

Finally, converting from delay to range, the RMS altitude error (in meters)

$$\sigma_R = \frac{1}{\sqrt{N_p}} \left[ \frac{\sigma_h^2}{\alpha^2} (k+\frac{1}{a})^2 \left( \frac{\Delta t}{T_E} + \frac{\Delta t}{T_L} \right) + \frac{T_E \Delta t}{12} \right]^{\frac{1}{2}} \quad (4.21)$$

where  $\Delta t$  can now be interpreted as a range resolution cell (since the samples are assumed to be independent) and  $T_E$  and  $T_L$  the range extent of the early and late gates, respectively.

An examination of equation 4.21 reveals the following characteristics associated with the RMS altitude error of a split-gate tracker. The error increases linearly with RMS wave height  $\sigma_h$ . It decreases as the number of resolution cells in the early and late gate increases and as the tracking point k is made smaller.

Thus, for a non-adaptive split-gate tracker (a tracker with fixed early and late gates), the quarter power tracker,  $k=.25$ , performs better than the half power tracker ( $k=.5$ ) as shown in Figure 4.2. In this case, the maximum width of the early gate is limited by the smallest RMS wave height to be encountered. Thus under smooth sea conditions, the early gate can only be made one resolution cell wide. Furthermore, with a one resolution cell

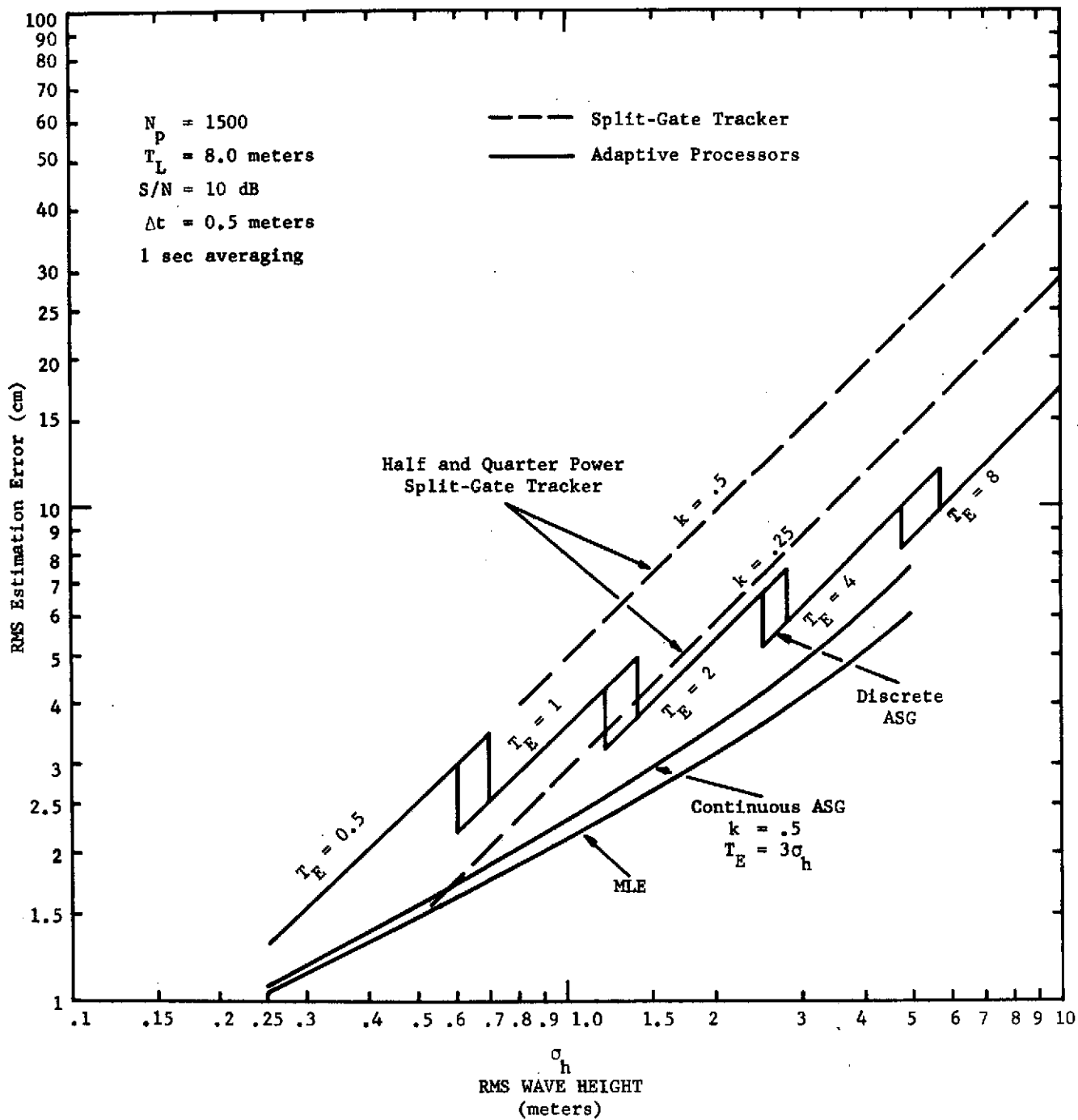


Figure 4.2 Comparison of Tracking Accuracies of Split-Gate Trackers and Adaptive Processors

early gate, little is to be gained by marking the late gate much wider than 16 resolution cells. That is, increasing the late gate from 16 to an infinite number of resolution cells only reduces  $\sigma_R$  by 3%.

Improved tracking performance can, however, be achieved with an adapting split-gate tracker. This is accomplished by estimating the RMS wave height and increasing the width of the early gate as the estimated wave height increases. The early gate width can be increased in discrete steps as suggested by MacArthur (2) or continuously as illustrated in Figure 4.2. The performance comparison of the split-gate trackers given in Figure 4.2 was based on typical SEASAT-A system parameters. The MLE performance is included in the figure to indicate the ultimate improvement achievable with an optimum tracker.

#### 4.2 Range Sidelobe Bias

In a pulse compression system, the major effect of amplitude and phase errors is to increase the level of the range sidelobes of the system. These sidelobes in general do not significantly affect the altitude tracker variance, or the accuracy of estimating wave height. They do, however, cause bias errors in the altimeter. In this section, an approximate expression is derived for the bias errors due to range sidelobes. The expression is then evaluated for typical SEASAT-A parameters. It is shown that peak sidelobes as large as -10 dB only produce an altitude bias of about 1 cm, thus receiver weighting to reduce the peak sidelobes will not be necessary for SEASAT-A. It is also shown, however, that the average far out sidelobe level must be less than -50 dB RMS in order to keep the altitude bias less than 6.0 cm.

##### 4.2.1 Theoretical Development

The mean power versus time output from an altimeter can be written as:

$$\bar{V}(\tau) = \int_{-\infty}^{\infty} \sigma(t) |\rho(\tau-t)|^2 dt \quad (4.22)$$

where

$\sigma(t)$  is the distribution of target cross-section with time (i.e., sea surface impulse response)

$\rho(\tau)$  is the normalized radar system point target response

and  $\bar{V}(\tau)$  is the mean power output.

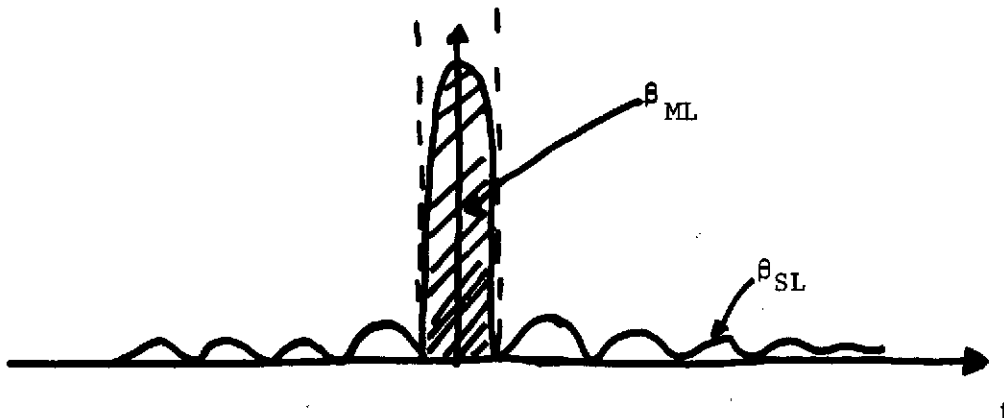
The standard split-gate tracker adjusts the epoch so that the early gate output exactly balances one-half the late gate output.

Thus, the tracker finds  $t_0$  such that

$$\bar{V}(t_0) = \frac{1}{2} \bar{V}(t_0 + \Delta) \quad (4.23)$$

where  $\Delta$  is the separation between the early and late gate.

Now, for typical pulse compression systems, the point target response consists of a narrow main lobe response plus extended sidelobes as sketched below:



Thus we may decompose the response function  $|\rho(t)|^2$  as

$$|\rho(t)|^2 = \beta_{ML}(t) + \beta_{SL}(t) \quad (4.24)$$

The mean power output is given by:

$$\begin{aligned} \bar{V}(\tau) = & \int_{-\infty}^{\infty} \sigma(t) \beta_{ML}(\tau-t) dt \\ & + \int_{-\infty}^{\infty} \sigma(t) \beta_{SL}(\tau-t) dt \end{aligned} \quad (4.25)$$

As long as the wave height is large compared to the system range resolution,  $\beta_{ML}(t)$  acts as essentially a delta function, thus

$$\bar{V}(\tau) \approx \tau_c \sigma(\tau) + \bar{V}_{SL}(\tau) \quad (4.26)$$

where

$\tau_c$  is the compressed pulse width and  
 $\bar{V}_{SL}(\tau)$  is the distortion in the response due to the presence of the sidelobes.

That is,

$$\bar{V}_{SL}(\tau) = \int_{-\infty}^{\infty} \sigma(t) \beta_{SL}(\tau-t) dt \quad (4.27)$$

From (4.26) and (4.23) we have at the estimated epoch:

$$\tau_c \sigma(t_o) + \bar{V}_{SL}(t_o) = \frac{1}{2} \left[ \tau_c \sigma(t_o + \Delta) + \bar{V}_{SL}(t_o + \Delta) \right] \quad (4.28)$$

Now for small bias errors,

$$\sigma(t_o) \approx \sigma(0) + \delta(0)t_o \quad (4.29)$$

and

$$\sigma(t_0 + \Delta) = \sigma(\Delta) + \dot{\sigma}(\Delta)t_0 \quad (4.30)$$

Where we assume the true epoch is  $t_0 = 0$ . Further, at the true epoch,

$$\sigma(0) = \frac{1}{2} \sigma(\Delta) \quad (4.31)$$

Applying (4.29), (4.30), and (4.31) to (4.28) yields:

$$t_0 \left[ \tau_c (\dot{\sigma}(0) - \frac{1}{2} \dot{\sigma}(\Delta)) \right] = \frac{1}{2} \bar{v}_{SL}(t_0 + \Delta) - \bar{v}_{SL}(t_0) \quad (4.32)$$

Now, in general,  $\bar{v}_{SL}$  is a slowly varying function, and we may write approximately:

$$\bar{v}_{SL}(t_0) \approx \bar{v}_{SL}(0) \quad (4.33)$$

and

$$\bar{v}_{SL}(t_0 + \Delta) \approx \bar{v}_{SL}(\Delta) \quad (4.34)$$

So that finally, the bias is given by:

$$t_0 = \frac{\frac{1}{2} \bar{v}_{SL}(\Delta) - \bar{v}_{SL}(0)}{\tau_c [\dot{\sigma}(0) - \frac{1}{2} \dot{\sigma}(\Delta)]} \quad (4.35)$$

We assume an impulse response corresponding to a pencil beam antenna as given by Barrick (3). That is:

$$\sigma(t) = \frac{1}{2} \left[ \phi(t/t_h) + \phi((t_I + t)/t_h) \right] \quad (4.36)$$

Where

$$\phi(LCX) = \frac{1}{\sqrt{2\pi}} \int_{-\infty}^{LCX} e^{-\frac{1}{2}t^2} dt$$

is the normal integral, and

$$t_h = \frac{2\sigma_h}{c}$$

is the (one sigma) pulse stretching due wave height  $\sigma_h$ , and

$$t_I = .125 \left( H(1+H/a)\psi_B^2 \right)$$

is the duration of the impulse response for beam width  $\psi_B$  and altitude H, where "a" is the earth radius.

In general,  $t_I \gg t_h$ , so that we may write

$$\dot{\sigma}(t) = \frac{1}{\sqrt{2\pi} t_h} e^{-\frac{1}{2}(t/t_h)^2} \quad (4.37)$$

And, the bias is given by

$$\frac{t_o}{t_h} = \frac{\sqrt{2\pi}}{\tau_c} \left( \frac{1}{2} \bar{V}_{SL}(\Delta) - \bar{V}_{SL}(0) \right) \quad (4.38)$$

where we have assumed  $\Delta \geq 3t_h$ .

#### 4.2.2 Evaluation of the Bias

To evaluate (4.38), we will assume that the sidelobes consist of a decaying term plus a uniform level term. The decaying term follows a power law, thus:

$$\beta_{SL}(t) = \gamma_o \left( \frac{1.5 \tau_c}{t} \right)^n + \gamma_1 \quad \tau_c < |t| \leq T_u \quad (4.39)$$

where  $\tau_c$  is the compressed pulse width

and  $T_u$  is the uncompressed pulse width

$\gamma_o$  is the (nominal) height of the first sidelobe

$\gamma_1$  is the "far-out" sidelobe level  
 $n$  is assumed to be even since it is the decay law  
for the power sidelobes.

For simplicity, we assume the uncompressed pulse length,  $T_u \gg t_h$ , so that the error function becomes essentially a step function when compared to the sidelobe envelope, thus the impulse response is approximately a pulse of duration  $t_I$ .

Substituting (4.36) and (4.39) into (4.27) and making the above approximation yields:

$$\bar{V}_{SL}(\tau) = \gamma_0 (1.5)^n \int_{\tau_c}^{\tau} \left(\frac{\tau_c}{t}\right)^n dt + \int_{\tau_c}^{t_I - \tau} \left(\frac{\tau_c}{t}\right)^n dt + \frac{\gamma_1 t_I}{\tau_c}$$

$$\frac{\bar{V}_{SL}(\tau)}{\tau_c} = \frac{\gamma_0 (1.5)^n}{n-1} \left[ 1 - \left(\frac{\tau_c}{\tau}\right)^{n-1} + \left(\frac{\tau_c}{t_I - \tau}\right)^{n-1} \right] + \frac{\gamma_1 t_I}{\tau_c} \quad (4.40)$$

Where for simplicity we have assumed that  $T_u > t_I$  and note that the term  $\left(\frac{\tau_c}{\tau}\right)^{n-1}$  is zero when  $\tau = 0$ .

Substituting (4.40) into (4.38) yields:

$$\frac{t_o}{t_h} = \sqrt{2\pi} \frac{\gamma_0 (1.5)^n}{(n-1)} \left[ -\frac{1}{2} \left[ \left(\frac{\tau_c}{\Delta}\right)^{n-1} + \left(\frac{\tau_c}{t_I - \Delta}\right)^{n-1} \right] + \left(\frac{\tau_c}{t_I}\right)^{n-1} \right]$$

$$- \sqrt{2\pi} \frac{\gamma_1}{2} \frac{t_I}{\tau_c}$$

Thus the total error is the sum of the error due to the decaying sidelobes, and the error due to the uniform sidelobes.

In most cases of interest,  $t_I > 50 \tau_c$ , so that we may neglect terms of order  $\tau_c/t_I$ . Secondly, for purposes of specifying a sidelobe budget, we will assume an upper bound roll-off  $n = 2$ . Thus,

$$\frac{t_o}{t_h} \approx -\sqrt{\frac{\pi}{2}} \left( (1.5)^2 \gamma_o \frac{\tau_c}{\Delta} + \gamma_1 \frac{t_I}{\tau_c} \right) \quad (4.42)$$

Table 4.1 gives the altitude bias due to the close-in sidelobes versus peak sidelobe for typical SEASAT-A parameters. Table 4.2 gives bias due to the far-out sidelobes.

Table 4.1

Bias in Centimeters Due to Close-In Sidelobes

$$t_I/\tau_c = 1000, \quad \Delta/\tau_c = 44$$

| Peak Sidelobe<br>( $2 \gamma_o$ ) | Wave-Height                |                            |
|-----------------------------------|----------------------------|----------------------------|
|                                   | $\sigma_h = .25 \text{ m}$ | $\sigma_h = 5.0 \text{ m}$ |
| -10 (dB)                          | .07 (cm)                   | 1.52 (cm)                  |
| -12                               | .04                        | .97                        |
| -14                               | .03                        | .60                        |
| -16                               | .02                        | .38                        |
| -18                               | .012                       | .24                        |
| -20                               | .008                       | .15                        |

Table 4.2

Bias in Centimeters Due to Far-Out Sidelobes

$$t_I/\tau_c = 1000, \quad \Delta/\tau_c = 44$$

| Average<br>Sidelobe Level | Wave-Height                |                            |
|---------------------------|----------------------------|----------------------------|
|                           | $\sigma_h = .25 \text{ m}$ | $\sigma_h = 5.0 \text{ m}$ |
| -30 (dB)                  | 32.0 (cm)                  | 632 (cm)                   |
| -35                       | 10.0                       | 194                        |
| -40                       | 3.2                        | 64                         |
| -45                       | 1.0                        | 20                         |
| -50                       | .3                         | 6                          |

### 4.3 Transmitter Noise Bias

In the recommended SEASAT-A system, the TWT must be turned on prior to (and kept on after) transmitting the LFM waveform, so that the transient response of the TWT is not superimposed on the desired signal. This results in a burst of noise being transmitted before and after the signal. This degrades the sidelobe response of the receiver as shown in Figure 4.3. To maintain these far out receiver sidelobes at -50 dB (altitude bias less than 6 cm) requires that the ratio of total transmit signal energy to total transmit noise energy be at least 17 dB.

#### 4.3.1 Analysis

Let  $S(t)$  be the desired transmit signal, and  $\eta_T(t)$  be a noise burst on transmit. In general  $\eta_T(t)$  will have a time varying power level as sketched below.



Thus the transmitted signal may be represented by:

$$Z_T(t) = S(t) + \eta(t) \quad (4.43)$$

Let  $\rho(\tau)$  be the target (distributed) reflection coefficient at range  $c\tau/2$ . Then the received signal may be represented by:

$$Z_R(t) = \int_{\tau} \rho(\tau) Z_T(t-\tau) d\tau \quad (4.44)$$

If the receiver is not matched, but has receiver characteristic  $w(u)$ , then the (complex) amplitude of the receiver output at time  $t$  is given by

$$X(t) = \int w^*(u) Z_R(t+u) du \quad (4.45)$$

Substituting (4.43) and (4.44) into (4.45) yields.

$$X(t) = \int \rho(\tau) \chi_{sw}(t-\tau) d\tau + \int \rho(\tau) N(t-\tau) d\tau \quad (4.46)$$

where  $\chi_{sw}(\tau)$  is the cross ambiguity function given by (zero doppler):

$$\chi_{sw}(t) = \int w^*(u) S(t+u) du \quad (4.47)$$

and  $N(t)$  is the noise process which results from passing  $\eta(t)$  through the receiver. Thus

$$N(t) = \int w^*(u) \eta(t+u) du \quad (4.48)$$

The mean receiver output is then given by:

$$\begin{aligned} P_R(t) &= E X^*(t)X(t) \\ &= \int \sigma(\tau) \left\{ |\chi_{sw}(t-\tau)|^2 + E|N(t-\tau)|^2 \right\} d\tau \end{aligned} \quad (4.49)$$

where  $\sigma(\tau) = E\rho(\tau)\rho^*(\tau)$  is the mean cross-section of the target with range.

If the noise pulse is time-varying white, we may write

$$E\left(\eta(t_1)\eta^*(t_2)\right) = P_N(t_1) \frac{\text{Sin } \pi B_N(t_1-t_2)}{\pi B_N(t_1-t_2)} \quad (4.50)$$

where  $P_N(t)$  is the noise power at time  $t_1$ .

Thus

$$\begin{aligned} E|N(t)|^2 &= \int_{u_1} \int_{u_2} w^*(u_1)w(u_2)E\eta(t+u_1)\eta^*(t+u_2)du_1du_2 \\ &= \int_{u_1} \int_{u_2} P_N(t+u_1) \frac{\text{Sin } \pi B_N(u_1-u_2)}{\pi B_N(u_1-u_2)} w^*(u_1)w(u_2)du_1du_2 \\ &\approx \int \frac{P_N(t+u)}{B_N} |w(u)|^2 du \\ &= \int N_o(t+u) |w(u)|^2 du \end{aligned} \quad (4.51)$$

where  $N_o$  is the power spectral density.

Substituting (4.51) into (4.49) yields

$$P_R(t) = \int \sigma(\tau) \left[ |\chi_{sw}(t-\tau)|^2 + \int_u N_o(t-\tau+u) |w(u)|^2 du \right] d\tau \quad (4.52)$$

Thus the effect of the noise burst is to additively distort the idealized ambiguity function by the term:

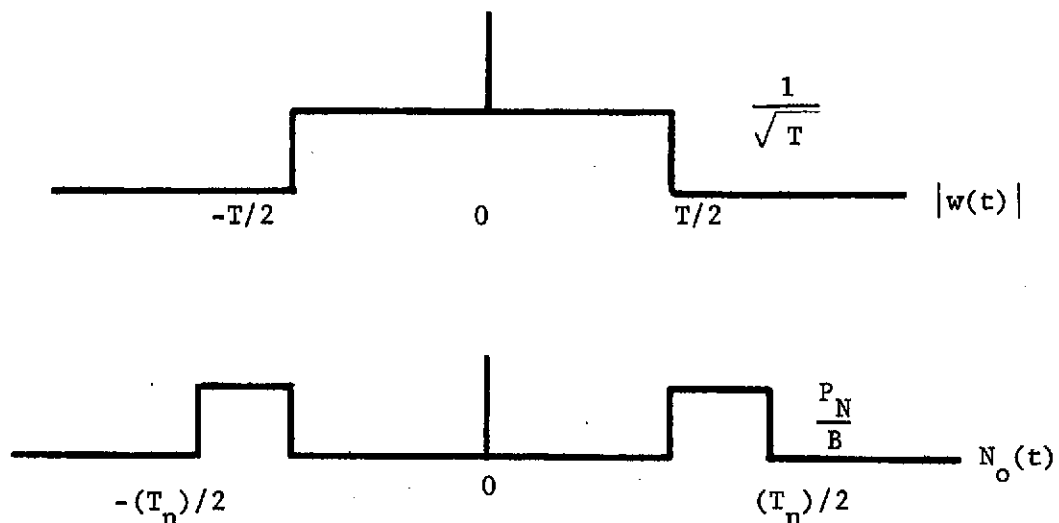
$$D(t) = \int N_o(t+u) |w(u)|^2 du \quad (4.53)$$

Let  $P_N(t)$  be the noise power (in the signal band) at time  $t$ , (relative to the signal). Then  $N_o(t) = P_N(t)/B$  where  $B$  is the signal bandwidth. Thus

$$D(t) = \frac{1}{B} \int P_N(t+u) |w(u)|^2 du \quad (4.54)$$

#### 4.3.2 Approximate Evaluation

To evaluate (4.54) approximately, we assume that the noise burst is completely suppressed by the signal, when the signal is present. Further, we assume the envelope of the noise burst is square, and we assume that the receiver weight is uniform. Thus, the situation is as sketched below:



For these assumptions, the distortion is given by

$$\begin{aligned}
 D(t) &= t \frac{P_N}{BT} & |t| < \Delta T/2 \\
 &= \frac{\Delta T}{2} \frac{P_N}{BT} & \Delta T/2 < |t| < T/2 \\
 &= (T_n/2 - t) \frac{P_N}{BT} & T/2 \leq |t| < T_n/2 \quad (4.55)
 \end{aligned}$$

where  $\Delta T = T_n - T$

Referenced to the signal, the distortion term results in the more or less uniform sidelobe structure shown below:

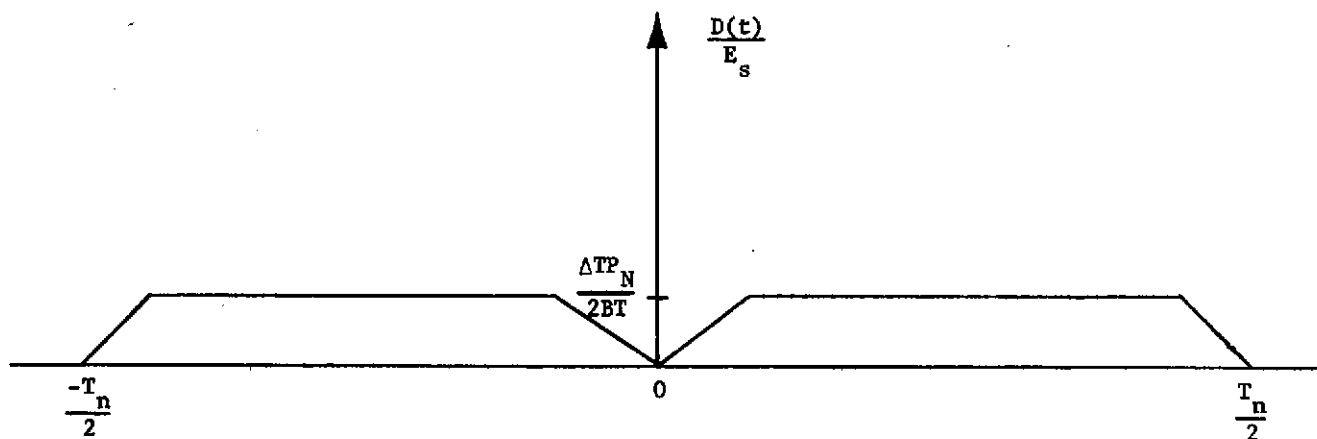


Figure 4.3

Receiver Sidelobes Resulting From Transmit Noise Burst

Then the maximum sidelobes

$$SL = \frac{E_N}{2E_s BT} \quad (4.56)$$

where

$E_N$  = total noise energy

$E_s$  = total signal energy

As was shown in Section 4.2, far out sidelobes should be kept at less than -50 dB to maintain an altitude bias of less than 6 cm at large RMS wave heights. Since for the recommended SEASAT-A system  $2BT \approx 2000$ , to achieve a -50 dB sidelobe (from equation 4.56) requires that

$$\frac{E_s}{E_N} > 17 \text{ dB} \quad (4.57)$$

While this requirement should not be difficult to achieve in practice, it does point out the fact that care should be taken to minimize the time the TWT is gated on prior to (and left on after) transmitting the LFM signal.

## 5.0 ALTIMETER POWER RETURN

In this section, the radar equation for a distributed target is derived and applied to the particular case of a satellite altimeter. The target is modeled as a continuous distribution of independent scattering points distributed in the three dimensions ( $\tau$ ,  $\nu$ ,  $u$ ). Here,  $\tau$  is range delay,  $\nu$  is the Doppler shift, and  $u$  is the sine of the angle to the scattering point measured from the antenna boresight. Since the scattering points are assumed to be incoherent, the total power is simply the integral over delay, Doppler shift, and angle of the differential power received from each point. Although the altimeter equation has been derived more rigorously elsewhere (e.g., Barrick (3),(4) or Harger (7)), this derivation is included for completeness, and to define the notation used to obtain an approximate, closed-form solution for the shape of the mean power return.

### 5.1 Theoretical Development

From the theory of high resolution radar (e.g., Rihaczek (8) or Deley (9)), the power received from a mis-matched filter can be written in terms of the cross-ambiguity function. That is, let the received narrow-band signal be represented as:

$$S_r(t) = \sqrt{2E_r} g(t-\tau) \exp[j2\pi(f_o - \nu)(t-\tau)] \quad (5.1)$$

where  $\tau$  is the round-trip delay to the scatterer,  
 $\nu$  is the Doppler shift produced by the scatterer,  
 $f_o$  is the carrier frequency,  
 $g(t)$  is the complex modulation impressed on the carrier,  
and  $E_r$  is the received signal energy.

If the receiver is matched to a complex modulation  $w(t)$ , a Doppler frequency  $\phi$ , and a delay,  $\tau$ , then the video power out of the filter at time  $t$  is given by:

$$\bar{V}(t) = \frac{1}{2} E_r G_o B |\chi_{gw}(t-\tau, \phi-\nu)|^2 \quad (5.2)$$

where  $|\chi_{gw}|^2$  is the normalized cross-ambiguity function defined by:

$$\chi_{gw}(\tau, \nu) = \int_{-\infty}^{\infty} g(\xi) w^*(\xi+\tau) \exp[-j2\pi\nu\xi] d\xi \quad (5.3)$$

and

$$G_o B = \int |G(f)|^2 df = \int |g(t)|^2 dt$$

is the product of receiver gain, times its noise bandwidth. Note that  $\chi_{gw}$  has been normalized so that

$$|\chi_{gw}|^2 \leq 1$$

If the scattering point has differential cross-section,  $d\sigma$ , and is located at angular position  $u$  (in sine theta space), then the signal energy can be computed from the standard radar equation (Skolnik (10)). That is:

$$E_r = \frac{E_T GA(u)}{4\pi R^2} \frac{d\sigma}{4\pi R^2} \frac{\lambda^2 GA(u)}{4\pi} L \quad (5.4)$$

where  $E_T$  is the transmitted energy,  
 $G$  is the peak antenna gain,  
 $A(u)$  is the one way loss factor when the target is not on boresight,  
 $R$   $c\tau/2$  is the range to the scatterer,  
 $\lambda$  is the R.F. wave length  
 $d\sigma$  is the differential cross-section at the scattering point, and is generally a function of all three parameters ( $\tau, \nu, u$ ),  
 and  $L$  is the total system losses (except for processing mis-match which is included in the cross-ambiguity function).

Combining Equations (5.2) and (5.4), gives the differential power received from a scattering point located at  $(\tau, \nu, u)$ :

$$d\bar{V}(t) = \frac{(\frac{1}{2}E_T) G^2 \lambda^2 L G_o B}{(4\pi)^3} \frac{A^2(u)}{R^4} | \chi_{gw}(t-\tau, \phi-\nu) |^2 d\sigma(\tau, \nu, u) \quad (5.5)$$

Integrating this equation over the three variables, and adding the receiver noise, yields the total average video power for a distributed target:

$$\bar{V}(t) = \frac{\frac{1}{2}E_T G^2 \lambda^2 L G_o B}{(4\pi)^3} \int_{u=0}^1 \int_{\nu=-\infty}^{\infty} \int_{\tau=-\infty}^{\infty} \frac{A^2(u)}{R^4} | \chi_{gw}(t-\tau, \phi-\nu) |^2 d\sigma(\tau, \nu, u) \quad (5.6)$$

$$+ \frac{1}{2}kT_o F_N G_o B$$

where  $k$  is Boltzman's Constant,  
 $T_o$  is the reference temperature,  
and  $F_N$  is the receiver noise figure.

Equation (5.6) is a fairly general representation of the power received from a distributed target. To apply it to the satellite altimeter, one must now compute an expression for the differential cross-section  $d\sigma(\tau, \nu, u)$  which is appropriate to the altimeter. The geometry being considered is shown in Figure 5.1.

Consider a scattering point located at height,  $h$ , above the mean sea surface. Then, if  $\sigma^o(\theta)$  is the mean cross-section per unit surface area (at angle  $\theta$  relative to radar) and if  $p_h(h/\sigma_n)$  is the probability density function of the distribution of scatterers with height, (scaled to RMS wave height  $\sigma_h$ ) then the differential cross-section at that point is:

$$d\sigma = \sigma^o(\theta) p_h(h/\sigma_h) dV \quad (5.7)$$

where  $dV$  is the differential volume at the point of interest. Now, in the spherical coordinate system  $(R, \theta, \psi)$  located at the satellite, the differential element of volume is:

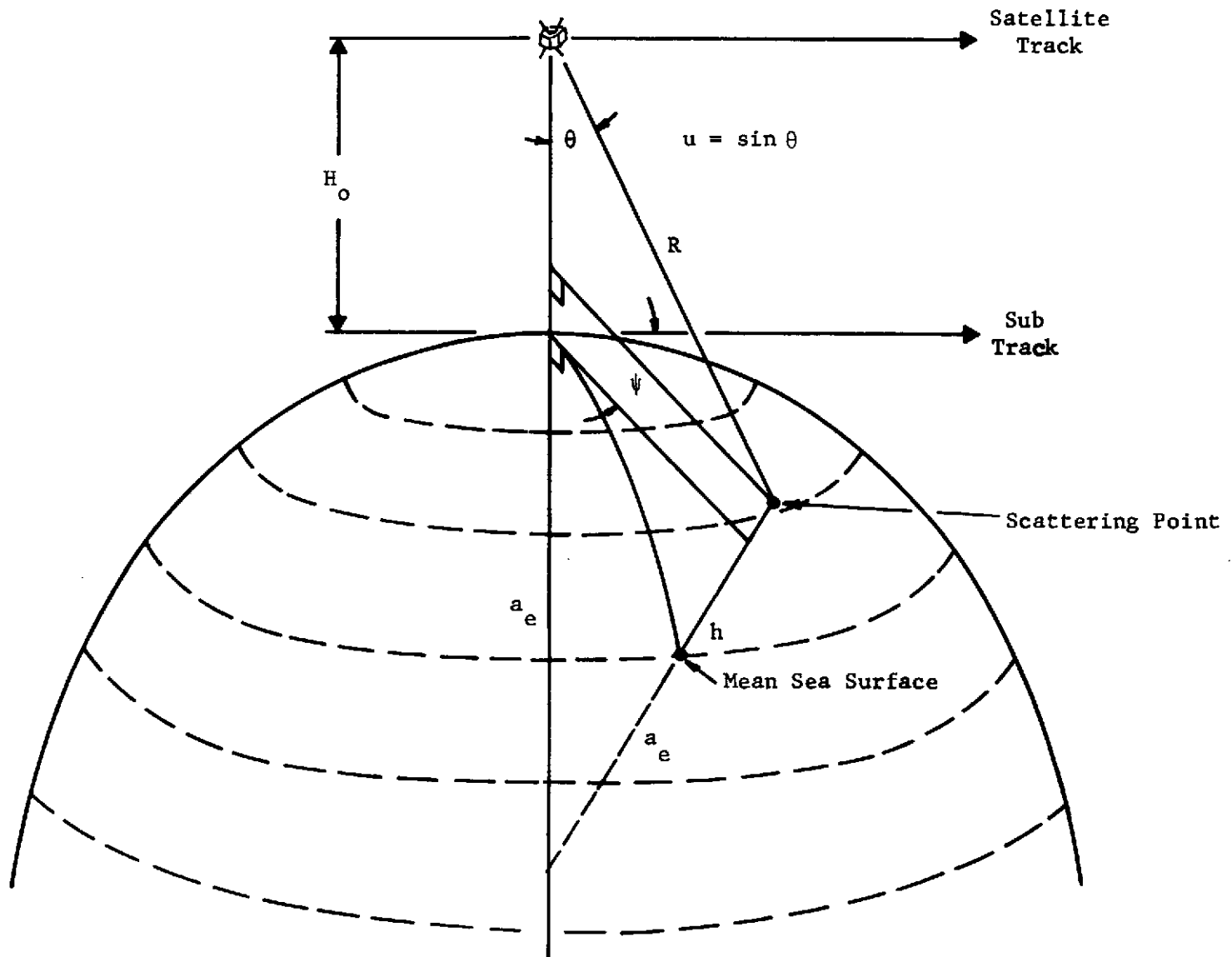


Figure 5.1 Geometry for Computing Mean Power Return

$$\begin{aligned}
 dV &= dR (Rd\theta) (R \sin \theta d\psi) \\
 &= R^2 \sin \theta dR d\theta d\psi
 \end{aligned}
 \tag{5.8}$$

The final step, then is to compute  $\tau$ ,  $v$ ,  $u$  and  $h$  in terms of  $R$ ,  $\theta$  and  $\psi$ , substitute the results into Equation (5.6) and then substitute Equation (5.8) into Equation (5.6) to obtain the final expression. But from Figure 5.1, it is seen that

$$\begin{aligned}
 \tau &= \frac{2R}{c} \\
 v &= \frac{2V}{\lambda} \sin \theta \cos \psi \\
 u &= \sin \theta
 \end{aligned}
 \tag{5.9}$$

and

$$h = \left( (H_o - R \cos \theta + a_e)^2 + R^2 \sin^2 \theta \right)^{\frac{1}{2}} - a_e
 \tag{5.10}$$

where  $V$  is the satellite velocity,  
 $H_o$  is the satellite altitude,  
and  $a_e$  is the radius of the earth.

Before making the indicated substitutions, the equations will be simplified by making some approximations. That is, it is assumed that the beam width of the altimeter is narrow (less than  $5^\circ$ ) so that small angle, and related consistent approximations can be made. Thus, it is assumed that:

$$\begin{aligned}
 u &= \sin \theta \ll 1, \\
 R &= H_o + \Delta R, \\
 \Delta R &\ll H_o \\
 \Delta R &\ll a_e
 \end{aligned}
 \tag{5.11}$$

With these approximations, one can write:

$$\tau = \frac{2H_o}{c} + \frac{2\Delta R}{c} = \tau_o + \frac{2\Delta R}{c}$$

$$h \approx -\Delta R + \frac{H_o \theta^2}{2} \left(1 + \frac{H_o}{a_e}\right) \quad (5.12)$$

$$d\sigma \approx \sigma^o(\theta) P_h (h/\sigma_h) H_o^2 \theta d\Delta R d\theta d\psi$$

and

$$v \approx \frac{2V\theta}{\lambda} \cos \psi$$

Thus, the average video power can be written finally as:

$$V(t) = \frac{\frac{1}{2} E_T G^2 \lambda^2 L^o G_o B}{(4\pi)^3 H_o^3 (1+H_o/a_e)} \int_{-\infty}^{\infty} d\Delta R \int_0^{\pi/2} [H_o (1+H_o/a_e) \theta d\theta] \cdot$$

$$\gamma(\theta) A^2(\theta) P_h \left( -\frac{\Delta R}{\sigma_h} + \frac{H_o \theta^2}{2\sigma_h} (1+H_o/a_e) \right) \cdot$$

$$\cdot \int_0^{2\pi} d\psi \left| \chi_{gw} \left( t - \tau_o - \frac{2\Delta R}{c}, \phi - \frac{2V\theta}{\lambda} \cos \psi \right) \right|^2$$

$$+ \frac{1}{2} k T_o F_n G_o B \quad (5.13)$$

where  $\gamma(\theta)$  is defined by  $\sigma^o(\theta) = \sigma^o \gamma(\theta)$  and defines the variation of  $\sigma^o(\theta)$  with angle.

## 5.2 Approximate Evaluation

A closed form solution for the mean power return can now be obtained from the triple integral of Equation 5.13. To achieve such a solution requires some additional approximations and simplifying assumptions. First assume that the cross ambiguity function is essentially constant over the doppler variation of the scattering points, then

$$\int_0^{2\pi} d\psi \left| \chi_{gw} \left( t - \tau_0 - \frac{2\Delta R}{c}, \phi - \frac{2V\theta}{\lambda} \cos \psi \right) \right|^2$$

$$\approx 2\pi \left| \chi_{gw} \left( t - \tau_0 - \frac{2\Delta R}{c}, 0 \right) \right|^2 \quad (5.14)$$

Further assume that the variation of the cross ambiguity function with range delay can be approximated by a Gaussian function, thus

$$|\chi_{gw}^2(t_1)| \simeq \exp\left[-\frac{1}{2}\left(\frac{t_1}{\sigma_\tau}\right)^2\right] = \sqrt{2\pi} \sigma_\tau \eta\left(\frac{t_1}{\sigma_\tau}\right) \quad (5.15)$$

where  $\eta$  is the normal density function and  $\sigma_\tau =$  RMS pulse width.

Now from Barricks (3) model, the wave height density is also normal, hence

$$p_h\left(\frac{h}{\sigma_h}\right) = \eta\left(\frac{h}{\sigma_h}\right) \quad (5.16)$$

Letting

$$H = H_0 \left(1 + \frac{H}{a_e}\right) \quad (5.17)$$

and

$$x = \frac{H\theta^2}{2}$$

$$dx = H\theta d\theta \quad (5.18)$$

and substituting equation 5.14 through 5.18 into the triple integral of equation 5.13, denoted  $I_3$ , yields

$$I_3 = (2\pi)^{3/2} \sigma_R \int_0^{\frac{H\pi^2}{8}} dx \gamma(x) A^2(x) \int_{-\infty}^{+\infty} d\Delta R \cdot$$

$$\eta\left(\frac{x - \Delta R}{\sigma_h}\right) \eta\left(\frac{\frac{c(t - \tau_0)}{2} - \Delta R}{\sigma_R}\right) \quad (5.19)$$

where

$$\sigma_R = \frac{c\sigma_\tau}{2} = \text{RMS range resolution}$$

Thus the integral over  $\Delta R$  is simply the convolution of two normal densities having different means and variances. As may readily be shown, this convolution produces a normal density with a mean equal to the sum of the means and a variance equal to the sum of the variances. Letting

$$y = \frac{c(t-\tau_0)}{2} = \text{range measured from the mean sea surface} \quad (5.20)$$

and performing the indicated convolution of equation 5.19

$$I_3 = (2\pi)^{3/2} \sigma_R \int_0^{\frac{H\pi^2}{8}} \gamma(x) A^2(x) \eta\left(\frac{y-x}{\sigma_e}\right) dx \quad (5.21)$$

where

$$\sigma_e^2 = \sigma_R^2 + \sigma_h^2 \quad (5.22)$$

Now assuming that the two way antenna pattern function can be approximated by a Gaussian function

$$A^2(\theta) \simeq e^{-\ln 2 \left(\frac{2\theta}{\theta_{BW2}}\right)^2} \quad (5.23)$$

where

$$\theta_{BW2} = \text{the two way 3 dB beamwidth}$$

And from Barricks (3) model the surface shaping function

$$\gamma(\theta) \simeq e^{-\ln 2 \left(\frac{2\theta}{\theta_s}\right)^2} \quad (5.24)$$

where

$$\theta_s = \text{the 3 dB spread of the slope distribution}$$

Then utilizing the change of variable given by equation 5.18, the product of the surface shaping function and beam pattern can be written as

$$G(x) = \gamma(x)A^2(x) = e^{-8\ln 2 \frac{x}{H\theta_e^2}} \quad (5.25)$$

where

$$\theta_e = \left[ \frac{1}{\theta_{BW}^2} + \frac{1}{\theta_s^2} \right]^{-1/2} \quad (5.26)$$

is the effective 3 dB beam width.

The remaining integral of equation 5.21 can now be expressed as

$$\begin{aligned} F(y) &= (G * \eta) [x] \\ &= \frac{1}{\sqrt{2\pi} \sigma_e} \int_0^\infty \exp \left[ -\frac{1}{2} \left( \frac{y-x}{\sigma_e} \right)^2 \right] \exp [-\mu x] dx \end{aligned} \quad (5.27)$$

where

$$\mu = \frac{8\ln 2}{H \theta_e^2} \quad (5.28)$$

To evaluate the remaining integral requires completing the square in the exponent, let

$$\begin{aligned} \frac{1}{2} \left( \frac{y-x}{\sigma_e} \right)^2 + \mu x &= \frac{1}{2} \frac{y^2 - 2xy + x^2}{\sigma_e^2} + \frac{1}{2} \frac{2\sigma_e^2 \mu x}{\sigma_e^2} \\ &= \frac{1}{2\sigma_e^2} [y^2 - 2x(y - \sigma_e^2 \mu) + x^2] \\ &= \frac{1}{2\sigma_e^2} [y^2 - (y - \sigma_e^2 \mu)^2 + (y - \sigma_e^2 \mu)^2 - 2x(y - \sigma_e^2 \mu) + x^2] \end{aligned}$$

$$\begin{aligned}
&= \frac{1}{2\sigma_e^2} [y^2 - y^2 + 2y\sigma_e^2\mu - \sigma_e^4\mu^2] + \frac{1}{2\sigma_e^2} [x - (y - \sigma_e^2\mu)]^2 \\
&= (y\mu - \frac{1}{2}\sigma_e^2\mu^2) + \frac{1}{2} \left[ \frac{x - (y - \sigma_e^2\mu)}{\sigma_e} \right]^2
\end{aligned}$$

Thus

$$F(y) = \exp[\frac{1}{2}(\sigma_e\mu)^2 - y\mu] \frac{1}{\sqrt{2\pi}\sigma_e} \int_0^\infty \exp\left[-\frac{1}{2}\left(\frac{x - (y - \sigma_e^2\mu)}{\sigma_e}\right)^2\right] dx \quad (5.29)$$

Letting

$$t = \frac{(y - \sigma_e^2\mu) - x}{\sigma_e}$$

$$F(y) = \exp[\frac{1}{2}(\sigma_e\mu)^2 - y\mu] \int_{-\infty}^{\frac{y}{\sigma_e} - \sigma_e\mu} \frac{1}{\sqrt{2\pi}} \exp(-\frac{1}{2}t^2) dt \quad (5.30)$$

So that finally

$$F(y) = \exp[\frac{1}{2}(\sigma_e\mu)^2 - y\mu] \Phi\left[\frac{y}{\sigma_e} - \sigma_e\mu\right] \quad (5.31)$$

where  $\Phi$  is the cumulative normal distribution function. Thus  $F(y)$  describes the shape of the mean power return as a function of range measured from the mean sea surface.

Substituting equation 5.31 into equation 5.21 and the result into equation 5.13 yields the approximate closed form solution for the average video power

$$\begin{aligned}
V(y) &= \frac{\frac{1}{2}(2\pi)^{3/2} E_T G^2 \lambda^2 L G_o B \sigma_R}{(4\pi)^3 H_o^3 (1 + \frac{H_o}{a_e})} \cdot \sigma_o(\sigma_h) \exp[\frac{1}{2}(\sigma_e\mu)^2 - y\mu] \Phi\left[\frac{y}{\sigma_e} - \sigma_e\mu\right] \\
&+ \frac{1}{2} k T_o F_n G_o B \quad (5.32)
\end{aligned}$$

where

$$10 \log \left( \sigma^{\circ}(\sigma_h) \right) = 13.6 - 5 \log \sigma_h \quad (5.33)$$

is the variation in cross section per unit area of the sea at normal incidence as a function of RMS wave height (in meters) as given by Barricks (3) model.

Figure 5.2 illustrates the shape of the mean power return as given by equation 5.32 as a function of RMS wave height  $\sigma_h$  for typical SEASAT-A parameters. The factor of 4 or 5 variation in power at the so called "plateau" of the return can be attributed to the change in cross section as given by equation 5.33. If this variation in  $\sigma^{\circ}(\sigma_h)$  is normalized (as with a late gate on the plateau) the mean power return of Figure 5.3 is obtained. The droop in the plateau region shown in Figure 5.3 is caused by the rather narrow effective beam width  $\theta_e$ . A small  $\theta_e$  also causes a distortion in the shape of the leading edge, producing a wave height dependent bias. As shown in Figure 5.4, a bias of 19 m occurs at a 5 m RMS wave height due to this effect. A plot of distortion and bias as a function of antenna beam width, Figure 5.5, shows that an antenna beam width of  $5^{\circ}$  to  $10^{\circ}$  would essentially eliminate this problem. The bias as a function of antenna beam width for a 5 meter RMS wave height is shown in Figure 5.6. While a wider antenna beam width would also reduce the effects of antenna pointing errors, the reduction in gain would require a corresponding increase in peak transmitter power and/or compression ratio to achieve the recommended signal-to-noise ratio.

The scope of the present program precluded an in depth study of the effects of pointing error on the shape of the mean power return (although it is presently felt that the effect of pointing error could be included in the closed form solution given by equation 5.32). It is recommended that a study be made of all the trade offs involved in order to determine an optimum antenna beam width.

I-5-12

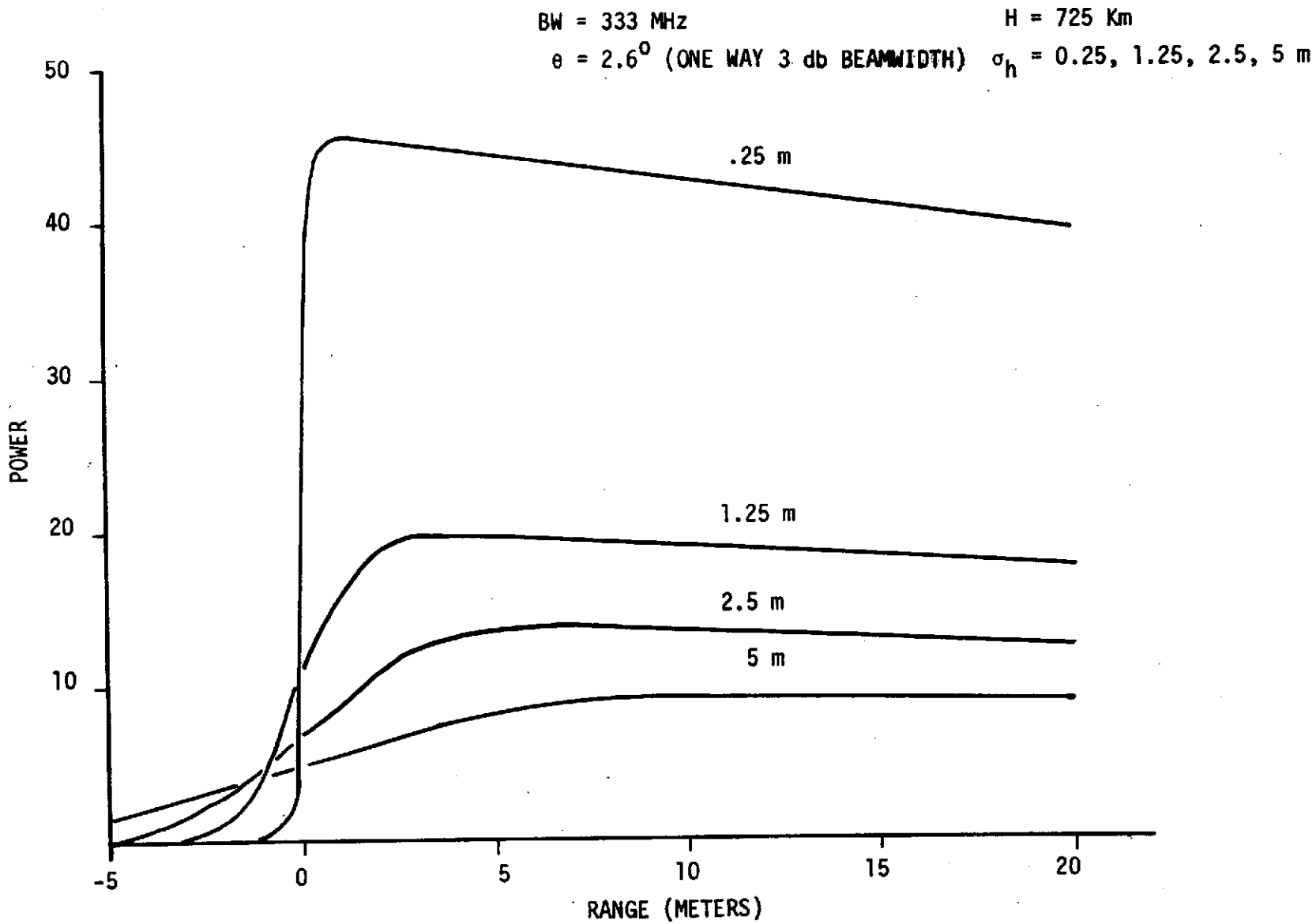


Figure 5.2 Mean Sea Return

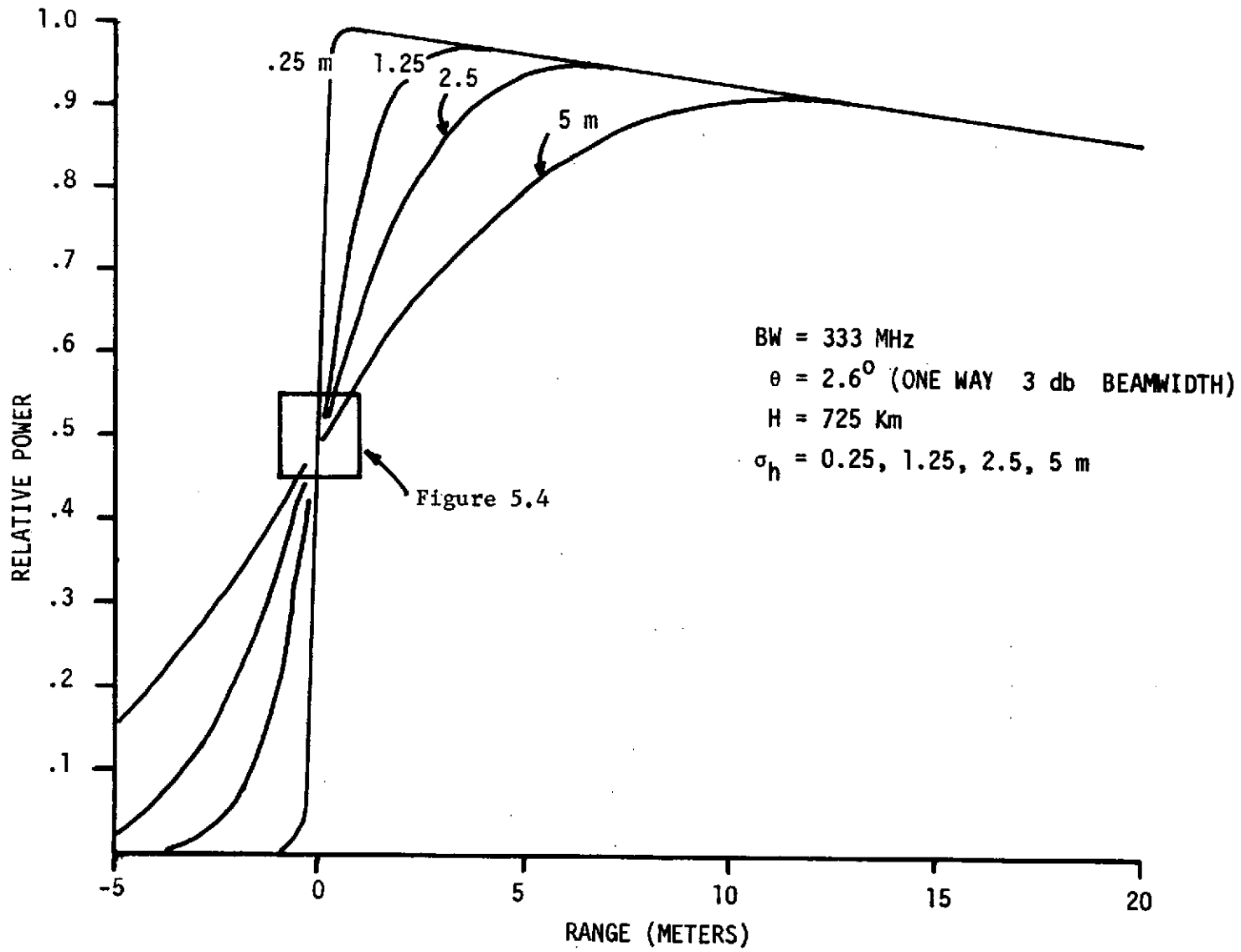


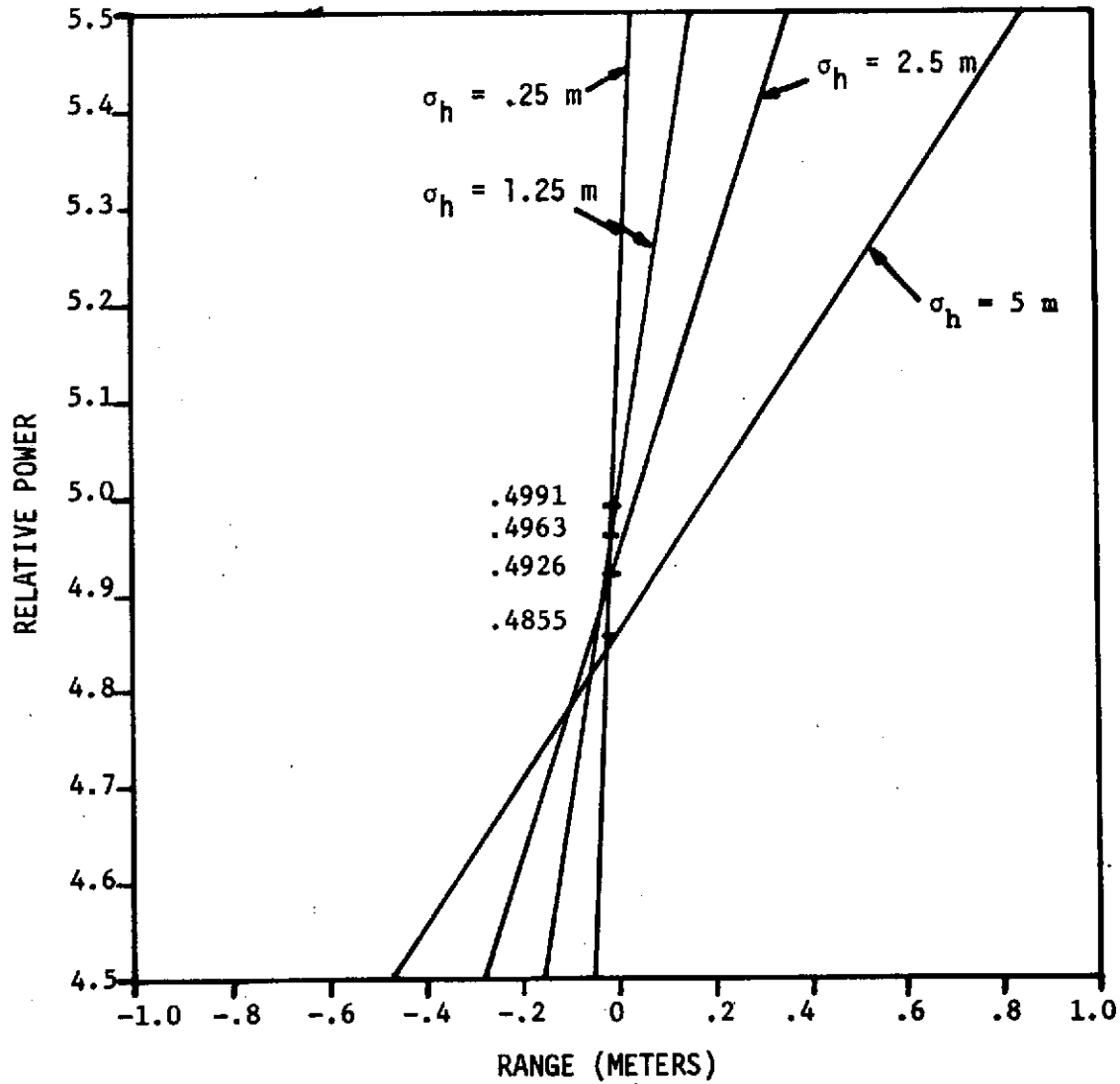
Figure 5.3 Normalized Mean Sea Return

BW = 333 MHz

H = 725 Km

$\theta = 2.6^\circ$  (ONE WAY 3 db BEAMWIDTH)

$\sigma_h = 0.25, 1.25, 2.5, 5$  m



I-5-14

Figure 5.4 Bias in Normalized Mean Surface Return

SI-5-1

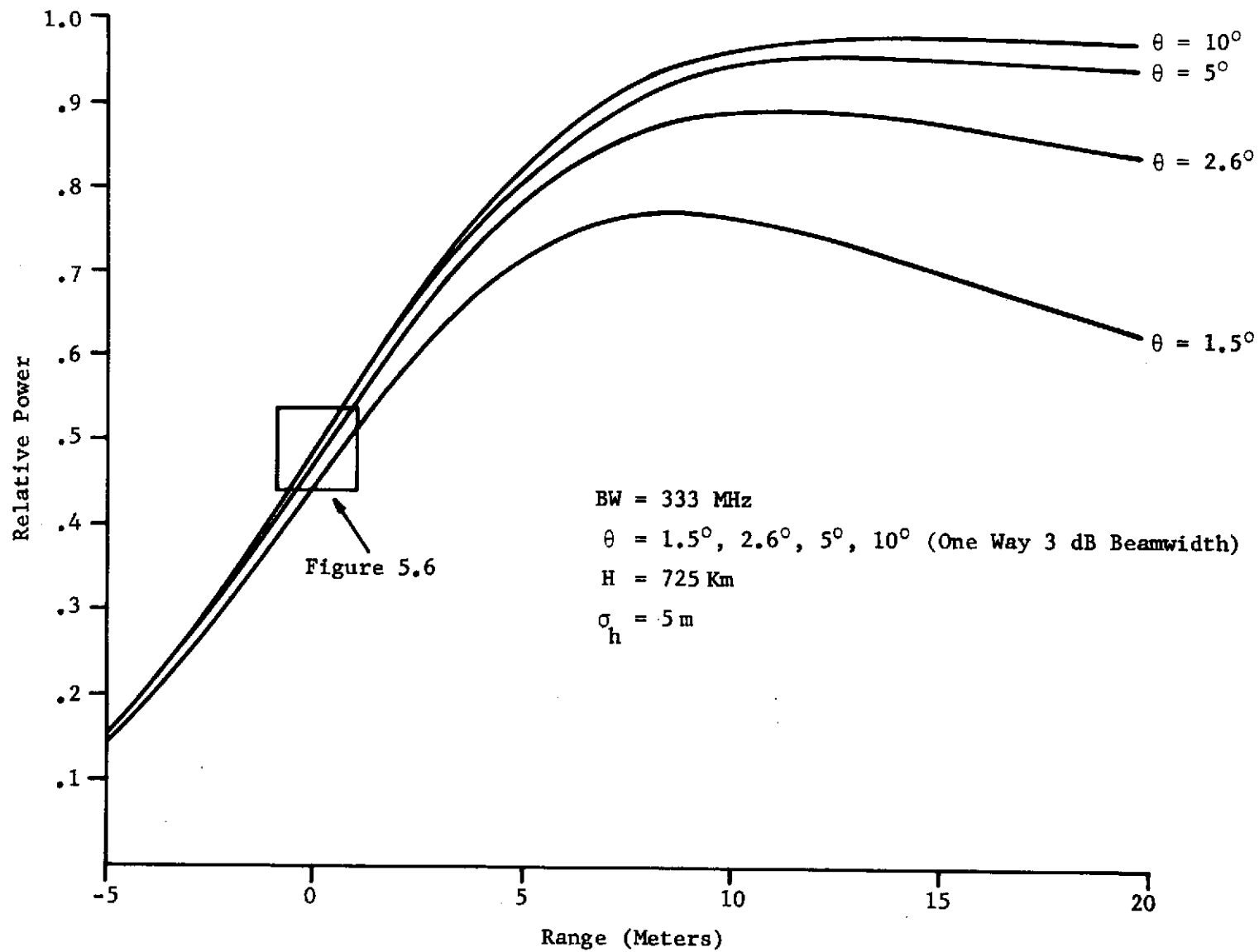


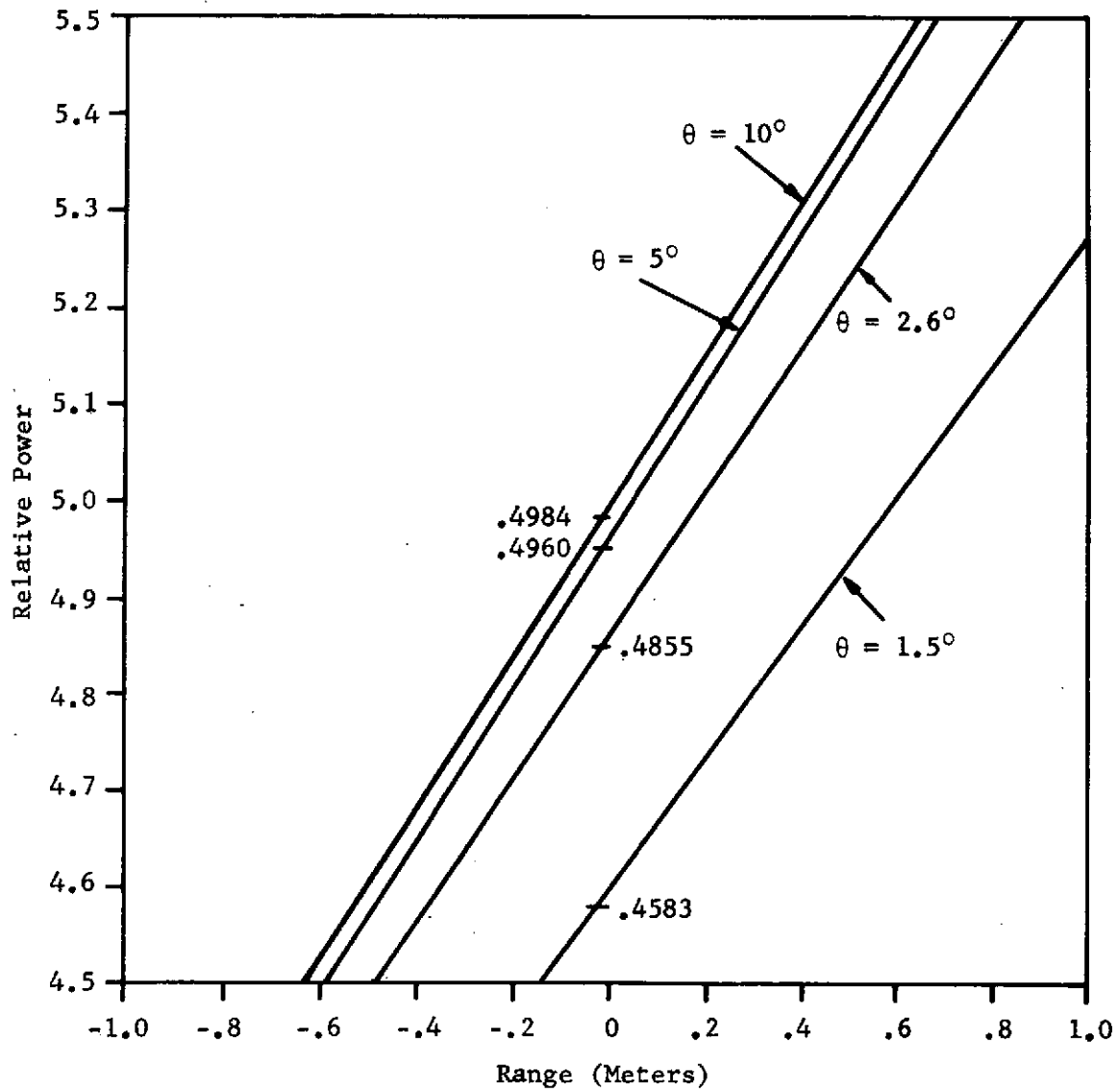
Figure 5.5 Distortion Due to Antenna Beamwidth in Mean Surface Return

BW = 333 MHz

H = 725 Km

$\theta = 1.5^\circ, 2.6^\circ, 5^\circ, 10^\circ$  (One Way 3 dB Beamwidth)

$\sigma_h = 5$  m



I-5-16

Figure 5.6 Bias Due to Antenna Beamwidth in Mean Surface Return

6.0      REFERENCES - PART I

- (1)      R. P. Dooley, F. E. Nathanson, L. W. Brooks, "Study of Radar Pulse Compression for High Resolution Satellite Altimetry," NASA CR # 137474, May 1, 1973.
- (2)      J. L. MacArthur, "Simplified Altimeter Design for SEASAT-A," The Johns Hopkins University, Applied Physics Laboratory, Memo S3R-74-077, June 3, 1974.
- (3)      Donald E. Barrick, "Determination of Mean Surface Position and Sea State from the Radar Return of a Short Pulse Satellite Altimeter," BATTELLE, Columbus Laboratories, October 4, 1971.
- (4)      Donald E. Barrick, "Remote Sensing of Sea State by Radar," Chapter 12 of "Remote Sensing of the Teoposphere," by V. E. Derr, National Oceanic and Atmospheric Administration, Boulder, Colorado, August 15, 1972.
- (5)      David E. Weissman, "Two Frequency Radar Interferometer Applied to the Measurement of Wave Height," IEEE, P-GAP, Volume AP-21, No. 5, pp. 649 - 656, September 1973.
- (6)      David Barton and Harold Ward, "Handbook of Radar Measurement," Prentice-Hall, Table 6.1, p. 170, 1969.
- (7)      R. O. Harger, "Radar Altimetry Optimization for Geodesy Over the Sea," IEEE Trans., Vol. AES-8, No. 6, pp. 728 - 742, November 1972.
- (8)      A. W. Rihaczek, "Principles of High-Resolution Radar," McGraw-Hill, New York, 1969.
- (9)      G. W. Deley, "Waveform Design," Chapter 3, Radar Handbook, M. I. Skolnik (Ed.), McGraw-Hill, New York, 1970.
- (10)     M. I. Skolnik, "An Introduction to Radar," Chapter 1, Radar Handbook, M. I. Skolnik (Ed.), McGraw-Hill, New York, 1970.

APPENDIX A  
(Part 1)

THEORETICAL DERIVATIONS FOR THE MLE ANALYSIS

A.0 INTRODUCTION

In Reference (1), a maximum likelihood estimator (MLE) was proposed which would simultaneously estimate the epoch, wave height, and signal-to-noise ratio for a satellite altimeter. In that reference, the asymptotic performance, when many pulses are integrated, is analyzed. In Reference (2), a technique for implementing the processor using feedback loops is proposed, but its performance is not analyzed. In this appendix, a somewhat broader class of estimators is considered. That is, those estimators which are obtained by minimizing a penalty functional which depends on both the observed data and on the parameters to be estimated. Maximum likelihood estimators (MLE) are special cases of this class of estimators.

In this appendix, formulas for computing the asymptotic bias and variance of the estimators are derived. In addition, an appropriate implementation scheme is discussed which is based on feedback loops. Finally, formulas for computing the mean response, and the variance of the loop estimators are derived. The general formulas are then evaluated for the satellite altimeter case. The resulting formulas provide the basis for the results discussed in Section 3.0.

A.1 Problem Definition

It is assumed that for each pulse (or data interval), a vector of K data values are measured. Thus, let:

$V_i$  be a K dimensional vector of measurements  
taken on the  $i^{\text{th}}$  pulse.

For the altimeter problem, the vector  $V_i$  represents the video outputs from K range cells. For a given set of parameters, represented by the M dimensional vector  $\theta$ , a penalty function is defined, call it:

$$Q(V_i/\theta)$$

Then, for an entire sequence of N pulses, the total penalty is

$$\sum_{i=1}^N Q(v_i/\theta)$$

The class of estimators to be considered are those estimates  $\hat{\theta}$  which minimize the total penalty, i.e.,

$$\sum_{i=1}^N Q(v_i/\hat{\theta}) = \min_{\theta} \sum_{i=1}^N Q(v_i/\theta) \quad (A-1)$$

If one lets  $\nabla^T = (\partial/\partial\theta_1, \partial/\partial\theta_2, \dots, \partial/\partial\theta_M)$  be the gradient with respect to  $\theta$ , then (assuming existence of the derivatives) a necessary condition on the estimator is:

$$\sum_{i=1}^N [\nabla Q(v_i/\hat{\theta})] = 0 \quad (A-2)$$

Before concluding this section, it should be noted that to derive a MLE estimate from this formulation, one lets the penalty function be the negative logarithm of the likelihood function. That is:

$$Q(v_i/\theta) = -\ln(P(v_i/\theta))$$

where  $P(v_i/\theta)$  is the joint probability density function (likelihood function) of the observed values given the parameter vector  $\theta$ .

Note that minimizing Q is equivalent to maximizing P. Note also, to derive a least mean square estimate, one lets

$$Q(v_i/\theta) = [v_i - \bar{v}(\theta)]^T W [v_i - \bar{v}(\theta)]$$

where  $\bar{v}(\theta)$  is a model for the mean value which depends on the parameters to be estimated,

and W is a normalizing matrix. (Note for  $W = I$ , one gets the usual unweighted least square formulation.)

## A.2 Asymptotic Bias and Variance

The asymptotic bias and variance can be estimated by expanding (A-2) in a Taylor Series about the true parameter values. Thus, Equation (A-2) becomes:

$$0 = \sum_{i=1}^N \nabla Q(V_i/\theta) + \sum_{i=1}^N [\nabla \nabla^T Q(V_i/\theta)] (\hat{\theta} - \theta) + \text{higher order terms.} \quad (\text{A-3})$$

Asymptotically, two assumptions are made:

- a)  $\hat{\theta}$  is close enough to  $\theta$  so that only the first term in the Taylor Series expansion needs to be kept.
- b) Enough independent pulses are included so that the second summation may be replaced by its mean value.

Thus:

$$\sum_{i=1}^N [\nabla \nabla^T Q(V_i/\theta)] \approx N E \nabla \nabla^T Q(V_i/\theta)$$

If one lets:

$$R(\theta) = E \nabla \nabla^T Q(V_i/\theta) \quad (\text{A-4})$$

and

$$e_i(\theta) = \nabla Q(V_i/\theta) \quad (\text{A-5})$$

Then Equation (A-3) becomes:

$$N R(\theta) (\hat{\theta} - \theta) = - \sum_{i=1}^N e_i(\theta)$$

or

$$\boxed{(\hat{\theta} - \theta) = -N^{-1} R^{-1}(\theta) \sum_{i=1}^N e_i(\theta)} \quad (\text{A-6})$$

From (A-6) the asymptotic bias and cross correlation matrix of  $\hat{\theta}$  is given by:

$$E(\hat{\theta} - \theta) = -R^{-1}(\theta) E e(\theta) \quad (\text{A-7})$$

and

$$E(\hat{\theta} - \theta) (\hat{\theta} - \theta)^T = N^{-1} R^{-1}(\theta) [E e(\theta) e^T(\theta)] R^{-1}(\theta) \quad (\text{A-8})$$

A.3 Special Case: MLE

For the MLE, Q has the special form:

$$Q(V/\theta) = -\ln P(V/\theta) \quad (\text{A-9})$$

And thus:

$$\epsilon(\theta) = \nabla Q(V/\theta) = -\frac{1}{P(V/\theta)} \nabla (P(V/\theta)) \quad (\text{A-10})$$

The bias is computed by:

$$\begin{aligned} E \epsilon(\theta) &= -\int \frac{1}{P(V/\theta)} [\nabla P(V/\theta)] P(V/\theta) dV \\ &= -\int \nabla P(V/\theta) dV \\ &= -\nabla \int P(V/\theta) dV \\ &= -\nabla 1 = 0 \end{aligned} \quad (\text{A-11})$$

Thus, by (A-7) the MLE is asymptotically unbiased. It should be noted that the above manipulations are formal, and can be justified only for regular distributions.

The information matrix,  $R(\theta)$ , is computed by:

$$\begin{aligned} R(\theta) &= E \nabla \nabla^T Q(V/\theta) \\ &= -E \nabla [P(V/\theta)]^{-1} \nabla^T P(V/\theta) \\ &= E (P(V/\theta))^{-2} (\nabla P(V/\theta)) (\nabla^T P(V/\theta)) \\ &\quad - E P(V/\theta)^{-1} \nabla \nabla^T P(V/\theta) \end{aligned} \quad (\text{A-12})$$

Now recall, (Equation (A-10)):

$$\epsilon(\theta) = (P(V/\theta))^{-1} \nabla P(V/\theta) \quad (\text{A-10})$$

Thus:

$$R(\theta) = E \epsilon(\theta) \epsilon^T(\theta) - E P(V/\theta)^{-1} \nabla \nabla^T P(V/\theta) \quad (\text{A-13})$$

But

$$\begin{aligned} E P(V/\theta)^{-1} \nabla \nabla^T P(V/\theta) &= \int P(V/\theta)^{-1} (\nabla \nabla^T P(V/\theta)) P(V/\theta) dV \\ &= \nabla \nabla^T \int P(V/\theta) dV = \nabla \nabla^T 1 = 0 \end{aligned} \quad (\text{A-14})$$

Again, the above manipulations are only justified for regular distributions. From (A-13) and (A-14) one has finally:

$$R(\theta) = E \epsilon(\theta) \epsilon^T(\theta) \quad (\text{A-15})$$

In summary, the asymptotic bias and covariance of the MLE estimates are:

$$E(\hat{\theta} - \theta) = 0 \quad (\text{A-16})$$

and

$$E(\hat{\theta} - \theta)(\hat{\theta} - \theta)^T = N^{-1} [E \epsilon(\theta) \epsilon^T(\theta)]^{-1} \quad (\text{A-17})$$

where

$$\epsilon(\theta) = -\nabla \ln P(V/\theta) \quad (\text{A-18})$$

Equation (A-17) is equal to the Cramer-Rao lower bound, thus, as is well known, the MLE is asymptotically efficient.

#### A.4 A Feedback Loop Implementation

Equation (A-2) stated that a necessary condition to obtain the desired estimator is to find  $\hat{\theta}$  so that the average error signal is zero. That is,  $\hat{\theta}$  must satisfy:

$$\sum_{i=1}^N \epsilon_i(\hat{\theta}) = 0 \quad (\text{A-2})$$

One technique for solving this equation is to let the error signal be an input to an integrator

$$\frac{d\tilde{\theta}}{dt} = -k \sum_{i=1}^N \epsilon_i(\tilde{\theta}(t)) \quad (\text{A-19})$$

If the loops are stable, then at steady state,  $d\tilde{\theta}/dt = 0$ , and the steady state value of  $\tilde{\theta}$  must satisfy Equation (A-2). Hence, at steady state  $\tilde{\theta}$  converges to the desired estimate  $\hat{\theta}$  which minimizes the total penalty.

The loop equation, (A-19), can be shown to always converge by the following argument. By differentiating the penalty function, one gets:

$$\frac{d}{dt} \sum_{i=1}^N Q(v_i/\tilde{\theta}) = \sum_{i=1}^N \nabla^T Q(v_i/\tilde{\theta}) \frac{d\tilde{\theta}}{dt} = \sum_{i=1}^N \epsilon_i^T(\tilde{\theta}) \frac{d\tilde{\theta}}{dt} \quad (\text{A-20})$$

But, by Equation (A-19) this results in:

$$\frac{d}{dt} \sum_{i=1}^N Q(v_i/\tilde{\theta}) = -k \left[ \sum_{i=1}^N \epsilon_i^T(\tilde{\theta}) \right] \left[ \sum_{i=1}^N \epsilon_i(\tilde{\theta}) \right] \leq 0 \quad (\text{A-21})$$

Thus, the total penalty is decreasing with time and must, therefore, converge to a local minimum.

The loop convergence time may be computed approximately by using the asymptotic linearization:

$$\sum_{i=1}^N \epsilon_i(\tilde{\theta}) \approx \sum_{i=1}^N \epsilon_i(\theta) + N R(\theta)(\tilde{\theta} - \theta) \quad (\text{A-22})$$

But, by using Equation (A-6), the first term may be written in terms of  $\hat{\theta}$ , thus:

$$\begin{aligned} \sum_{i=1}^N \epsilon_i(\tilde{\theta}) &= N R(\theta) [ -(\hat{\theta} - \theta) + \tilde{\theta} - \theta ] \\ &= N R(\theta) (\tilde{\theta} - \hat{\theta}) \end{aligned} \quad (\text{A-23})$$

And one has:

$$\frac{d\tilde{\theta}}{dt} = -kN R(\theta) (\tilde{\theta} - \hat{\theta}) \quad (\text{A-24})$$

The solution to Equation (A-24) is:

$$\tilde{\theta}(t) = e^{-kN R(\theta)t} \tilde{\theta}_0 + e^{-kN R(\theta)t} \int_0^t e^{kN R(\theta)\tau} (kN R(\theta) \hat{\theta}(\tau)) d\tau \quad (\text{A-25})$$

where  $\tilde{\theta}_0$  is the initial value for the estimate  $\tilde{\theta}$ . Note in the above expression,  $\hat{\theta}$  may vary during the loop settling time, but it is assumed that  $\theta$  is not varying. By assumption  $\hat{\theta}(t)$  represents the minimum penalty estimate for  $N$  pulses centered at time  $t$ . For simplicity, we assume that the estimates are only computed at discrete times. Thus:

$$\hat{\theta}(t) = \frac{N}{\text{PRF}} \sum_j \hat{\theta}_j \delta(t - jN/\text{PRF}) \quad (\text{A-26})$$

where PRF is the pulse repetition frequency  
 $\delta$  is the Dirac delta function  
and  $\hat{\theta}_j$  is the minimum penalty estimate computed for the pulses occurring from time  $(j - \frac{1}{2})N/PRF$  to time  $(j + \frac{1}{2})N/PRF$ .

From (A-25) and (A-26) one has that the mean of  $\tilde{\theta}(t)$  is given by:

$$E \tilde{\theta}(t) = e^{-kN R(\theta)t} \tilde{\theta}_0 + \frac{N}{PRF} \sum_{j < t \frac{PRF}{N}} e^{-kN R(\theta)(t - jN/PRF)} kN R(\theta) E(\hat{\theta}) \quad (A-27)$$

Assuming that the loop time constant is large compared to  $N/PRF$ , then

$$\begin{aligned} E \tilde{\theta}(t) &\approx e^{-kN R(\theta)t} \tilde{\theta}_0 + e^{-kN R(\theta)t} \int_0^t e^{kN R(\theta)\tau} kN R(\theta) d\tau (E \hat{\theta}) \\ &= E \hat{\theta} + e^{-kN R(\theta)t} (\tilde{\theta}_0 - E \hat{\theta}) \end{aligned} \quad (A-28)$$

Thus, the behavior of the mean of  $\tilde{\theta}$  is determined by the eigenvalues of the matrix:

$$R(\theta) = E \nabla \nabla^T Q(V/\theta) \quad (A-29)$$

In particular, if all the eigenvalues of  $R(\theta)$  are positive, then:

$$\lim_{t \rightarrow \infty} e^{-kN R(\theta)t} = 0$$

and

$$E \tilde{\theta}(t) \xrightarrow[t \rightarrow \infty]{} E \hat{\theta}$$

Further, the convergence time of the loops is determined by the minimum eigenvalue of  $R(\theta)$ , thus the maximum loop time constant is given by:

$$T_c = (kN \lambda_{\min})^{-1} \quad (A-30)$$

where  $\lambda_{\min}$  is the minimum eigenvalue of  $R(\theta)$ .

The variance of the estimate  $\tilde{\theta}$  is computed as follows. From (A-25) and (A-28), one has:

$$\tilde{\theta}(t) - E \tilde{\theta}(t) = e^{-kN R(\theta)t} \int_0^t e^{kN R(\theta)\tau} kN R(\theta) (\hat{\theta}(\tau) - E \hat{\theta}) d\tau \quad (A-31)$$

Thus:

$$\begin{aligned} \text{Cov} \left( \tilde{\theta}(t) \right) &= E \left( \tilde{\theta}(t) - E \tilde{\theta}(t) \right) \left( \tilde{\theta}(t) - E \tilde{\theta}(t) \right)^T \\ &= \int_0^t \int_0^t e^{-kN R(\theta)(t - \tau_1)} \left( kN R(\theta) \right) \text{Cov} \left( \hat{\theta}(\tau_1), \hat{\theta}(\tau_2) \right) \\ &\quad \bullet \left( kN R(\theta) \right) e^{-kN R(\theta)(t - \tau_2)} d\tau_1 d\tau_2 \end{aligned} \quad (\text{A-32})$$

Now, consider  $\text{Cov} \left( \hat{\theta}(\tau_1), \hat{\theta}(\tau_2) \right)$ , from (A-26) one has:

$$\text{Cov} \left( \hat{\theta}(\tau_1), \hat{\theta}(\tau_2) \right) = \left( \frac{N}{\text{PRF}} \right)^2 \sum_{\ell, m} \text{Cov} \left[ \hat{\theta}_\ell, \hat{\theta}_m \right] \delta \left( \tau_1 - \ell N / \text{PRF} \right) \delta \left( \tau_2 - m N / \text{PRF} \right) \quad (\text{A-33})$$

But, assuming independent pulses, one has:

$$\begin{aligned} \text{Cov} \hat{\theta}_j \hat{\theta}_\ell &= \text{Cov} \hat{\theta} \quad j = \ell \\ &= 0 \quad j \neq \ell \end{aligned} \quad (\text{A-34})$$

Thus

$$\begin{aligned} \text{Cov} \hat{\theta}(\tau_1) \hat{\theta}(\tau_2) &= \left( \frac{N}{\text{PRF}} \right)^2 \sum_{j, \ell} \text{Cov} \left( \hat{\theta}_j, \hat{\theta}_\ell \right) \delta \left( \tau_1 - j N / \text{PRF} \right) \delta \left( \tau_2 - j N / \text{PRF} \right) \\ &= \left( \frac{N}{\text{PRF}} \right)^2 \text{Cov} \hat{\theta} \sum_j \delta \left( \tau_1 - j N / \text{PRF} \right) \delta \left( \tau_2 - j N / \text{PRF} \right) \end{aligned} \quad (\text{A-35})$$

Substituting the above expression into Equation (A-32) gives:

$$\begin{aligned} \text{Cov} \tilde{\theta}(t) &= \left( \frac{N}{\text{PRF}} \right)^2 \sum_{j < t \frac{\text{PRF}}{N}} e^{-kN R(\theta)(t - jN/\text{PRF})} \left( kN R(\theta) \right) \text{Cov} \hat{\theta} \left( kN R(\theta) \right) \\ &\quad \bullet e^{-kN R(\theta)(t - jN/\text{PRF})} \end{aligned} \quad (\text{A-36})$$

Now if it is assumed that the loop time constant is large compared to  $N/\text{PRF}$ , then

$$\text{Cov} \left( \tilde{\theta}(t) \right) \approx \frac{N}{\text{PRF}} \int_0^t e^{-kN R(\theta)(t - \tau)} \left( kN R \right) \text{Cov} \hat{\theta} \left( kN R \right) e^{-kN R(\theta)(t - \tau)} d\tau \quad (\text{A-37})$$

The above equation can be evaluated by expanding  $\exp [-kN R(\theta)(t - \tau)]$  in terms of the eigenvalues and eigenvectors of  $R$ . Thus:

$$e^{-kN R(\theta)(t - \tau)} kN R(\theta) = \sum_{\ell=1}^K e^{-kN \lambda_\ell (t - \tau)} kN \lambda_\ell \varphi_\ell \varphi_\ell^T \quad (\text{A-38})$$

where  $\lambda_\ell$  is the  $\ell^{\text{th}}$  eigenvalue of  $R(\theta)$   
and  $\varphi_\ell$  is the corresponding eigenvector.

Thus:

$$\begin{aligned} \text{Cov}[\tilde{\theta}(t)] &= \frac{N}{\text{PRF}} \sum_{\ell, m} \int_0^t e^{-kN(\lambda_\ell + \lambda_m)(t - \tau)} (k^2 N^2 \lambda_\ell \lambda_m) d\tau \varphi_\ell \varphi_\ell^T [\text{Cov } \hat{\theta}] \varphi_m \varphi_m^T \\ &= \frac{kN^2}{\text{PRF}} \sum_{\ell, m} \left[ \frac{1 - e^{-kN(\lambda_\ell + \lambda_m)t}}{\lambda_\ell + \lambda_m} (\lambda_\ell \lambda_m) \right] \varphi_\ell \varphi_\ell^T [\text{Cov } \hat{\theta}] \varphi_m \varphi_m^T \end{aligned} \quad (\text{A-39})$$

For the special case of the MLE,

$$\text{Cov } \hat{\theta} = R^{-1}(\theta) = N^{-1} \sum_j \lambda_j^{-1} \varphi_j \varphi_j^T$$

Thus (A-39) becomes:

$$\begin{aligned} \text{Cov}[\tilde{\theta}(t)] &= \frac{kN}{2\text{PRF}} \sum_\ell (1 - e^{-2kN \lambda_\ell t}) \varphi_\ell \varphi_\ell^T \\ &= \frac{kN}{2\text{PRF}} (\text{I} - e^{-2kN R(\theta)t}) \end{aligned} \quad (\text{A-40})$$

Further, as  $t \rightarrow \infty$

$$\text{Cov}[\tilde{\theta}(t)] \rightarrow \frac{kN}{2\text{PRF}} \text{I} \quad (\text{A-41})$$

Equation (A-41) shows that the steady-state variance of  $\tilde{\theta}$  can be made small by reducing the feed-back loop gain. However, Equation (A-30) shows that this increases the settling time of the loops. Thus the reduced variance is achieved by increasing the loop averaging time.

#### A.5 Evaluation of the Satellite Altimetry Case

In the previous sections, the asymptotic variance of a MLE was shown to depend only on the information matrix:

$$R(\theta) = E e(\theta) e^T(\theta) \quad (\text{A-15})$$

where

$$e(\theta) = \nabla Q(V/\theta) \quad (\text{A-18})$$

and

$$Q(V/\theta) = -\ln P(V/\theta)$$

where  $P(V/\theta)$  is the joint likelihood function of the vector of observed values,  $V$ , given the parameter values  $\theta$ . In this section, the information matrix will be evaluated for the satellite altimetry case.

For this section, it is assumed that the vector

$$V = \{V_j\}_{j=1}^K \quad (A-42)$$

represents the sampled video output of the altimeter. It is assumed that the sampled values occur at least one range resolution cell apart, thus the sampled values are statistically independent. Further, square law detection is assumed so that the video samples follow an exponential distribution. With these assumptions, the likelihood function can be written:

$$P(V/\theta) = \prod_{j=1}^K \left( \bar{V}_j(\theta) \right) \exp \left( -V_j / \bar{V}_j(\theta) \right) \quad (A-43)$$

where

$$\bar{V}_j(\theta) = E(V_j/\theta) \quad (A-44)$$

Thus, the likelihood function depends only on the mean power return as a function of range.

Applying (A-43) to (A-18), one obtains the penalty function

$$Q(V/\theta) = \sum_{j=1}^K \ln \bar{V}_j + V_j / \bar{V}_j \quad (A-45)$$

Thus:

$$\begin{aligned} \epsilon(\theta) &= \nabla Q(V/\theta) \\ &= \sum_{j=1}^K (\bar{V}_j - V_j) (\bar{V}_j)^{-2} \nabla \bar{V}_j \end{aligned} \quad (A-46)$$

And the information matrix is given by:

$$\begin{aligned}
R(\theta) &= E \epsilon(\theta) \epsilon^T(\theta) \\
&= E \sum_{j=1}^K \sum_{\ell=1}^K (\bar{V}_j - V_j) (\bar{V}_j)^{-2} \nabla \bar{V}_j \nabla^T \bar{V}_\ell (V_\ell)^{-2} (\bar{V}_\ell - V_\ell) \\
&= \sum_{j=1}^K (\bar{V}_j^{-1} \nabla \bar{V}_j) (\bar{V}_j^{-1} \nabla \bar{V}_j)^T \\
&= \sum_{j=1}^K B_j B_j^T
\end{aligned} \tag{A-47}$$

Where the vector  $B_j$  is given by:

$$B_j = \bar{V}_j^{-1} \nabla \bar{V}_j \tag{A-48}$$

Note that the summation in Equation (A-47) is over range. In general, the range resolution cell is small, therefore the summation can be approximated by an integral so that:

$$R(\theta) \approx \frac{1}{\Delta t} \int_{T_{\min}}^{T_{\max}} B(t) B^T(t) dt \tag{A-49}$$

where the limits of integration in (A-49) are from the minimum to the maximum range sampled, and  $B_j$  is treated as a function of time delay,  $B(t)$ . In (A-49)  $\Delta t$  is the time in seconds between adjacent range samples. Note that the dependence on the parameters is contained entirely in  $\bar{V}$ .

To evaluate (A-49) further, an expression for  $\bar{V}(t/\theta)$  is required (i.e., the mean power return versus time given the parameter values). In Section 5.0 a fairly detailed derivation of the mean power returned from a distributed target is given, and a reasonably good approximation for the altimeter case is derived. The resulting expression depends on compressed pulse length, RMS wave height, antenna beamwidth, and the RMS surface slopes. However, from the results in that section, it can be shown that when the compressed pulse length is small compared to the wave height, and when the antenna beamwidth is broad ( $>5^\circ$ ), the mean power return can be written approximately as:

$$\bar{V}(t/\theta) = a \Phi(\beta(t - \tau_0)) + 1 \tag{A-50}$$

where the significant parameters to be estimated are:

$$\theta = (a, \tau_o, \beta)$$

with  $a =$  signal-to-noise ratio

$$\tau_o = \text{epoch}$$

and  $\beta = \frac{c}{2\sigma_n}$  is a measure of the RMS wave height.

In Equation (A-50)  $\Phi(\cdot)$  is the unit normal cumulative density function. Further, for convenience, the known receiver noise power is assumed to be unity.

With these assumptions, one can write:

$$B(t) = \begin{pmatrix} B_a(t) \\ B_{\tau_o}(t) \\ B_{\beta}(t) \end{pmatrix} \quad (\text{A-51})$$

with

$$B_a(t) = a^{-1} \frac{\Phi(\beta(t - \tau_o))}{\Phi(\beta(t - \tau_o)) + 1/a}$$

$$B_{\tau_o}(t) = \beta \left( \frac{-\dot{\Phi}(\beta(t - \tau_o))}{\Phi(\beta(t - \tau_o)) + 1/a} \right) \quad (\text{A-52})$$

$$B_{\beta}(t) = \beta^{-1} \left( \frac{\beta(t - \tau_o) \dot{\Phi}(\beta(t - \tau_o))}{\Phi(\beta(t - \tau_o)) + 1/a} \right)$$

If the above expressions are substituted directly into Equation (A-50), the resulting integrals are difficult to evaluate. Therefore, to simplify the computations, the cumulative normal is approximated by three straight line segments. That is:

$$\begin{aligned} \Phi(u) &\approx 0 & u < -\frac{1}{2}\alpha^{-1} \\ &\approx \alpha u + \frac{1}{2} & |u| \leq \frac{1}{2}\alpha^{-1} \\ &\approx 1 & u > \frac{1}{2}\alpha^{-1} \end{aligned} \quad (\text{A-53})$$

where the constant,  $\alpha = .3227$ , is chosen to make the straight line segments fit the cumulative normal in a least squares sense.

Using the above approximation, and making the change of variable:

$$Z = \alpha \beta (t - \tau_0) + \frac{1}{2} + 1/a \quad (\text{A-54})$$

one finds that the components of the vector  $B(t)$  can be written in terms of  $Z$  as follows:

$$\begin{aligned} \text{Since } \Phi(\beta(t - \tau_0)) &= \alpha \beta (t - \tau_0) + \frac{1}{2}, \quad |\beta(t - \tau_0)| \leq \frac{1}{2}\alpha^{-1} \\ &= Z - 1/a, \quad 1/a \leq Z \leq 1 + 1/a \\ &= 1, \quad Z > 1 + 1/a \end{aligned} \quad (\text{A-55})$$

$$\begin{aligned} \text{and } \dot{\Phi}(\beta(t - \tau_0)) &= \alpha, \quad |\beta(t - \tau_0)| \leq \frac{1}{2}\alpha^{-1} \\ &1/a \leq Z \leq 1 + 1/a \\ &= 0, \quad \text{otherwise} \end{aligned} \quad (\text{A-56})$$

$$\begin{aligned} \text{Then } B_a(t) &= a^{-1} \left[ \frac{Z - 1/a}{Z} \right], \quad 1/a \leq Z \leq 1 + 1/a \\ &= a^{-1} (1 - 1/a Z), \quad 1/a \leq Z \leq 1 + 1/a \\ &= a^{-1} (a/a + 1), \quad Z > 1 + 1/a \end{aligned} \quad (\text{A-57})$$

$$B_{\tau_0}(Z) = \beta(-\alpha/Z), \quad 1/a \leq Z \leq 1 + 1/a$$

$$B_{\beta}(Z) = \beta^{-1} \left( \frac{Z - \frac{1}{2} - 1/a}{Z} \right) = \beta^{-1} \left( 1 - \frac{a+2}{2aZ} \right), \quad 1/a \leq Z \leq 1 + 1/a$$

Substituting the above equations into (A-50) and integrating over  $Z$  gives the results:

$$R(\theta) = \frac{1}{\alpha \beta \Delta t} D C D \quad (\text{A-58})$$

where  $D$  is the diagonal matrix.

$$D = \begin{pmatrix} a^{-1} & 0 & 0 \\ 0 & \beta & 0 \\ 0 & 0 & \beta^{-1} \end{pmatrix} \quad (\text{A-59})$$

and C is given by:

$$C = \begin{pmatrix} C_{aa} & C_{a\tau_o} & C_{a\beta} \\ C_{a\tau_o} & C_{\tau_o\tau_o} & C_{\tau_o\beta} \\ C_{a\beta} & C_{\tau_o\beta} & C_{\beta\beta} \end{pmatrix} \quad (A-60)$$

where

$$\begin{aligned} C_{aa} &= \int_{1/a}^{1+1/a} \left(1 - \frac{1}{aZ}\right)^2 dZ + \int_{1+1/a}^{\alpha\beta T_{\max}^{+1/2} - 1/a} \left(\frac{a}{1+a}\right)^2 dZ \\ &= 1 - \frac{2}{a} \log(1+a) + \frac{1}{1+a} + (\alpha\beta T_{\max} - \frac{1}{2}) \left(\frac{a}{1+a}\right)^2 \end{aligned}$$

$$\begin{aligned} C_{a\tau_o} &= - \int_{1/a}^{1+1/a} \left(1 - \frac{1}{aZ}\right) \left(\frac{\alpha}{Z}\right) dZ \\ &= -\alpha \left[ \log(1+a) - \frac{a}{1+a} \right] \end{aligned} \quad (A-61)$$

$$\begin{aligned} C_{a\beta} &= \int_{1/a}^{1+1/a} \left(1 - \frac{1}{aZ}\right) \left(1 - \frac{a+2}{2aZ}\right) dZ \\ &= 1 - \frac{a+4}{2a} \log(1+a) + \frac{a+2}{2(a+1)} \end{aligned}$$

$$C_{\tau_o\tau_o} = \alpha^2 \int_{1/a}^{1+1/a} \frac{dZ}{Z^2} = \frac{\alpha^2 a^2}{(1+a)}$$

$$\begin{aligned} C_{\tau_o\beta} &= - \int_{1/a}^{1+1/a} \frac{\alpha}{Z} \left(1 - \frac{a+2}{2aZ}\right) dZ \\ &= -\alpha \left[ \log(1+a) - \frac{(a+2)a}{2(a+1)} \right] \end{aligned}$$

$$C_{\beta\beta} = \int_{1/a}^{1+1/a} \left(1 - \frac{a+2}{2az}\right)^2 dz$$

$$= 1 - \frac{a+2}{a} \log(1+a) + \frac{(a+2)^2}{4(1+a)}$$

Since the variance of the MLE is given by  $N^{-1}R^{-1}(\theta)$ , it would be useful to have a general formula for  $C^{-1}$  (from which  $R^{-1}(\theta)$  could be computed). Although it is feasible to write down the inverse of a 3 by 3 matrix, the resulting formulas are unmanageably cumbersome. Therefore, we proceed differently.

Let

$$C'_{aa} = 1 - \frac{2}{a} \log(1+a) + \frac{1}{1+a} + \frac{1}{2} \left(\frac{a}{1+a}\right)^2 \quad (\text{A-62})$$

Then if

$$C' = \begin{pmatrix} C'_{aa} & C_{a\tau_0} & C_{a\beta} \\ C_{a\tau_0} & C_{\tau_0\tau_0} & C_{\tau_0\beta} \\ C_{a\beta} & C_{\tau_0\beta} & C_{\beta\beta} \end{pmatrix} \quad (\text{A-63})$$

one has

$$C = C' + d \begin{pmatrix} 1 \\ 0 \\ 0 \end{pmatrix} \begin{pmatrix} 1 & 0 & 0 \end{pmatrix} \quad (\text{A-64})$$

where

$$d = (\alpha\beta T_{\max} - 1) \left(\frac{a}{1+a}\right)^2 \quad (\text{A-65})$$

The advantage of writing  $C$  in this form is that  $C'$  depends only on signal-to-noise ratio; therefore,  $(C')^{-1}$  can be easily tabulated. Further, using the Woodbury identity,  $C^{-1}$  can be computed from  $(C')^{-1}$ . That is, let

$$F = (C')^{-1}$$

Then:

$$C^{ij} = F_{ij} - \frac{d}{1+dF_{11}} F_{1i} F_{1j} \quad (\text{A-66})$$

where  $C^{ij}$  is the  $(i,j)$  element of  $C^{-1}$ . Table A-I tabulates  $F_{ij}$  versus signal-to-noise ratio from -10 dB to 30 dB in 5 dB steps.

TABLE A-I  
F Matrix vs S/N

| S/N (dB) | F <sub>11</sub> | F <sub>12</sub> | F <sub>13</sub> | F <sub>22</sub> | F <sub>23</sub> | F <sub>33</sub> |
|----------|-----------------|-----------------|-----------------|-----------------|-----------------|-----------------|
| -10      | 242.0           | 374.96          | -242.0          | 1640.5          | -440.0          | 1563.6          |
| - 5      | 34.649          | 53.686          | - 34.649        | 212.78          | - 76.271        | 194.19          |
| 0        | 8.0             | 12.395          | - 8.0           | 41.587          | - 21.408        | 33.579          |
| 5        | 3.4649          | 5.3686          | - 3.4649        | 15.416          | - 9.8626        | 9.978           |
| 10       | 2.42            | 3.7496          | - 2.42          | 9.8201          | - 6.5847        | 5.141           |
| 15       | 2.1285          | 3.2979          | - 2.1285        | 8.2012          | - 5.4429        | 3.7847          |
| 20       | 2.0402          | 3.1611          | - 2.0402        | 7.6221          | - 4.9907        | 3.3143          |
| 25       | 2.0127          | 3.1185          | - 2.0127        | 7.3857          | - 4.7978        | 3.1303          |

Example

Suppose it is required to compute the variance in the epoch estimate when  $N = 1500$ ,  $\frac{c \Delta t}{2} = .5 \text{ m}$  and  $\frac{c T_{\max}}{2} = 23 \text{ m}$ ,  $\sigma_n = 5 \text{ m}$  and  $a = 10 \text{ dB}$ . Now from Equation (A-58),

$$R^{-1}(\theta) = \alpha \beta \Delta t \ D^{-1} \ C^{-1} \ D^{-1} \quad (\text{A-67})$$

where  $D^{-1} = \text{diag} (a, \beta^{-1}, \beta)$  is a diagonal matrix.

Now,

$$\begin{aligned} d &= (\alpha \beta T_{\max} - 1) \left( \frac{a}{1+a} \right)^2 = \left( \frac{.3227 \ c T_{\max}}{2 \sigma_n} - 1 \right) \left( \frac{a}{a+1} \right)^2 \\ &= .4003 \end{aligned} \quad (\text{A-68})$$

From Table A-I,

$$F_{11} = 2.42, \ F_{12} = 3.75, \ F_{22} = 9.82$$

Thus

$$C^{\tau_o \tau_o} = 6.961$$

and

$$\sigma_{\tau_o \tau_o}^2 = [N^{-1} R^{-1}(\theta)]_{\tau_o \tau_o} = (\alpha \beta \Delta t) N^{-1} \beta^{-2} C^{\tau_o \tau_o}$$

or

$$\begin{aligned} \frac{c}{2} \sigma_{\tau_o} &= \sqrt{\alpha \left( \frac{c \Delta t}{2} \right) \sigma_h N^{-1} C^{\tau_o \tau_o}} \\ &= 6.1 \text{ cm} \end{aligned} \quad (\text{A-69})$$

**A.6 Bias in the MLE Due to Range Sidelobes**

In the satellite altimeter case, the MLE minimizes the penalty functional:

$$Q(V/\theta) = \sum_{j=1}^K [V_j / \bar{V}_j(\theta)] + \ln \bar{V}_j(\theta) \quad (\text{A-45})$$

where the summation is over range. In (A-45),  $\bar{V}_j(\theta)$  is a model of the mean power returned versus range. The model, of course, depends on  $\theta$  the vector of parameters to be estimated. The resulting estimate of  $\theta$  is a true MLE and will be unbiased only when the mean power model is complete and includes all significant parameters. In particular, the mean return model derived in Section 5.0 does not include the effect of range sidelobes. Therefore, when range sidelobes are significant, and a model such as proposed in Section 5.0 is used, the resulting estimate will not be a MLE, and will, in general, have biases. However, the estimate is still minimizing the functional (A-45), therefore the previously developed theory may be applied to compute the bias.

Recall from (A-7), the bias is given by:

$$E(\hat{\theta} - \theta) = -R^{-1}(\theta) E \epsilon(\theta) \quad (A-7)$$

where

$$R(\theta) = E \nabla \nabla^T Q(V/\theta) \quad (A-4)$$

and

$$E \epsilon(\theta) = E \nabla Q(V/\theta) \quad (A-5)$$

To apply (A-7), (A-4), and (A-5) to (A-45) let

$$E V_j = \tilde{V}_j$$

be the true returned power including the effects of range sidelobes.

Then,

$$\nabla Q(V/\theta) = \sum_{j=1}^K (V_j - \bar{V}_j) \bar{V}_j^{-2} \nabla \bar{V}_j \quad (A-70)$$

and

$$E \epsilon(\theta) = E \nabla Q(V/\theta) = \sum_{j=1}^K (\tilde{V}_j - \bar{V}_j) \bar{V}_j^{-2} \nabla \bar{V}_j \quad (A-71)$$

Differentiating (A-71) again, and taking expected values, one obtains:

$$\begin{aligned}
R(\theta) &= E \nabla \nabla^T Q(V/\theta) \\
&= - \sum_{j=1}^K (\bar{v}_j^{-2}) (\nabla \bar{v}_j) (\nabla \bar{v}_j)^T \\
&\quad + \sum_{j=1}^K (\tilde{v}_j - \bar{v}_j) \{ \bar{v}_j^{-2} \nabla \nabla^T \bar{v}_j - 2\bar{v}_j^{-3} \nabla \bar{v}_j \nabla^T \bar{v}_j \} \quad (A-72)
\end{aligned}$$

If the average sidelobe level is small, then one may assume:

$$\frac{\tilde{v}_j - \bar{v}_j}{\bar{v}_j} \ll 1 \quad (A-73)$$

Thus the second summation in Equation (A-72) is small compared to the first summation, and one has approximately:

$$R(\theta) \approx - \sum_{j=1}^K B_j B_j^T \quad (A-74)$$

where

$$B_j = \bar{v}_j^{-1} \nabla \bar{v}_j \quad (A-75)$$

Note that this is exactly the negative of the matrix which was evaluated in the last section. Thus, to evaluate the bias due to range sidelobes, one only needs evaluate  $E \epsilon(\theta)$  as given by Equation (A-71), and then evaluate Equation (A-7) using the matrix derived in the last section.

To evaluate the mean error signal as given by Equation (A-7), an expression for  $\tilde{v} - \bar{v}$  is required. This can be derived by including a uniform sidelobe level in the ambiguity function used in Section 5.0. That is, in Section 5.0 the ambiguity function was approximated by:

$$|\chi^2(t_1)| \simeq e^{-\frac{1}{2}(t_1/\sigma_T)^2} \quad (5.15)$$

If a uniform sidelobe level is added to the above expression, then one has:

$$|\chi^2(t_1)| \simeq e^{-\frac{1}{2}(t_1/\sigma_T)^2} + \gamma_1 \quad ; \quad |t_1| \leq T_u \quad (\text{A-76})$$

where  $T_u$  is the uncompressed pulse length, and  $\gamma_1$  is the average sidelobe level. In the approximation (A-76), only the far-out, uniform, range sidelobes are considered. This is felt to be a reasonable approach since the results in Section 4.2, on the split-gate tracker bias, indicate that the far-out sidelobes are the most important ones to consider.

If the approximation (A-76) is substituted into (5.13), and all the various variable changes required to get to Equation (5.19) are made, and if the main lobe contribution is subtracted, one obtains:

$$\tilde{V}(t) - \bar{V}(t) = \frac{\frac{1}{2}E_T G^2 \lambda^2 L O^2 G_o B}{(4\pi)^3 H_o^3 (1+H_o/a_e)} \bullet I_3 \quad (\text{A-77})$$

where  $I_3$  is the integral:

$$I_3 = 2\pi\gamma_1 \int_0^{\frac{H\pi^2}{8}} dx \gamma(x) A^2(x) \int_{c/2(t-\tau_o-T_u)}^{c/2(t-\tau_o+T_u)} d\Delta R \eta_{ph} \left(\frac{x-\Delta R}{\sigma_h}\right) \quad (\text{A-78})$$

where all the various symbols are defined in Section 5.0. Assuming that  $\frac{c}{2}T_u \gg \sigma_h$ , then the second integral above can be evaluated approximately as:

$$\int_{\frac{c}{2}(t-\tau_o-T_u)}^{\frac{c}{2}(t-\tau_o+T_u)} d\Delta R \eta_{ph} \left(\frac{x-\Delta R}{\sigma_h}\right) \approx 1 \quad ; \quad \frac{c}{2}(t-\tau_o-T_u) \leq x \leq \frac{c}{2}(t-\tau_o+T_u) \quad (\text{A-79})$$

Thus the integral  $I_3$  becomes:

$$I_3 = (2\pi)\gamma_1 \int_{x_{\min}}^{x_{\max}} dx \gamma(x) A^2(x) \quad (\text{A-80})$$

where:

$$x_{\min} = \text{Max} [0, c/2(t - \tau_o - T_u)]$$

$$x_{\max} = \text{Max} [0, c/2(t - \tau_o + T_u)]$$

By Equation (5.25)  $\gamma(x) A^2(x)$  can be written:

$$\gamma(x) A^2(x) = \exp [-(8 \ln 2 / H\theta_e^2)x] \quad (5.25)$$

Thus  $I_3$  becomes:

$$I_3 = \frac{2\pi \gamma_1 H\theta_e^2}{8 \ln 2} \left\{ 1 - \exp \left[ -\frac{8 \ln 2}{H\theta_e^2} \left( \frac{c}{2} (t - \tau_o + T_u) \right) \right] \right\} \quad (A-81)$$

where it has been assumed that only those times for which  $x_{\min} = 0$  and  $x_{\max} \neq 0$  are of interest (i.e.,  $|t - \tau_o| < T_u$ ).

Substituting (A-81) into (A-77) yields:

$$\tilde{V}(t) - \bar{V}(t) = \frac{\frac{1}{2} E_T G^2 \lambda^2 L \sigma^o G_o B}{(4\pi)^3 H_o^3 (1 + H_o/a_e)} (2\pi) \gamma_1 \frac{H\theta_e^2}{8 \ln 2} \left( 1 - \exp \left[ \frac{8 \ln 2}{H\theta_e^2} \frac{c(t - \tau_o + T_u)}{2} \right] \right) \quad (A-82)$$

Now, from Equation (5.32), the signal-to-noise ratio is given by:

$$a = \frac{\frac{1}{2} E_T G^2 \lambda^2 L \sigma^o G_o B (2\pi)^{3/2} \sigma_R}{(4\pi)^3 H_o^3 (1 + H_o/a_e) (\frac{1}{2} k T_o F_n G_o B)} \quad (A-83)$$

Substituting into (A-82) yields:

$$\tilde{V}(t) - \bar{V}(t) = \frac{a}{\sqrt{2\pi} \sigma_R} \gamma_1 \frac{H\theta_e^2}{8 \ln 2} \left\{ 1 - \exp \left[ -\left( \frac{8 \ln 2}{H\theta_e^2} \right) \frac{c}{2} (t - \tau_o + T_u) \right] \right\} \quad (A-84)$$

where (as before) it is assumed that the noise power has been normalized to unity (i.e.,  $\frac{1}{2} k T_o F_n G_o B = 1$ ). In most cases of interest, it may be assumed that:

$$\frac{c(t - \tau_o)}{2} \ll \frac{H\theta_e^2}{8 \ln 2} \frac{df}{\mu} \quad (A-85)$$

That is, the range over which the return is sampled is much smaller than the effective depth of the antenna beam. Here, the depth of the beam is defined as the range change on the earth's surface between the center and the edge of the antenna beam. In the above expression,  $\mu^{-1}$  is the depth of the beam divided by  $\ln 2$ .

With this assumption, the difference in the return due to side-lobes can be written:

$$\begin{aligned} \tilde{V}(t) - \bar{V}(t) &= \frac{a\gamma_1 \mu^{-1}}{\sqrt{2\pi} \sigma_R} \left( 1 - e^{-\frac{c(t - \tau_0 + T_u)}{2\mu^{-1}}} \right) \\ &\approx \frac{a\gamma_1 \mu^{-1}}{\sqrt{2\pi} \sigma_R} \left[ 1 - \exp(-cT_u/2\mu^{-1}) + \exp(-cT_u/2\mu^{-1}) [c(t - \tau_0)/2\mu^{-1}] \right] \quad (A-86) \end{aligned}$$

Making the change of variable,  $Z = \alpha\beta(t - \tau_0) + \frac{1}{2} + 1/a$ , and doing some manipulation yields finally:

$$\tilde{V} - \bar{V} \approx a g_1 [g_2 + Z] \quad (A-87)$$

where

$$g_1 = \frac{\gamma_1 \alpha_h}{2\pi \sigma_R \alpha} e^{-\left(\frac{c}{2\mu^{-1}} T_u\right)} \quad (A-88)$$

$$g_2 = \left[ \frac{\alpha\mu^{-1}}{\alpha_h} \left( e^{\frac{c}{2\mu^{-1}} T_u} - 1 \right) \right] - \frac{1}{2} - \frac{1}{a} \quad (A-89)$$

Substituting this expression into Equation (A-71) gives the following expression for the mean error signal:

$$\begin{aligned} E \epsilon(\theta) &= \sum_{j=1}^K \frac{\tilde{V}_j - \bar{V}_j}{\bar{V}_j} \frac{\nabla \bar{V}_j}{\bar{V}_j} = \sum_{j=1}^K \frac{\tilde{V}_j - \bar{V}_j}{\bar{V}_j} B_j \quad (A-90) \\ &\approx \frac{g_1}{\alpha\beta \Delta t} \int_{1/a}^{1+1/a} \left(1 + \frac{g_2}{Z}\right) B(Z) dZ + \frac{a}{a+1} \int_{1+1/a}^{\alpha\beta T_{\max} + \frac{1}{2} + 1/a} (g_2 + Z) B(Z) dZ \end{aligned}$$

where  $B(Z)$  was defined by Equation (A-75). The above integrals can be evaluated in closed form; the manipulations involved are fairly tedious, but straightforward, and will not be repeated here. The results are:

$$\begin{aligned} \epsilon_a &= \left[ \frac{g_1}{\alpha\beta \Delta t a} \right] \left[ 1 + \left(g_2 - \frac{1}{a}\right) \log(1+a) - \frac{g_2 a}{1+a} + \left(\frac{a}{1+a}\right)^2 g_2 (\alpha\beta T_{\max} - \frac{1}{2}) \right. \\ &\quad \left. + \frac{1}{2} \left(\frac{a}{1+a}\right)^2 (\alpha\beta T_{\max} + \frac{1}{2} + \frac{1}{a})^2 - \frac{1}{2} \right] \\ \epsilon_{\tau_0} &= \frac{-g_1}{\Delta t} \left( \log(1+a) + \frac{g_2 a^2}{1+a} \right) \\ \epsilon_\beta &= \frac{g_1}{\alpha\beta^2 \Delta t} \left[ 1 + \left(g_2 - \frac{a+2}{2a}\right) \log(1+a) - \frac{g_2(a+2)a}{2(a+1)} \right] \end{aligned} \quad (A-91)$$

These equations appear to involve too many parameters to easily tabulate or graph them. Therefore, they were programmed, and the bias errors were computed for a typical case of interest. For this table, the satellite height was 725 km, the (one-way) beamwidth was  $5^\circ$ , and the side-lobe level was -50 dB.

The  $5^\circ$  beamwidth is larger than what is proposed for SEASAT; however, the broader beam represents a "worst" case in that biases due to range sidelobes increase as the antenna beamwidth is increased. Further, the results in Section 5.0 indicate that the approximation (A-50) is not valid since it does not include "beamwidth roll-off". It should be noted that in a three loop tracker, which does not compensate for beamwidth roll-off, bias errors will develop. These biases are likely to be more significant than those due to range sidelobes. Unfortunately, funds on this contract ran out before this effect could be evaluated.

As stated earlier, Table A-2 shows the effect of range sidelobe errors. A surprising feature of the table (in view of the complexity of the equations) is that the results are independent of signal-to-noise

ratio, and that the epoch and wave height errors scale in proportion to RMS wave height. These results have not been verified analytically, but if they do hold generally, the biases have the simple form\*:

$$\Delta \tau_o \approx 880 \left( \frac{2 \sigma_h}{c} \right) \gamma_1$$

$$\Delta \sigma_h \approx 600 \sigma_h \gamma_1$$

$$\Delta a \approx 600 a \gamma_1$$

---

\* It can be shown analytically that the biases are proportional to average sidelobe level,  $\gamma_1$ .

Table A-2

MLE Altimeter Bias Due to Range Sidelobes

Average Sidelobe Level = -50 dB  
 Antenna Beamwidth = 5° (one way)  
 Satellite Altitude = 725 km

Epoch Error (cm)

| S/N (dB) | 5    | 10   | 20   | Sig. Waveheight (m) |
|----------|------|------|------|---------------------|
| 0        | -1.1 | -2.2 | -4.5 |                     |
| 5        | -1.1 | -2.2 | -4.5 |                     |
| 10       | -1.1 | -2.2 | -4.5 |                     |
| 20       | -1.1 | -2.2 | -4.5 |                     |

Waveheight Error (cm)

| S/N (dB) | 5   | 10  | 20  | Sig. Waveheight (m) |
|----------|-----|-----|-----|---------------------|
| 0        | .75 | 1.5 | 3.0 |                     |
| 5        | .75 | 1.5 | 3.0 |                     |
| 10       | .75 | 1.5 | 3.0 |                     |
| 20       | .75 | 1.5 | 3.0 |                     |

S/N Error (dB)\*

| S/N (dB) | 5   | 10  | 20  | Sig. Waveheight (m) |
|----------|-----|-----|-----|---------------------|
| 0        | .03 | .03 | .03 |                     |
| 5        | .03 | .03 | .03 |                     |
| 10       | .03 | .03 | .03 |                     |
| 20       | .03 | .03 | .03 |                     |

\* The quantity in the above table is  $10 \log (1 + \Delta SN/SN)$ .

## REFERENCES

- (1) R. P. Dooley, F. E. Nathanson, L. W. Brooks, "Study of Radar Pulse Compression for High Resolution Satellite Altimetry," NASA CR # 137474, May 1, 1973.
- (2) R. P. Dooley, L. W. Brooks, "Description and Preliminary Sizing of the MLP Processor for SEASAT-A," Technology Service Corporation Presentation to NASA, Langley, June 26, 1974.

Part II  
OCEAN WAVE SPECTRA

1.0 INTRODUCTION AND SUMMARY

In Part I, the design of a high resolution radar for altimetry and wave height estimation was discussed. The feasibility of utilizing this same radar for the measurement of ocean wave spectra as well is examined in this part of the report. A preliminary design analysis shows the resulting system parameters for the ocean wave spectrometer to correspond very closely to those of the radar altimeter design.

Section 2.0 examines the implementation and design of a high resolution radar for the measurement of directional ocean wave spectra. Commonality of the implementation with that of the radar altimeter leads to the recommendation of a short pulse wide-band radar technique instead of the mathematically equivalent two frequency correlation technique. Both techniques perform a spectral analysis of the amplitude modulation (caused by ocean waves) on the return signal at a given analysis direction. A preliminary analysis and design shows that the required modifications to the radar altimeter design which will allow the system to measure wave spectra are that the transmitter output is switched to a 2 meter antenna which is steered  $20^{\circ}$  away from nadir and scanned conically with a period of 5 sec. On receive the full deramp processor is replaced by a surface wave pulse compressor and detector followed by a band of 11 one-third (1/3) octave filters to perform the spectral analysis. The filter outputs are then detected and integrated for 26  $\mu$ sec per pulse. While this preliminary design meets all the specified performance requirements, it is based primarily on compatibility with the radar altimeter and probably does not represent an optimum configuration. A more detailed study of the trade-offs in achieving an optimum configuration is recommended.

Section 3.0 provides the preliminary analysis of the directional wave spectrometer upon which much of the system design is based. The analysis should be considered a quick "first cut" at the problem because of the many simplifying assumptions required in a study of this size. Nevertheless, the overall

approach, considerations, and conclusions are believed to be correct. It is shown that the input to the spectrum analyzer consists of two noise processes, one being the desired modulation of  $\sigma^{\circ}$  due to the gravity wave spectrum of the ocean surface and the other due to the fact that the modulation is riding on a noise process whose mean is  $\sigma^{\circ}$ . Standard statistical theory for the detection of a Gaussian signal in Gaussian noise is used to develop approximate expressions for the signal-to-noise ratio necessary for reliable detection of the modulation and resulting design constraint. It is shown that the problem of measuring ocean wave length is analogous to the beam limited satellite altimeter problem. Results developed during the TSC altimeter study are then used to establish the resulting design equation for measurement accuracy. As with the altimeter, measurement accuracy improves with S/N ratio up to a point, after which further increases in S/N provide little improvement (saturation effect). In the wave spectrometer, this effect occurs at unity signal-to-noise into the spectrum analyzer,  $(S/N)_{isa}$ . Furthermore to achieve unity  $(S/N)_{isa}$  with a 2 dB modulation, it is necessary to resolve to the order of a 19th of a (water) wavelength.

In addition to altimetry and wave height, a high resolution satellite radar may also be used to measure directional wave spectra. A nominal performance requirement for such an instrument is the measurement of spatial frequencies from 50 meters to 400 meters with an accuracy of 25%. This requirement is then compatible with a wave height measurement of 2.5 to 20 meters (peak-to-trough) with an accuracy of 25% since wave period is approximately twenty times peak-to-trough wave height. A directional resolution of at least ( $18^\circ$ ) is also assumed as a nominal requirement.

There are at least three types of satellite radar implementations capable in principle of achieving the above directional ocean wave spectra requirements. First, there is the high resolution side looking imaging radar. With this technique both image and directional wave spectra are continuously measured along the strip illuminated by the side looking antenna. The other two radar techniques provide a more coarse measurement of ocean wave spectra with a corresponding significant reduction in output data rate when compared to the radar imaging technique. The two frequency correlation technique of Ruck, Barrick and Kaliszewski<sup>(1)</sup> and the short pulse wide-band radar technique discussed by Tomiyasu<sup>(2)</sup> are in fact mathematically equivalent. Both techniques perform a spectral analysis of the amplitude modulation (caused by ocean waves) on the return signal at a given analysis direction. A slow mechanically conical scanned antenna then permits the spectral measurement to be performed every  $\Delta\theta^\circ$  over the full  $360^\circ$  scan.

The choice of implementing the short pulse wide-band radar technique is based primarily on the commonality of the implementation with that of the radar altimeter. In fact, a preliminary design analysis shows the resulting system parameters to correspond very closely to those of the altimeter design. The projected altimeter design can be fairly easily modified to perform ocean wave spectra measurements. The major modifications to the altimeter design which will allow it to measure directional surface spectra are:

1. The transmitter output is switched to the 2 meter antenna. The antenna beam is then steered  $20^\circ$  away from nadir and scanned conically with a period of 5.0 seconds.
2. On receive the current full deramp processor is replaced by a surface wave pulse compressor. The compressed pulse output is detected and passed through a bank of 11 one-third ( $1/3$ ) octave\* filters which span the frequency range of 1 MHz to 9.0 MHz in logarithmic steps. The filter outputs are then detected and integrated for 26  $\mu$ sec per pulse.

## 2.1 Basic Principles and Recommended Approach

The basic purpose of this instrument is to measure the significant lower end (50-400 meters) of the gravity wave spectrum of the ocean surface as a function of angular direction. For an off nadir looking radar this requires the measurement of the low frequency portion of the spectrum of the mean power response of a matched filter receiver. This mean power response is the radar cross-section versus range,  $\sigma(R)$ , which for a large enough off nadir look angle ( $20^\circ$  for the present SEASAT-A geometry) will contain an amplitude modulation spectrum corresponding to the gravity wave spectrum.

As described in section 2.0 of Part I of this report, a two frequency correlation technique measures the Fourier transform of  $\sigma(R)$  as a function of frequency separation  $\Delta f$  thus providing a direct measure of the desired amplitude modulation spectrum. A rigorous theoretical development of this technique for the measurement of ocean wave surface spectra is given in reference (1). With the short pulse radar technique (2),  $\sigma(R)$  is measured at the output of the matched filter receiver and hence must be further processed (spectrum analyzed) in order to obtain the desired amplitude modulation spectrum. As mentioned previously, both techniques are mathematically equivalent and simply represent different implementations of the same measurement process. The short pulse radar technique is chosen only because of the commonality of equipment with

---

\* A  $1/3$  octave filter has a bandwidth which is 25% of its center frequency.

the short pulse altimeter. The following gives a rather simplistic view of the principles involved in the measurement of ocean surface spectra by means of a short pulse satellite radar.

Consider a short pulse satellite radar looking at some angle  $\theta_0$  off nadir in the direction normal to the ocean wave (upwind or downwind) as illustrated in Figure 2.1. Then, as shown, there is a decrease in resolution along the surface  $\Delta X$  inversely proportional to the off nadir angle  $\theta_0$  i.e.  $\Delta R = \frac{c\tau}{2}$  and  $\Delta X = \frac{c\tau}{2 \sin \theta_0}$ . Thus in order to faithfully produce an amplitude modulation on  $\sigma(R)$  corresponding to the smallest spatial frequency of interest (50 meters) requires that  $\Delta X \simeq 25$  meters. Note, however, that even if the pulse width  $\tau$  were a delta function; the amplitude modulation of  $\sigma(R)$  can be distorted at large wave heights (peak-to-trough) if  $\theta_0$  is made too small. For 20 meter peak-to-trough wave heights this consideration places a lower bound on  $\theta_0$  at  $8^\circ$ . But the differential path length at the edge of the beam must also be on the order of the smallest wave period of interest. This length

$$\Delta \ell = \frac{H (1 - \cos \theta_{B/2})}{\cos \theta_0 \sin \theta_0} ,$$

which for a 2 meter antenna is about 50 meters at  $\theta_0 = 20^\circ$ . It is this consideration then that places the lower bound on  $\theta_0$  at about  $20^\circ$ .

At this  $20^\circ$  off nadir angle the previous range resolution consideration ( $\Delta X \simeq 25$  meters) places a constraint on the maximum pulse length  $\tau$  at about 57 nsec. However, in order to have adequate S/N to detect small peak-to-peak amplitude modulations on the return it is required that

$$\frac{1}{B_m \tau_c} \geq \frac{1}{\gamma^2}$$

where the peak-to-peak modulation is given by

$$m = \frac{1 + \gamma}{1 - \gamma} , \quad \tau_c = \text{compressed pulse width,}$$

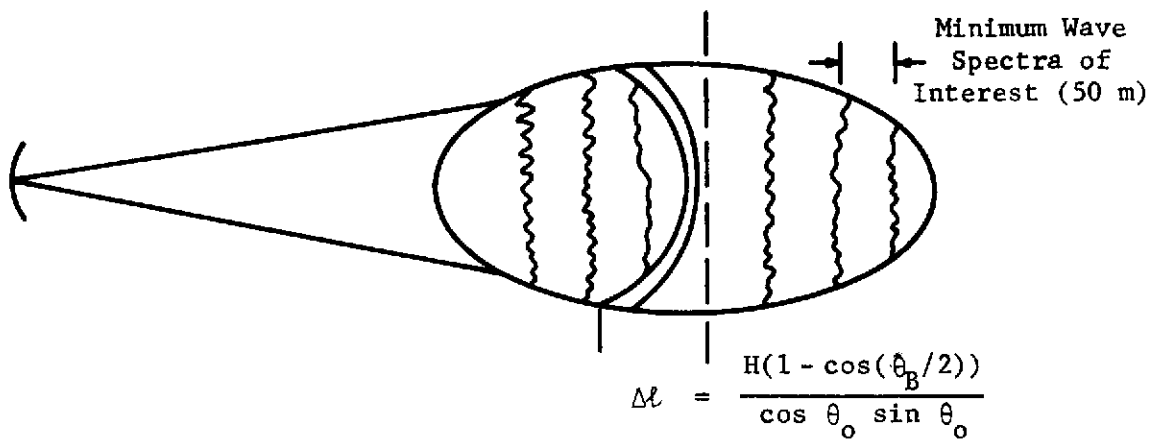
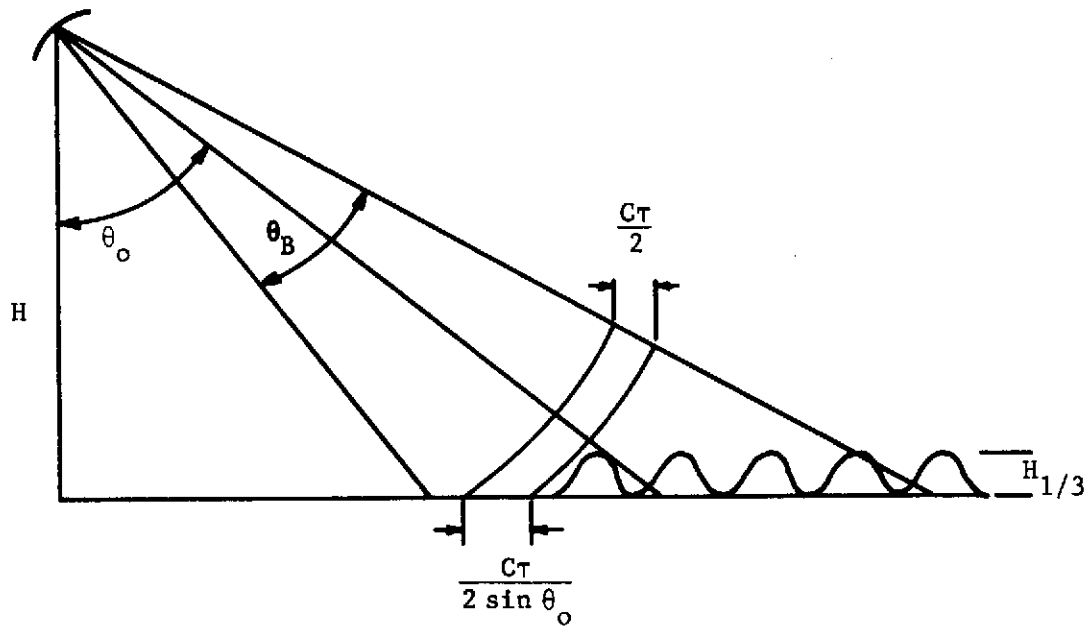


Figure 2.1 High Resolution Radar Geometry and Constraints for Measuring Ocean Surface Spectra

and  $B_m$  is the bandwidth of the modulation. For ocean wave spectra the bandwidth is about equal to the frequency. Assuming the detection of a 2 dB modulation as a reasonable design goal, this consideration places the maximum pulse width at 6.0 nsec (for  $B_m = 9.0$  MHz corresponding to 50 meter wave periods).

Under the conditions described above the output of the matched filter would appear as illustrated in Figure 2.2. The modulation of course would not have the regularity illustrated in the figure. Since spatial frequencies,  $\ell$ , of 50 to 400 meters are to be measured, the corresponding modulation frequencies of interest are from 9.0 MHz to 1.0 MHz since the relationship between the two is given by

$$f = \frac{c}{2 \sin \theta_o \ell} \cdot$$

Since the bandwidth of the modulation is approximately equal to  $f$ , a spectral analysis of this modulation by means of filters spaced at logarithmic intervals would seem to be a logical choice. With this selection, 11 filters having a 1/3 octave bandwidth are sufficient to cover the 1.0 to 9.0 MHz frequency band of interest as shown in Figure 2.3.

## 2.2 System Design Summary

The preliminary design of a high resolution satellite radar for measuring directional ocean wave spectra is described in the following tables. This design meets all the specified performance requirements. These performance requirements are summarized in Table 2.1 and the system design is summarized in Table 2.2. The design presented in Table 2.2 was selected on the basis of compatibility with the altimeter design and as such probably does not represent an optimum configuration. A study to determine the trade offs involved in achieving an optimum configuration should be made during the initial phase of the program. A block diagram of the system is shown in Figure 2.4 and Table 2.3 presents a preliminary power budget for this sensor.

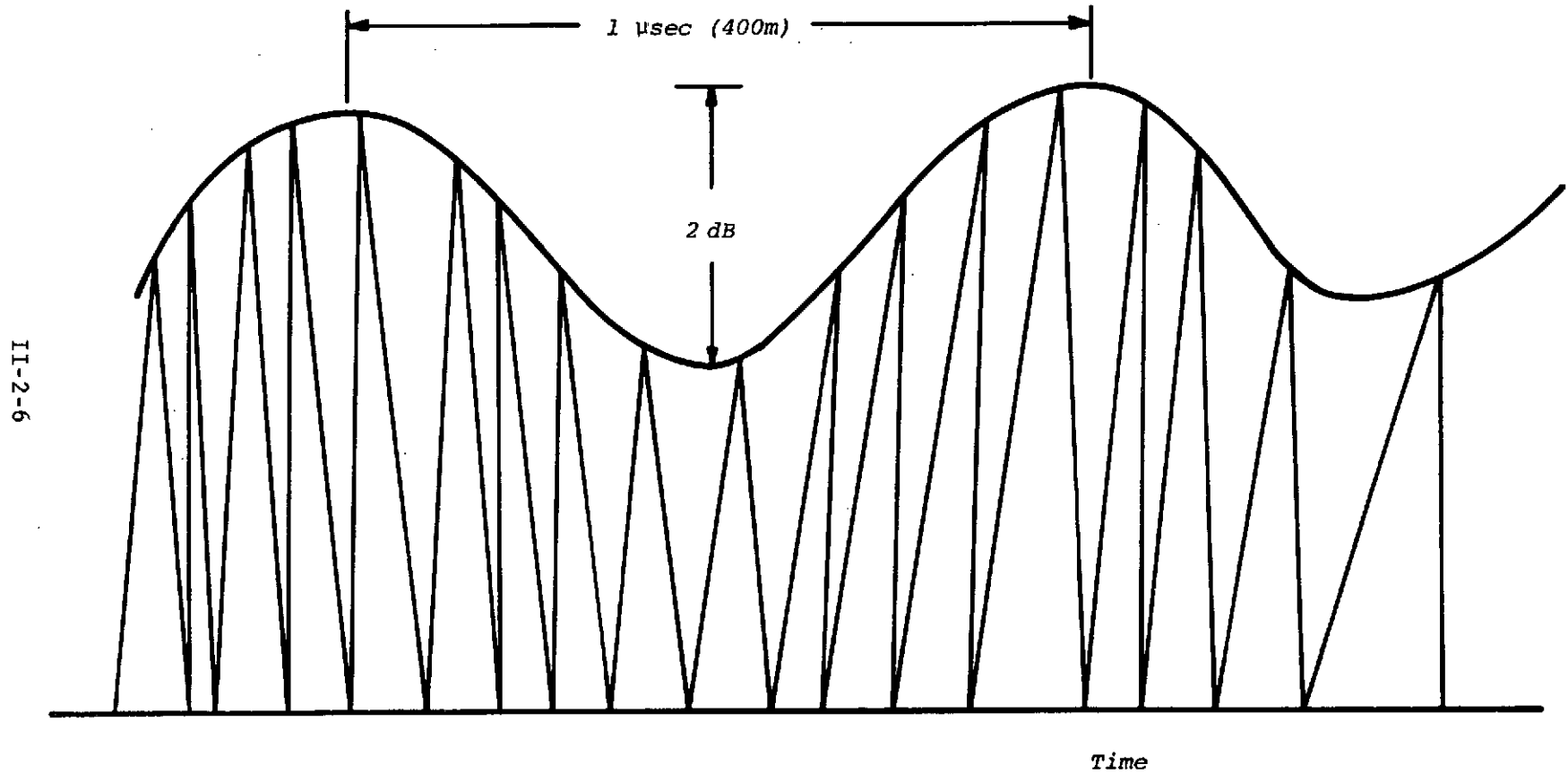


Figure 2.2 An Illustration of the Amplitude Modulation  $\sigma(R)$  Due to Wave Spectra

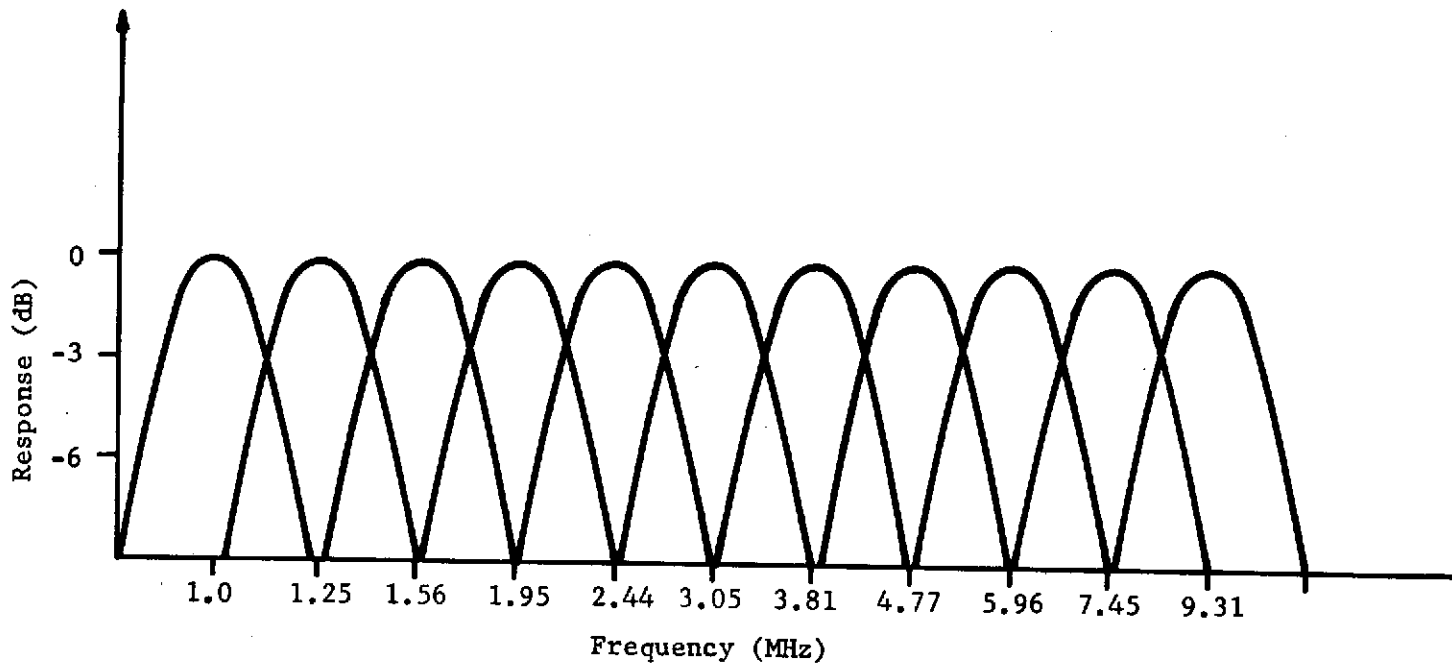


Figure 2.3 Selected Filter Bank

Table 2.1

System Performance Requirements

|      |                            |
|------|----------------------------|
| I.   | Ocean Wave Spectra         |
|      | Range 50-400 m             |
|      | Accuracy 25%               |
| II.  | Angular Directivity        |
|      | Range 360°                 |
|      | Resolution 18° (5%)        |
| III. | Detectable Modulation 2 dB |

Table 2.2  
Design Summary

|      |   |                          |
|------|---|--------------------------|
| I.   | <u>Orbit Parameters</u>   |                          |
|      | a) Height   | 725 km                   |
|      | b) Inclination  | 90° retrograde           |
|      | c) Eccentricity   | 0.0064 maximum           |
| II.  | <u>Radar Parameters</u>   |                          |
|      | a) Antenna beamwidth  | 0.8° (2m dish)           |
|      | b) Pointing accuracy  | $2\sigma_{\theta} = 0.1$ |
|      | c) Antenna gain   | 46.7 dB                  |
|      | d) Peak power   | 2 kW                     |
|      | e) System losses (other than processing losses in pulse compressor) | 5 dB                     |
|      | f) Noise figure   | 5.5 dB                   |
|      | g) Frequency  | 13.9 GHz                 |
|      | h) Uncompressed pulse width   | 5.6 $\mu$ s              |
|      | i) Uncompressed pulse bandwidth                                     | 180 MHz                  |
|      | j) Compressed pulse width   | 6.0 ns                   |
|      | k) Compression ratio  | 1000/1                   |
|      | l) PRF  | $\geq 400$ Hz            |
|      | m) S/N (single pulse)   | 3.0 dB                   |
|      | n) Ocean cross section  | -10 dB                   |
|      | o) Scan period  | 5 sec                    |
|      | p) Number of footprints in 360°                                     | 154                      |
| III. | <u>Linear FM Generation</u>   |                          |
|      | Type  | Surface wave             |
|      | Bandwidth   | 180 MHz                  |
|      | Pulse length  | 5.6 $\mu$ s              |
|      | Linearity of FM   | $\leq 0.2\%$             |
|      | Peak frequency deviation (one circle of variation across pulse)     | 25 kHz                   |
| IV.  | <u>Pulse Compression</u>  |                          |
|      | Type  | Surface wave             |
|      | Bandwidth   | 167 MHz                  |
|      | Weighting   | -26 dB modified Taylor   |
|      | Processing loss   | 0.55 dB                  |
| V.   | <u>Spectral Processing</u>  |                          |
|      | Type  | Filter band              |
|      | Number of filters   | 11                       |
|      | Frequency range   | 1.0 to 9.0 MHz           |
|      | Filter spacing  | Logarithmic              |
|      | Filter bandwidth  | 1/3 octave               |
|      | Integration time  | 25 $\mu$ s               |

II-2-10

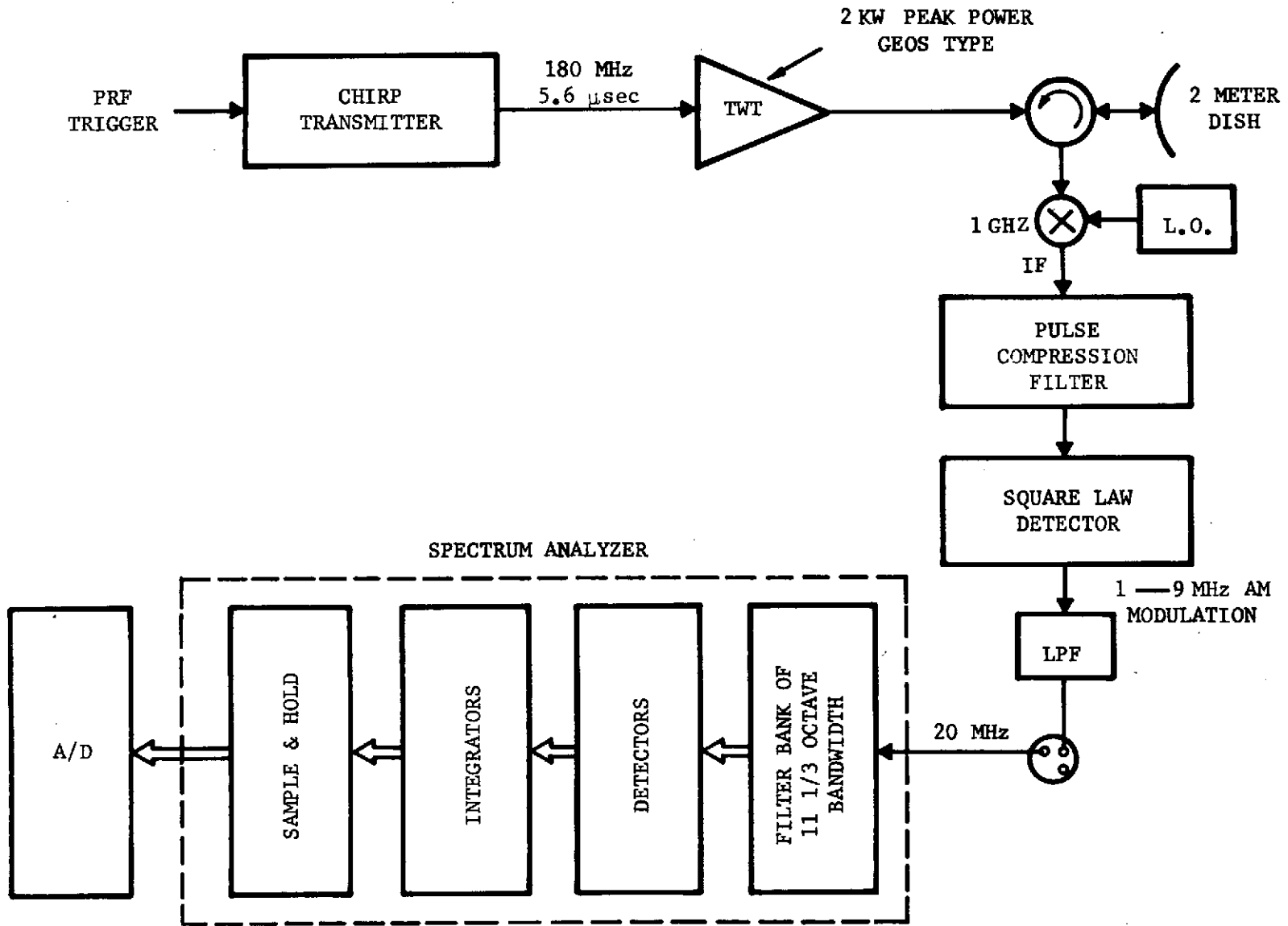


Figure 2.4 High Resolution Radar Block Diagram

Table 2.3  
Signal-to-Noise Computation

|   |                          |
|---|--------------------------|
| $\frac{S}{N} = \frac{\pi P_t \frac{c\tau}{2 \sin \theta_o} L_g^2 L_s}{4^3 \lambda \left(\frac{H}{\cos \theta_o}\right)^3 K T_o F_N \frac{k}{\tau}} \sigma_o D^3 CR$ |                          |
| $P_t$   | 33 dBW                   |
| $\frac{c\tau}{2 \sin \theta_o}$   | 4.2 dB/m                 |
| $\frac{L_g^2 L_s}{k}$   | -5.5 dB                  |
| $\frac{\pi}{4^3}$   | -13.09 dB                |
| $\lambda$   | -16.65 dB/m              |
| $\left(\frac{H}{\cos \theta_o}\right)^3$  | 176.62 dB/m <sup>3</sup> |
| $K T_o$   | -204 dBW                 |
| $F_N$   | 5.5 dB                   |
| $\frac{1}{\tau}$  | 82.218 dB/s              |
| $CR$  | 30 dB                    |
| $D^3$   | 9.03 dB/m <sup>3</sup>   |
| $\frac{S}{N}$   | 13.952 dB + $\sigma_o$   |

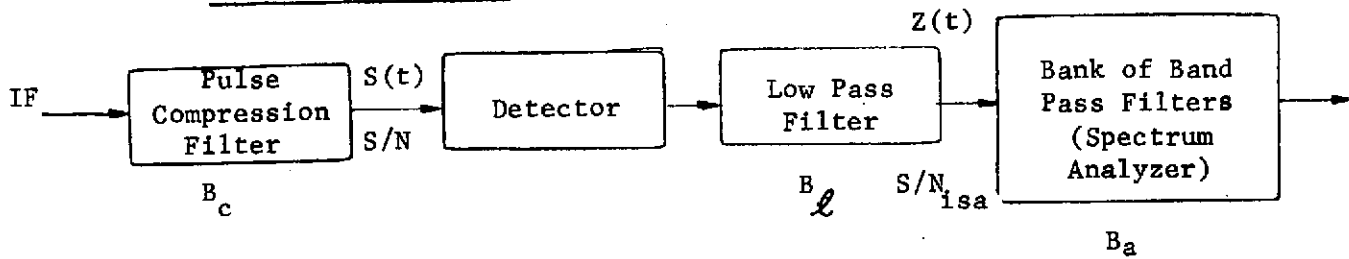
This section of the report describes the analysis of a directional wave spectrometer upon which much of the material presented in the previous section is based. While the overall approach and considerations presented here are believed to be correct, the following analysis should be considered a quick "first cut" at the problem because of the many simplifying and/or unsubstantiated assumptions.

In section 3.1, the required receiver processing and underlying assumptions are established and used to develop design equations for the signal-to-noise ratio necessary for detection of the modulation caused by the gravity wave spectrum of the ocean surface. It is shown that the input to the spectrum analyzer consists of two noise processes, one being the desired modulation of  $\sigma^{\circ}$  and the other due to the fact that the modulation is riding on a noise process whose mean is  $\sigma^{\circ}$ . Standard statistical theory for the detection of a Gaussian signal in the presence of Gaussian noise is then used to develop an approximate expression for the resulting design constraint.

In section 3.2, an expression for the standard deviation of the ocean wavelength measurement is derived. It is shown that the problem of measuring ocean wavelength is just the satellite altimeter (beam limited) problem in disguise. Results developed during the TSC altimeter study are then used to establish the resulting design equation for measurement accuracy. As with the altimeter, a saturation effect occurs when the "signal-to-noise" into the spectrum analyzer,  $(S/N)_{isa}$ , is near unity. Thus, a further increase in  $(S/N)_{isa}$  beyond this value provides little improvement in measurement accuracy. However, the  $(S/N)_{isa}$  is found to be a function of modulation index,  $\gamma$ , and the number of resolution cells per ocean wavelength. To achieve unity  $(S/N)_{isa}$  with a 2 dB (peak-to-peak) modulation it is necessary to resolve to the order of a 19th of a (water) wavelength.

### 3.1 Detection of Modulation on a Noise Process

#### 3.1.1 Assumed Processing



At the output of the pulse compression filter the signal is given by:

$$S(t) = [N + S + \gamma S m(t)]^{\frac{1}{2}} [a(t)] \cos(\omega t + \phi(t)) \quad (3.1)$$

where

- N is the mean noise power
- S is the mean signal power
- $m(t)$  is the modulation of the received signal power
- $\gamma$  is a modulation index
- $a(t)$  is a Rayleigh process
- $\phi(t)$  is a random phase

Then,  $a(t) \cos \phi(t)$  and  $a(t) \sin \phi(t)$  are independent Gaussian processes with bandwidth,  $B_c$ , equal to the pulse bandwidth.  $a(t)$  is assumed to have unity power.

Let  $B_l$  be the bandwidth of the low pass filter. Assume that:

$$B_c > B_l$$

But

$$B_l \gg B_m$$

where  $B_m$  is the bandwidth of the modulation process  $m(t)$ .

After detection and low pass filtering:

$$z(t) = \int s^2(t-\tau)h(t)dt \quad (3.2)$$

$$\approx [N+S+\gamma Sm(t)] \int a^2(t-\tau)\cos^2(\omega(t-\tau)+\phi(t-\tau))h(t)dt$$

where  $[N+S+\gamma Sm(t)]$  is taken outside the integral since it is assumed  $m(t)$  is constant over the response time of the filter ( $B_c > B_\ell$ ).

The integral:

$$q(t) = \int a^2(t-\tau)\cos^2(\omega(t-\tau) + \phi(t-\tau))h(t)dt \quad (3.3)$$

Represents the result of passing the square of a narrow band Gaussian process  $(a(t)(\cos \omega t + \phi(t)))$  through a low pass filter. The result of such an operation is to yield a Chi-square process with  $2 (B_c/B_\ell)$  degrees of freedom.

But the Chi-square process can be approximated by a normal process with mean  $2(B_c/B_\ell)$  and variance  $4(B_c/B_\ell)$

Let

$$q(t) \approx 2 \frac{B_c}{B_\ell} + 2 \sqrt{\frac{B_c}{B_\ell}} \quad \eta(t) \quad (3.4)$$

where  $\eta(t)$  is a unit variance normal process.

Thus

$$Z(t) \approx [(N+S) + \gamma Sm(t)] \left[ 2 \frac{B_c}{B_\ell} + 2 \sqrt{\frac{B_c}{B_\ell}} \quad \eta(t) \right] \quad (3.5)$$

$$= (N+S) 2 \left( \frac{B_c}{B_\ell} \right) + 2\gamma S \frac{B_c}{B_\ell} m(t) + (N+S) 2 \sqrt{\frac{B_c}{B_\ell}} \quad \eta(t)$$

$$+ 2\gamma S \sqrt{\frac{B_c}{B_\ell}} \begin{matrix} \nearrow \text{negligible} \\ m(t) \eta(t) \end{matrix} \quad (3.6)$$

That is, the cross product is negligible since

$$\gamma < 1$$

and

$$\sqrt{\frac{B_c}{B_\ell}} \ll \frac{B_c}{B_\ell}$$

Thus

$$Z(t) \approx 2(N+S) \frac{B_c}{B_\ell} + 2\gamma S \left(\frac{B_c}{B_\ell}\right) m(t) + 2(N+S) \sqrt{\frac{B_c}{B_\ell}} \eta(t) \quad (3.7)$$

↑ DC                      ↑ Signal                      ↑ Noise

Thus using this approximation, the input to the spectrum analyzer consists of a DC bias plus two Gaussian noise processes ( $m(t)$  is simply assumed to be Gaussian). The process  $m(t)$  is the desired modulation, and the process  $\eta(t)$  is due to the fact that the modulation is riding on a (nearly white) noise process.

Define

$$2\gamma S \frac{B_c}{B_\ell} m(t) \text{ as "Signal"}$$

$$2(N+S) \sqrt{\frac{B_c}{B_\ell}} \eta(t) \text{ as "Noise"}$$

Then the signal to noise ratio into the spectrum analyzer is given by:

$$(S/N)_{isa} = \frac{\left[ \gamma S \left( \frac{B_c}{B_\ell} \right) \right]^2 \left[ S_m(\omega) \right]}{\left[ (N+S) \sqrt{\frac{B_c}{B_\ell}} \right]^2 \left[ S_\eta(\omega) \right]} \quad (3.8)$$

Where  $S_m(\omega)$  is the spectral density of the modulation process and  $S_\eta(\omega)$  is the spectral density of the noise process.

Assuming band limited processes

$$S_m(\omega) = \frac{1}{B_m} \quad (3.9)$$

and

$$S_\eta(\omega) = \frac{1}{B_\ell} \quad (3.10)$$

Recall that things are defined so that  $m$  and  $\eta$  have unit power.

Thus

$$(S/N) = \gamma^2 \left( \frac{S}{S+N} \right)^2 \left( \frac{B_c}{B_\ell} \right) \frac{B_\ell}{B_m} \quad (3.11)$$

or

$$(S/N)_{isa} = \gamma^2 \left( \frac{S}{N+S} \right)^2 \left( \frac{B_c}{B_m} \right) \quad (3.12)$$

### 3.1.2 Detection Criteria

Now the detection index<sup>(3)</sup> for detecting Gaussian signal in the presence of Gaussian noise is:

$$d = B_a T (S/N)^2 \quad (3.13)$$

where  $B_a$  is the analysis bandwidth, and  $T$  is the total analysis time. i.e.,  $B_a$  is the bandwidth of a filter in the spectrum analyzer, and  $T$  is the total integration time. Then

$$T \approx \left( \frac{2H\theta_B \sin\theta_o}{c \cos^2\theta_o} \right) N_p \quad (3.14)$$

where  $N_p$  is the number of pulses averaged in the spectrum analyzer.

Good detection<sup>(3)</sup> requires that

$$d > 25$$

Thus

$$\sqrt{B_a \frac{2H\theta_B \sin\theta_o}{c \cos^2\theta_o} N_p} \gamma^2 \left(\frac{S}{N+S}\right)^2 \left(\frac{B_c}{B_m}\right) > 5 \quad (3.15)$$

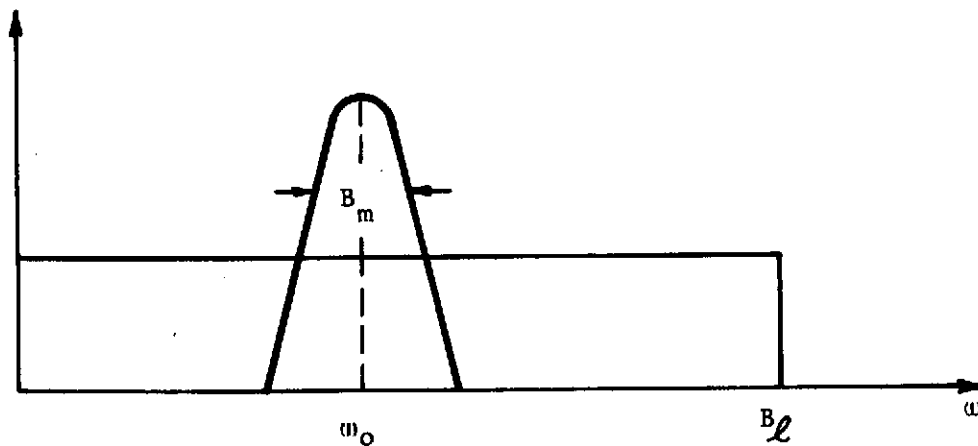
represents a design constraint based on the systems capability to detect the modulation caused by ocean waves.

### 3.2 Measurement of Ocean Wavelength

As was shown in the previous section, the input to the spectrum analyzer is a (nominally white) Gaussian process plus a process with a smaller bandwidth (Gaussian process) representing the modulation due to the wave structure, i.e.,

$$Z(t) \approx 2(N+S) \left(\frac{B_c}{B_\ell}\right) + 2\gamma S \left(\frac{B_c}{B_\ell}\right) m(t) + 2(N+S) \sqrt{\frac{B_c}{B_\ell}} \eta(t)$$

In the spectral domain:



the problem of measuring ocean wavelength is equivalent to locating the center of this hump in frequency.

Note this is just the satellite altimeter problem (beam limited) in disguise. In the spectral domain, what is required is to locate a hump of noise in the presence of uniform background noise. But this is just the problem solved in the altimeter study, reference.<sup>(4)</sup> (In fact, for a full stretch FM altimeter system, the altimeter problem is identical to this one since range becomes equivalent to frequency in a full stretch system.)

This being the case, much of the following relies heavily on the results developed in the altimeter study including a consistent notation.

Assume that a split-gate tracker is used to locate the center of the spectrum of the modulation as shown in Figure 3.1. Then the output of the tracker is given as

$$e(\omega_o) = \sum_{eg} V_i - \sum_{lg} V_i \quad (3.16)$$

where the  $V_i$  are independent samples of the power, and the notation eg and lg refer to early and late gate, respectively.

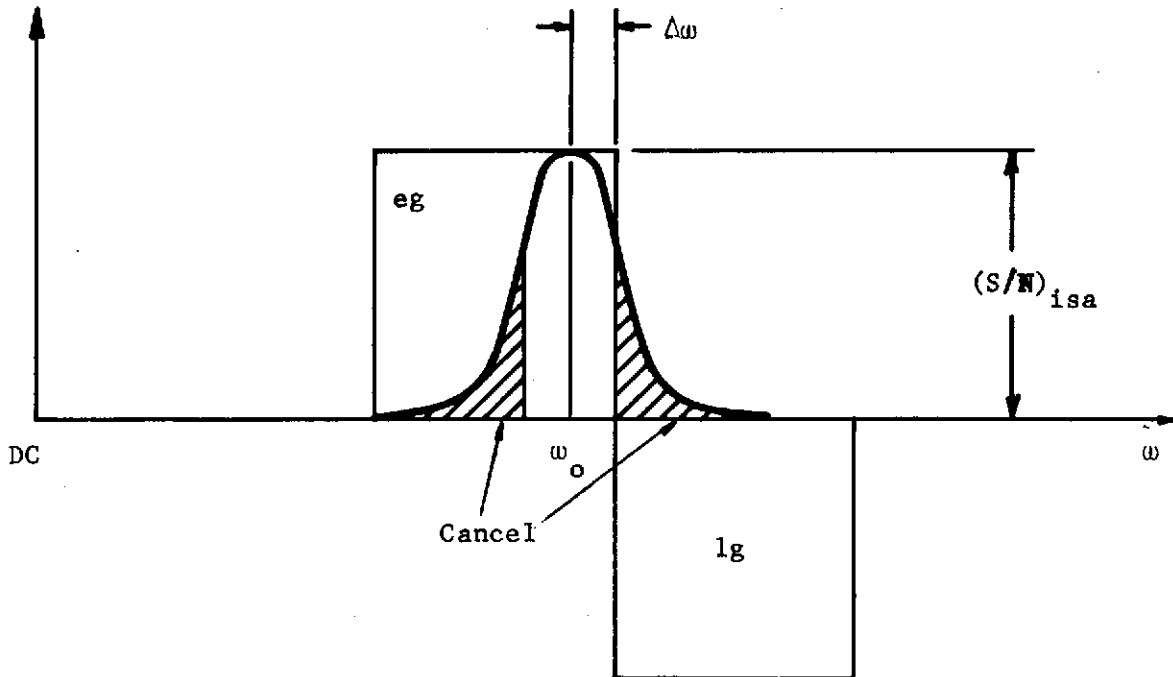


Figure 3.1 Split-Gate Tracker

Further assume, for simplicity, that the shape of the modulation spectrum is symmetric about its center frequency. (The actual non-symmetric spectrum will of course cause a bias in this type estimate.)

Then

$$E \epsilon(\omega_0) = 0 \quad (3.17)$$

and

$$E \epsilon(\omega_0 + \Delta\omega) = \left. \begin{aligned} & \sum_{eg} \bar{v}_i - \sum_{lg} \bar{v}_i \\ & \sim \frac{2\Delta\omega}{B_a} (S/N)_{isa} \end{aligned} \right\} \quad (3.18)$$

Now

$$\begin{aligned} \sigma^2 \epsilon(\omega_0) &= \left. \begin{aligned} & \sum_{lg} E v_i v_j + \sum_{eg} E v_i v_j \\ & = 2 \sum_{eg} E v_i v_j \quad (\text{by symmetry}) \\ & = 2 \left\{ \sum_i 2 \bar{v}_i^2 + \sum_{i \neq j} \bar{v}_i \bar{v}_j \right\} \end{aligned} \right\} \quad (3.19) \end{aligned}$$

since  $E v_i^2 = 2 \bar{v}_i^2$  for an exponential process.

Hence

$$\sigma^2 \epsilon(\omega_0) = 2 \left\{ \sum_i \bar{v}_i^2 + \left( \sum_i \bar{v}_i \right)^2 \right\} \quad (3.20)$$

Assuming the spectrum is nearly square:

$$\sum_i \bar{V}_i^{-2} = N_E (1 + S/N_{isa})^2 \quad (3.21)$$

$$\sum_i \bar{V}_i = N_E (1 + S/N_{isa}) \quad (3.22)$$

where  $N_E$  is the number of samples in the gate.

Substituting eq. (3.21) and (3.22) into 3.20 yields

$$\sigma_{\epsilon}^2(\omega_o) = 2(N_E + N_E^2) (1 + S/N_{isa})^2 \quad (3.23)$$

Now the slope of the error signal (from eq. (3.18))

$$\frac{E \epsilon(\omega_o + \Delta\omega)}{\Delta\omega} \approx \frac{2(S/N)_{isa} \Delta\omega}{B_a \Delta\omega} \quad (3.24)$$

Thus the error in estimating the center of the modulation hump is

$$\sigma_{\omega} \approx \frac{\sigma_{\epsilon} B_a}{2(S/N)_{isa}} = \sqrt{\frac{(N_E + N_E^2) B_a^2}{2}} \left[ 1 + \frac{1}{(S/N)_{isa}} \right] \quad (3.25)$$

Now, from Figure 3.1, it is seen that the gates are assumed to cover the entire modulation spectrum, thus

$$N_E B_a \approx B_m \quad (3.26)$$

and

$$\sigma_{\omega} \approx \sqrt{\frac{B_m B_a + B_m^2}{2}} \left[ 1 + \frac{1}{(S/N)_{isa}} \right] \quad (3.27)$$

Assuming that

$$B_a \ll B_m$$

$$\frac{\sigma_{\omega}}{B_m} \approx \frac{1}{\sqrt{2}} \left[ 1 + \frac{1}{(S/N)_{isa}} \right] \quad (3.28)$$

Here again, the normalization of the error to the modulation bandwidth is somewhat analogous to that of the altimeter error which normalizes to wave height. Thus, for a given set of system parameters the error in estimating 50 meter ocean wave lengths will be a factor of 8.0 greater than the error in estimating 400 meter ocean wave lengths.

The error expression given by equation (3.28) is on a spectrum resolution basis. If more samples are averaged, the standard deviation decreases as  $\sqrt{\text{number}}$ .

But 
$$N = B_a T \quad (3.29)$$

$$= B_a \frac{2H\theta_B \sin\theta_o}{c \cos^2 \theta_o} N_p \quad (\text{see eq. 3.14})$$

therefore

$$\frac{\sigma_{\omega} \sqrt{N}}{B_m} \approx \left( \frac{B_a 4H\theta_B \sin\theta_o}{c \cos^2 \theta_o} \right)^{-1} \left( 1 + \frac{1}{(S/N)_{isa}} \right) \quad (3.30)$$

Figure 3.2 shows the effect of  $(S/N)_{isa}$  on estimation accuracy. Note that a saturation effect occurs near  $(S/N)_{isa} = 0$  dB.

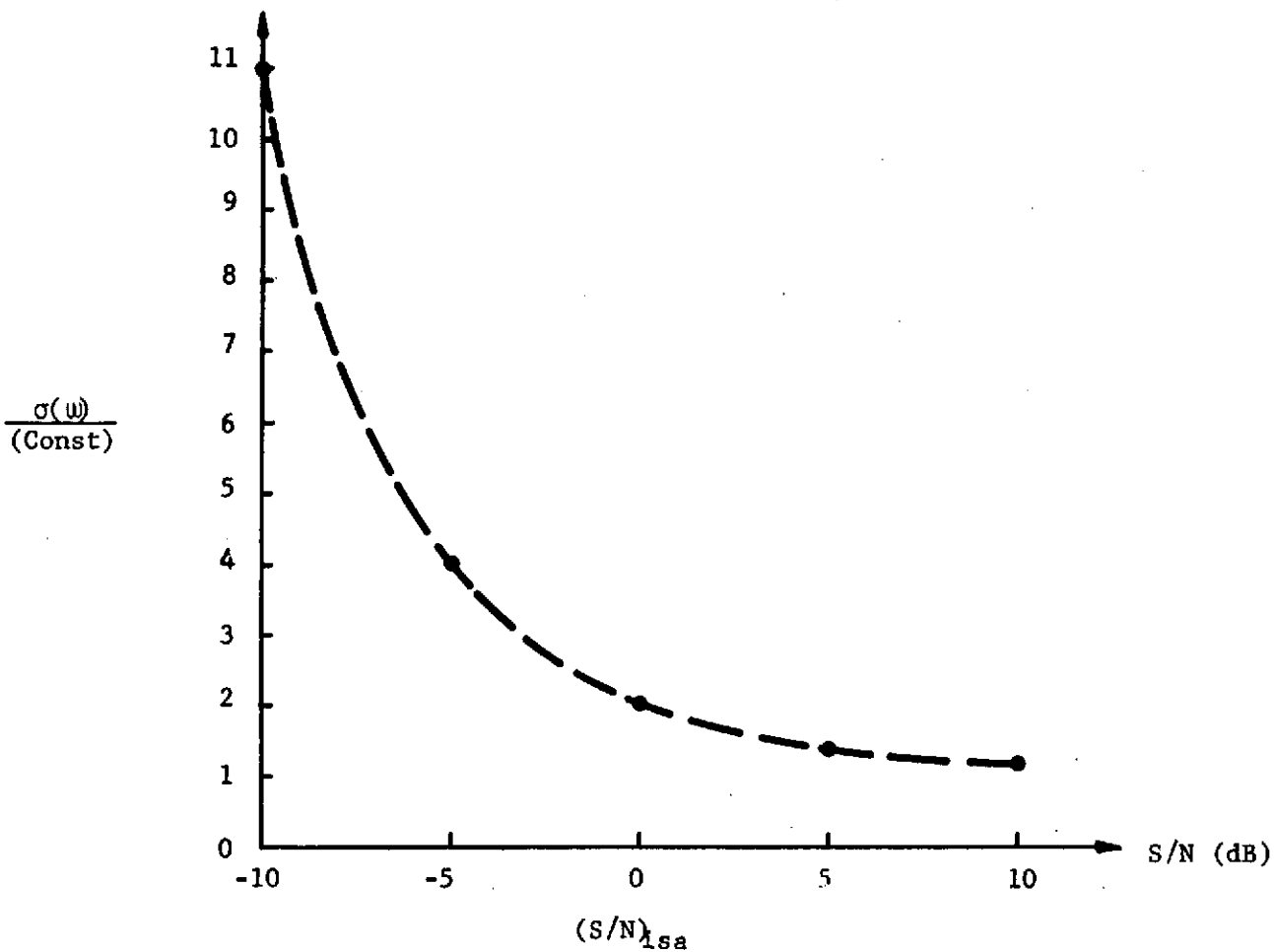


Figure 4.2 Estimation Accuracy vs  $(S/N)_{isa}$

Recall, however, that the "signal-to-noise" ratio is given by:

$$S/N_{isa} = \gamma^2 \left( \frac{S}{S+N} \right)^2 \frac{B_c}{B_m}$$

Thus, even for  $\infty$  receiver signal-to-noise ratio, the effective signal-to-noise ratio becomes

$$\gamma^2 \frac{B_c}{B_m} = \frac{\gamma^2}{B_m \tau_c} \quad (3.31)$$

Hence, to get in the neighborhood of unity "signal-to-noise"<sub>isa</sub> requires that

$$\boxed{\frac{1}{B_m \tau_c} > \frac{1}{\gamma^2}} \quad (3.32)$$

This effect arises because you are trying to measure the modulation of  $\sigma^\circ$ . But what you measure is a random return whose mean power is  $\sigma^\circ$ . Thus you have to average several samples to estimate the mean power level. The less variation in  $\sigma^\circ$ , then the more accurately you must measure the mean power level to pick up small variations in it. But the only way to do this (unless you want to integrate every range resolution cell for several pulses) is to get several range cells packed into one wavelength on the water. (i.e. make  $B_c/B_m$  large).

For  $\gamma = .23$  (2 dB modulation)

$$\boxed{\frac{1}{B_m \tau_c} > 19} \quad (3.33)$$

Thus it is necessary to resolve to the order of a 19th of a (water) wavelength in order to recover the modulation reliably.

Table 3.1 summarizes this requirement for various modulation indexes.

Table 3.1

| <u>Modulation (dB)</u><br><u>(peak-to-peak)</u> | <u><math>\gamma</math></u> | <u><math>(1/\gamma^2)</math></u> |
|---|----------------------------|----------------------------------|
| 2   | .23                        | 19                               |
| 4   | .43                        | 5.4                              |
| 6   | .60                        | 2.8                              |
| 8   | .73                        | 1.9                              |
| 10  | .83                        | --                               |

4.0      REFERENCES - PART II

- (1)      G. T. Ruck, D. E. Barrick and T. Kaliszewsk, "Bistatic Radar Sea State Monitoring," Batelle, Columbus Laboratories, June 1972.
- (2)      K. Tomiyasu, "Short Pulse Wide-Band Scatterometer Ocean Surface Signature," IEEE Transactions on Geoscience Electronics, Volume GE-9, Number 3, pp. 175 - 177, July 1971.
- (3)      W. W. Peterson, et. al., "The Theory of Signal Detectability," IRE Trans. on Information Theory, Volume 4, pp. 171 - 212, September 1954.
- (4)      R. P. Dooley, F. E. Nathanson, L. W. Brooks, "Study of Radar Pulse Compression for High Resolution Satellite Altimetry," NASA CR # 137474, May 1, 1973.